ENHANCING PROTEIN-RESISTANCE OF PEO-MODIFIED BIOMATERIALS

A Dissertation

by

RANJINI MURTHY

Submitted to the Office of Graduate Studies of
Texas A&M University
in partial fulfillment of the requirements for the degree of

DOCTOR OF PHILOSOPHY

May 2009

Major Subject: Materials Science and Engineering

ENHANCING PROTEIN-RESISTANCE OF PEO-MODIFIED BIOMATERIALS

A Dissertation

by

RANJINI MURTHY

Submitted to the Office of Graduate Studies of
Texas A&M University
in partial fulfillment of the requirements for the degree of

DOCTOR OF PHILOSOPHY

Approved by:

Chair of Committee,	Melissa A. Grunlan
Committee Members,	Hong Liang
	Kenith Meissner
	James Silas
Chair of Materials Science and Engineering Faculty,	Tahir Cagin

May 2009

Major Subject: Materials Science and Engineering

ABSTRACT

Enhancing Protein-Resistance of PEO-Modified Materials. (May 2009)

Ranjini Murthy, B.S., Arkansas State University;

M.S., Arkansas State University

Chair of Advisory Committee: Dr. Melissa A. Grunlan

The ultimate goal of this dissertation research is to enhance the protein resistant nature of poly(ethylene oxide) (PEO) or poly(ethylene glycol) by introduction of a siloxane linker and to subsequently prepare coatings which prevent surface-induced thrombosis. The hydrophobicity and flexibility of the siloxane tether should impart both amphiphilicity and conformational mobility to the PEO chain to further decrease protein adhesion. Because adsorption of plasma (blood) proteins initiates the clotting process, coating surfaces based on these new PEO-silanes should prevent or significantly diminish thrombosis. Thus, these coatings would be extremely useful for blood-contacting medical devices such as stents, grafts, arteriorintravenous shunts, and biosensors.

Novel amphiphilic PEO-silanes were prepared with systematic variations to several key structural features, including: siloxane tether length, PEO segment length, and PEO architecture. Thus, PEO-silanes were prepared having the general formulas: α-$(EtO)_3Si(CH_2)_2$-oligodimethylsiloxane$_n$-*block*-[PEO_8-OCH_3] (n = 0, 4, and 13; linear architecture) and α-$(EtO)_3Si(CH_2)_2$-oligodimethylsiloxane$_n$-*block*-[PEO_m-OCH_3]$_2$ (n = 0,

4, and 13; m = 6 and 12 branched architecture). The reactive triethoxysilane [$(EtO)_3Si$-] group serves as the crosslinking or grafting moiety. The PEO segment is distanced from the $(EtO)_3Si$- group by an oligodimethylsiloxane tether which is both hydrophobic and exhibits a high degree of chain flexibility. Crosslinked silicone coatings and surface-grafted coatings were prepared with amphiphilic *linear* PEO-silanes **(a-c)**. Crosslinked silicone coatings were also prepared with *branched* PEO-silanes **(1a-3a** and **1b-3b).** All coatings showed improved resistance to common plasma proteins compared to silicone coatings. Furthermore, protein adsorption generally decreased with siloxane tether length.

For crosslinked PEO-modified silicone coating systems based on *linear* **(a-c)** and *branched* PEO-silanes **(1a-3a** and **1b-3b)**, longer tethers enhanced PEO reorganization to the film-water interface to enhance protein resistance. In the absence of surface reorganization for surface grafted coatings prepared with *linear* PEO-silanes, longer siloxane tethers better inhibited protein adsorption despite a moderate decrease in graft density (σ) and decrease in surface hydrophilicity. This indicates that longer siloxane tethers enhance the configurational mobility of the PEO segments to better repel proteins.

DEDICATION

TO MY DAUGHTER

I love you so much and thank you for coming into my life. You inspire me with your presence.

TO MY HUSBAND

You are my best friend and the love of my life. Thank you for all your love encouragement and support.

TO MY PARENTS AND SISTER

I thank you for all the love and moral support throughout the course of my study. I love you all very much.

ACKNOWLEDGEMENTS

I express my gratitude to my research advisor, Professor Melissa A. Grunlan, for all the painstaking hours of input, guidance and encouragement that have been instrumental in the completion of my doctoral studies. My growth as a scientist, to be able to think, analyze and solve problems, has improved significantly under your guidance.

I wish to thank Professor Mariah Hahn for the guidance provided for protein adsorption studies. Our collaboration resulted in our publication in *Biomacromolecules* and *Biomaterials*. I thank Professor David E. Bergbrieter for the use of the goniometer for surface analyses.

I thank the members of my qualifying and dissertation committees: Professors James Silas, Hong Liang, Kenith Meissner, Zubeida Oeniaes, Haiyan Wang, and Richard Griffin for all the input to better my work and grow as a scientist.

I wish to extend my gratitude to all my research group members for all the emotional support that was provided in times of great need. This work would be incomplete without your support.

Finally, I wish to thank my daughter, parents, husband, sister and friends for making this task seem easier and all the emotional support that you have provided me in the course of my accomplishment. Thank you to all.

TABLE OF CONTENTS

CHAPTER Page

LIST OF FIGURES

FIGURE Page

FIGURE Page

FIGURE Page

LIST OF TABLES

CHAPTER I

INTRODUCTION

1.1 Overview

Millions of new blood-contacting medical devices such as coronary stents, vascular grafts, arteriorintravenous shunts, and biosensors are implanted in patients each year. These devices are highly prone to surface-induced thrombosis which compromises device function and may even cause a catastrophic event (e.g. embolism). Conventional materials used to prepare blood-contacting devices often suffer from poor blood-compatibility. These materials adsorb plasma proteins which triggers thrombosis. Thus, the current widespread approach to prevent surface-induced thrombosis is anti-coagulant or anti-platelet therapy which is costly and may cause undesirable complications. An attractive alternative are new materials which are resistant to the adsorption of blood proteins and hence prevent surface induced thrombosis. Poly(ethylene oxide) (PEO, or poly(ethylene glycol) (PEG)) is one of the most promising protein-resistant material. However, the long-term in vivo performance have been disappointing compared to in vitro[1] results. Thus, enhancing the protein resistant nature of PEO remains of significant interest.

This dissertation follows the style of *Biomaterials*.

1.2 Introduction

The hemostatic mechanisms of the body cause blood to coagulate thereby preventing uncontrolled blood loss during injury. Unfortunately, this mechanism also leads to thrombus formation on artificial implant surfaces which contact blood. This process is known as “surface-induced thrombosis” and is a major complication in the development of blood-contacting medical devices.[2] When blood comes in contact with an artificial surface, non-specific adsorption of plasma proteins results in platelet adhesion and activation of coagulation pathways which often leads to thrombus formation (Fig. 1.1).[3-5] Surface-induced thrombosis on biomaterial implant surfaces is therefore a frequent reason for diminished performance or even catastrophic failure of many devices.[6]

Thrombus formation leads to poor blood circulation and may cause complete embolism (occlusion) of a blood vessel. In addition, active adsorption of blood components on the surface of an artificial implant during thrombosis can lead to changes in the composition of blood. Thus, it is desirable for blood-contacting materials to eliminate or at least minimize the adsorption of blood proteins to prevent surface-induced thrombosis and improve device performance.

Millions of new blood-contacting medical devices are implanted into patients each year (Table 1.1). The most prevalent blood-contacting biomedical devices include vascular grafts, coronary stents, arteriovenous (AV) grafts, and prosthetic heart valves.[6] Unfortunately, conventional materials used to fabricate these devices illicit surface-induced thrombosis.

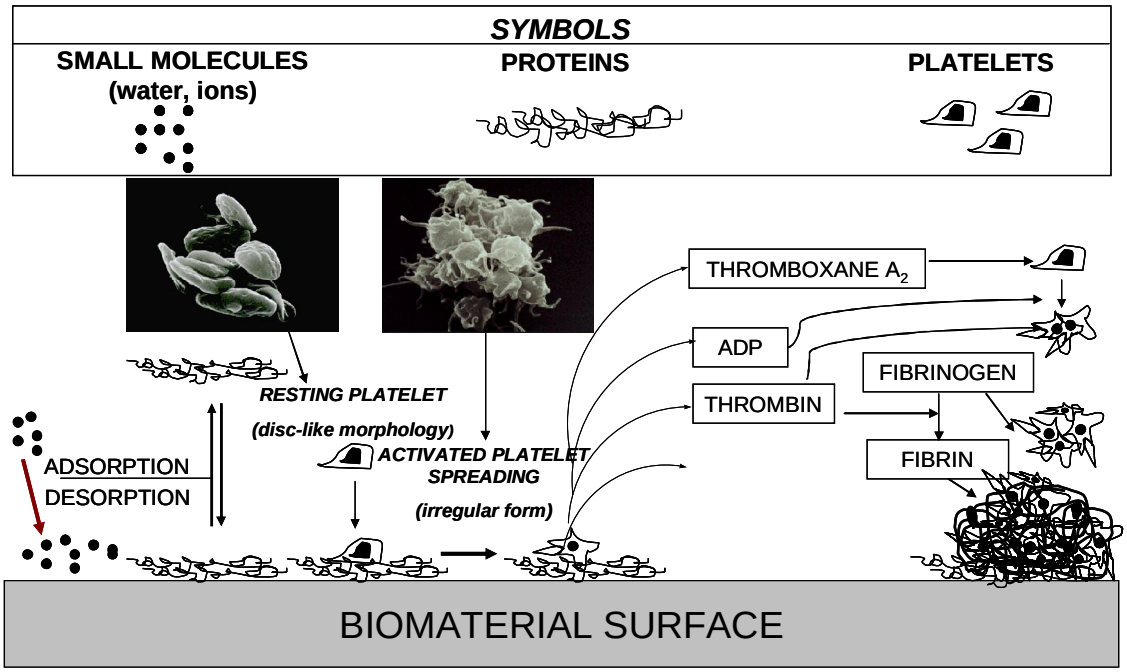

Figure 1.1. Surface-induced thrombosis. Blood proteins adsorb onto the surface of a biomaterial and thereby induce clot formation.

This requires the use of anti-coagulation or anti-platelet therapies such as heparin coatings in conjunction with these devices.[7] The necessity for drug therapy for both short and long-term blood-contacting devices, is often costly and imposes additional risks to the patient.[8] For instance, heparin usage has been linked to increased bleeding and heparin-induced thrombocytopenia.[7] Between January 1, 2007 and April 13, 2008, the food and drug administration (FDA) received over 700 reports of adverse events such as vasodilation, hypotension, facial swelling, abdominal pain vomiting and diarrhea that resulted in over 80 deaths in patients receiving heparin as a part of their dialysis treatment or surgical procedures.[9]

Given the prevalence of blood-contacting devices and the complications associated with surface-induced thrombosis and conventional drug therapeutics,

considerable research effort is being made to develop synthetic materials which are hemocompatible.[10] A “hemocompatible” or “blood-compatible” material is one which does not cause any change in blood functions, transform its components, have negative effects on the chemical composition of blood, distort the electrolytic composition of blood, provoke the formation of thromboses and thromboembolism or activate coagulating and fibrinolytic systems.

Table 1.1. Estimated usage of common blood contacting devices worldwide.[8]

Blood contacting device	Blood contacting material	No. per year
Vascular graft	Dacron, Teflon	200,000
Stents	Stainless steel, styrene-isobutylene polymer	4,000,000
Heart valve	Pyrolytic carbon, Dacron, fixed natural tissue	200,000
Pacemaker	Silicone, polyurethane, platinum	300,000
Catheters	Silicone, polyurethane, PVC, Teflon	200,000,000
Extracorporeal oxygenation	Silicone rubber	20,000
Guidewires	Stainless steel, nitinol	Millions
Artificial kidney	Polyacrylonitrile, polysulfone, cellulose	1,200,000
Left ventricular assist device (LVAD)	Polyurethane	1000

A principal approach to create hemocompatible surfaces is to design polymeric materials which are resistant or reduce the adsorption of blood proteins. Since blood proteins prefer to adsorb onto hydrophobic surfaces, polymers such as silicones have been hydrophilized with air or oxygen plasma treatment, etc. Hydrophilic polymers which reduce protein adhesion include poly(ethylene oxide) (PEO). Biodedegradable polymers also prevent the accumulation of proteins since, as the polymer degrades, the adsorbed protein layer is sloughed off. Zwitterionic polymers such as polyphosphorylcholine mimic the membrane of red blood cells which are naturally

thromobresistant. Polymers with hydrophilic and hydrophobic components (i.e. amphiphilic polymers) undergo surface phase segregation which can lead to formation of unique topography which reduced protein adhesion.[11, 12] Other approaches currently being explored as a means to reducing thrombogenesis is the use of body's own biological materials such as endothelial cells (ECs) to solve issues of hemocompatibility.[13] In the following sections, currently used materials for common blood-contacting devices and their modification to improve blood-compatibility are reviewed.

For vascular reconstruction, including coronary bypass surgery, autologenous saphenous vein is the most commonly used for small-caliber (< 5 mm diameter).[14] However, 10-40% of patients do not have a suitable saphenous vein due to size mismatch, venous disease or previous procedures. Additionally, four-year patency with saphenous veins is only 40-70%.[14] The thrombogenic potential as well as intimal hyperplasia (thickening of the neointima) are the main determinants of patency of vascular grafts with the former being mainly responsible for graft occlusion.[10] Therefore the success rates for these small caliber vascular grafts are disappointing.[15]

Dacron (PET) and expanded polytetrafluoroethylene (ePTFE) are among the materials that are known to have high success rates for large-vessel reconstructions but have failed when used as small-caliber grafts primarily due to early graft occlusion.[14] Typically, healing of synthetic grafts is delayed in humans as grafts never endothelialize and thrombus covers the inner surface long after implantation.[16]

Glutaraldehyde-(GA) fixed bovine and human umbilical vein grafts have been evaluated but discarded due to aneurysm formation two years post implantation. Patency rates of GA-fixed human umbilical vein in coronary bypass at 3-13 months is about 46% and for GA-fixed bovine artery grafts at 3-23 months is about 16%. Porcine common carotid arteries covalently linked with heparin to reduce thrombogeniety and provide a substrate for heparin-binding growth factors to promote cell infiltration and healing is currently being explored. These porcine carotid arteries are devoid of any cells to reduce immune reactions and are uncrosslinked to maintain compliance and microstructure of the vessel to allow host cell infiltration.[14]

Another approach explored to combat surface induced thrombosis is by endothelial cell seeding. The growth of ECs on the luminal surface of the ePTFE prosthetic graft prior to implantation results in a conduit covered by neo-intima with normal ECs that can counteract the biological mechanisms responsible for thrombosis. EC seeding has its own challenges. Short seeding times results in ECs losses up to 95% 24 hours post implantation whereas longer seeding times present the problem of applicability in humans thereby making human ECs difficult to grow.[13]

Protein adsorption and platelet adhesion are interfacial phenomena that is vastly influenced by the surface properties of the biomaterials. For this reason, biomaterial surface modification with protein-repulsive molecules is an attractive alternative for making more blood compatible biomaterials. Heparin is commonly used as a protein-repulsive molecule.[1, 17] Heparin and low molecular heparins are widely used in

treatment of various diseases as well as for their anticoagulant activity and can be found coating medical devices such as stents, catheters and filters.[9, 18]

Endoluminal metallic stents is used vastly during percutaneous transluminal coronary angioplasty for treatment of coronary arterial stenosis or obstructive coronary atherosclerotic narrowing.[19, 20] Bare metallic stents also trigger protein adhesion resulting in activation of coagulation cascade, and finally thrombosis.[19, 21] Thrombosis as well as neointimal hyperplasia are commonly reported among metallic stents.[22] Restenosis rates in patients who receive metallic stents is 20-40% at 6 months post procedure and is a rare occurrence after that time.[19, 23]

Stent material selection has been primarily based on their mechanical properties, including: a good expandability ratio (i.e. ability to expand and conform to the vessel wall once inserted at the target area and the balloon inflated), sufficient radial hoop strength and negligible recoil (i.e. ability to overcome the forces imposed by atherosclerotic arterial wall and not collapse), sufficient flexibility. In addition, magnetic resonance imaging (MRI) compatibility to assist clinicians in assessing the *in-vivo* location of the stent is also desirable.[24] Thus, stents have been traditionally prepared with metals such as: 316L stainless steel (316L SS), platinum-iridium (Pt-Ir) alloy, tantalum (Ta), Nitinol (Ni-Ti), cobalt-chromium (Co-Cr) alloy, titanium (Ti), pure iron (Fe) and magnesium alloys (Mg). Unfortunately, clotting on bare metallic stents remains a problem.

One approach to combat thrombosis and neointimal proliferation in metallic stents is to alter its surface characteristics without altering the bulk. Inorganic coatings

such as iridium oxide, silicon-carbide and gold are commonly used inorganic-coating materials on stents. Several polymers such as PET, PLLA, PLGA with previous medical or dental applications have been used for coating stents or used to make the stent itself.[22] Biostable polymers such as PET has been investigated for making stents due to its excellent mechanical properties. However, the use of PET resulted in chronic foreign body inflammatory reaction resulting in complete occlusion of the vessel. In another study, significant foreign body reactions and inflammatory reactions were reported.[25] Pure Fe and Mg alloys have been explored for biodegradable coronary stents which also reduces thrombosis.[22]

Drug-eluting stents (DES) have been in use since 2002 and have transformed the practice of interventional cardiology by drastically reducing restenosis. In DES, metal stents are coated with polymers with embedded drugs such that it serves as a "drug reservoir" to deliver therapeutics. Data on late stage thrombosis (up to 4 years) in the first generation DES have recently emerged. The drugs used in first generation DES are cytostatic and cytotoxic agents that have detrimental effects on endothelialization.[21] The next generation DES is using more complex hemocompatible materials such as phosphorylcholine polymer, a zwitterionic mimic of the red blood cell membrane.[26] Other fully biodegradable polymer coatings on stents such PLGA, which metabolizes to carbon dioxide and water thus leaving the bare metal stent after the drug has been released, are currently being explored.[21] For instance, biodegradable polymer matrices have been evaluated to deliver anti-proliferative drugs (e.g. heparin, rapamycin, sirolimus, zotarolimus or paclitaxel) during degradation.[26] In some cases, restenosis

rate has been reduced to less than 10%. Currently clinically available DES is the sirolimus-eluting stents (SES) which consists of a stainless steel platform coated with poly(ethylene-*co*-vinyl acetate) (PEVA) and poly-(*n*-butyl methacrylate) (PBMA). The polymer is a reservoir for sirolimus, a potent immunosuppressant used in transplant recipients. The taxus paclitaxel-eluting stent (PES) has also been widely studied in a range of patients. It incorporates a stainless steel platform coated with poly(styrene-*b*-isobutylene-*b*-styrene) (SIBS) combined with paclitaxel. The zotarolimus-eluting stent is also currently in use with a CoCr platform loaded with phosphorylcholine and a sirolimus analogue (70% released over 30 days). There are a number of DES and combination drug eluting stents currently in use or under investigation (Tables 1.2 and 1.3).[21, 26]

Dialysis grafts are used to obtain vascular access in patients with chronic renal failure undergoing hemodialysis. Patients undergoing chronic hemodialysis treatment represent a high risk group for thromoboembolic complications due to contact activation by extracorporeal devices. Nevertheless, grafts have continued to be more commonly used in the United States.[27, 28]

Thrombosis of a patient's dialysis grafts results in failed access for hemodialysis and will ultimately lead to death. The typical approach is declotting, with adjunctive therapy, to correct the underlying stenosis of the thrombosed shunt.[29] Percutaneous intravascular thrombolysis (PIT) is a method for treating thrombosed hemodialysis grafts. It is performed by applying a thrombolytic agent such as urokinase into the clot or by mechanically fragmenting the thrombotic material or a combination of the two. One

major drawback using this method is that pulmonary embolism upon fragmentation is an expected complication.[30]

Table 1.2. DES in clinical use or under investigation.[21]

Drug	Stent Platform	Coating
Sirolimus	SS	Durable Polymer
Sirolimus	SS	Biodegradable Polymer
Sirolimus	SS	
Sirolimus	CoCr	Biodegradable Polymer
Zotarolimus	CoCr	Durable Polymer
Paclitaxel	SS	Durable Polymer
Paclitaxel	SS	Biodegradable Polymer
Paclitaxel	CoCr	Biodegradable Polymer
Paclitaxel	SS	
Paclitaxel	Tyrosine polycarbonate	Biodegradable Polymer

SS: stainless steel; CoCr: cobalt chromium; Durable polymer:phosphorylcholine; Biodegradable polymer: polylactic acid or polylactic-co-polyglycolic acid.

Table 1.3. Combination DES under clinical investigation.[21]

Drug 1	Drug 2	Stent Platform	Coating
Sirolimus	Genistein		
Pimecrolimus	Paclitaxel	CoCr	Biodegradable Polymer
Sirolimus	Heparin	SS	Biodegradable Polymer
Zotarolimus	Dexamethasone		
Sirolimus	Estradiol	SS	

SS: stainless steel; CoCr: cobalt chromium; Biodegradable polymer: polylactic acid or polylactic-co-polyglycolic acid.

ePTFE is commonly used for vascular access for dialysis. However, problems with these grafts results in frequent hospitalization of the patient due to thrombosis and decreased efficiency of dialysis**.** Additionally, dialysis access placement, replacement, and maintenance results in medical costs that exceed millions annually.[31]

A more recent and increased approach for hemodialysis is the use of tunneled dialysis catheters (TDC) to gain vascular access. Over 70% of incident and 21% of

prevalent chronic hemodialysis patients use TDC as a method to receive dialysis treatment.[32, 33] As indicated by Centers for Medicare Services (CMS), at 90 days of dialysis the catheter is still the access of choice. From 2002 to 2005, the number of grafts being used at 90 days decreased whereas the number of fistulas increased, but the percentage of catheters being used remained approximately the same (Table 1.4).[14] Among several issues related to the use of TDCs are infection, biofilm formation and thrombus formation that lead to catheter dysfunction.

Table 1.4. Distribution of access types at 90 days of chronic outpatient dialysis (CMS 2006 report).[14]

Year	% of AV fistulas	% of dialysis grafts	% of catheters
2002	23	26	48
2003	25	19	52
2004	25	19	52
2005	32	11	52

Surface-treated catheters have been recently developed to combat infection, biofilm formation and thrombosis. Antimicrobial coatings and antithrombotic coatings are the two types of surface treatments available for catheters used in hemodialysis. Catheter complications are a major cause of morbidity and mortality in hemodialysis patients.[34] Antithrombotic coatings primarily use heparin bonded to the catheter as an anticoagulant. Heparin is a strong anticoagulant as well as reduces thrombin-activated factors thereby controlling thrombus formation. As a result, heparinization on medical surfaces has the potential to reduce infection, biofilm formation and thrombosis. However, this is based on inadequate clinical trials with the use of surface treatments on catheters for hemodialysis patients. In addition to inadequate clinical data, coated

catheters cost more than uncoated catheters. For instance, a tunneled catheter with surface heparinization costs $100 more than a standard catheter and this increased expense cannot be justified without sufficient clinical data. Therefore, more randomized, controlled clinical data is necessary to evaluate the effectiveness of this new technology.

As mentioned earlier, materials which prevent the adsorption of plasma proteins should eliminate or reduce surface-induce thrombosis. PEO's protein resistance has been attributed to its high water content,[35] excluded volume,[36] steric repulsion [37] and its blockage of adsorption sites on the underlying surface [38] that leads to the "exclusion effect" or "steric stabilization effect." The high chain mobility of PEO produces an entropic penalty of chain compression if protein adsorption were to occur (Fig. 1.2).

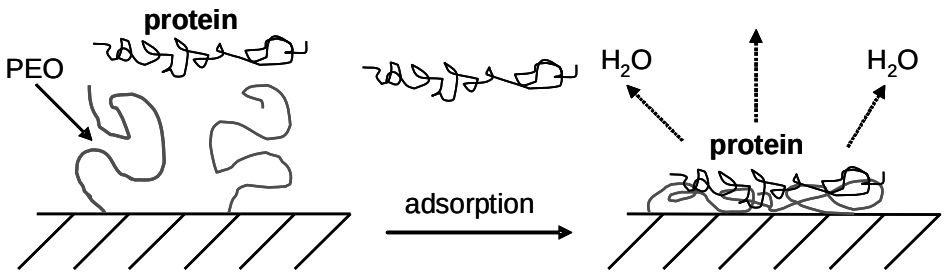

Figure 1.2. Protein resistance of PEO. The configurational mobility of the PEO chains produces a large excluded volume, steric repulsion and blockage of adsorption sites on the underlying surface.

Thus, enhancement of PEO's chain mobility may optimize protein resistance and improve blood-compatibility of biomedical devices. PEO has been incorporated onto polymer surfaces by various methods such as bulk crosslinking,[39] self-assembly,[40,

41] physisorption,[42] formation of surface physical interpenetrating networks (SPINs)[4, 43, 44] or covalent grafting.[45]

In this dissertation research, amphiphilic linear and branched PEO-silanes with "siloxane tethers" were prepared and incorporated into crosslinked and surface-grafted coatings. The effect of PEO-silane structure was related to protein resistance. These findings will enable the rationale design of PEO-based biomaterials with enhanced thromboresistance. In addition, this study provides an improved understanding of the mechanism of PEO's protein resistance, particularly the role of configurational mobility.

CHAPTER II

PROTEIN-RESISTANT SILICONES: INCORPORATION OF POLY(ETHYLENE OXIDE) VIA SILOXANE TETHERS*

2.1 Overview

Silicones with enhanced protein resistance were prepared by introducing PEO chains via siloxane tethers **(a-c)** of varying lengths. Three unique ambifunctional molecules **(a-c)** having the general formula α-$(EtO)_3Si(CH_2)_2$-oligodimethylsiloxane$_n$-*block*-poly(ethylene oxide)$_8$-OCH_3 [n = 0 **(a)**, 4, **(b)** and 13 **(c)**] were prepared via regioselective Rh-catalyzed hydrosilylation. Nine PEO-modified silicone films were subsequently produced by the H_3PO_4-catalyzed sol-gel crosslinking of **a-c** each with α,ω-bis(Si-OH)polydimethylsiloxane (**P**, M_n = 3000 g/mol) in varying ratios (1:1, 1:2, and 2:3 molar ratio **a**, **b**, or **c** to **P**). Films prepared with a 2:3 molar ratio (**a-c** to **P**) contained the least amount of uncrosslinked materials which may migrate to the film surface. For this set of films, surface hydrophilicity and protein resistance increased with siloxane tether length **(a-c)**. These results indicate that PEO was more effectively mobilized to the surface if incorporated into silicones via longer siloxane tethers.

2.2 Introduction

Silicones, particularly poly(dimethylsiloxane) (PDMS), have been utilized in many biomedical applications because of their thermal and oxidative stability, gas permeability, low modulus, flexibility, and good biocompatibility.[45, 46] Unfortunately, silicones generally exhibit poor resistance to blood proteins as a result of its extreme hydrophobicity.[47, 48] An adsorbed blood protein layer can invoke subsequent platelet adhesion and activation of coagulation pathways leading to thrombosis thereby compromising device success.[49, 50] In order to reduce protein adsorption, silicone surfaces have been hydrophilized by various approaches which involve physical or chemical treatments or a combination of both.[47, 50-53] Poly(ethylene oxide) (PEO; or poly(ethylene glycol) PEG) is a neutral, hydrophilic polymer which exhibits unusually high protein resistance.[54, 55] In order to improve the protein resistance of silicone surfaces, PEO has been incorporated into silicone materials. Typically, silyl methyl (Si-Me) groups at the surfaces of silicones are first converted to reactive silanol (Si-OH) groups by oxygen or air plasma,[56-58] UV radiation,[59, 60] UV/ozone radiation (UVO)[60, 61], or solution phase oxidation.[62] PEO may be subsequently grafted onto the silanol-covered silicone surfaces via silanization reactions of PEO-silanes containing appropriate end-functionalized silane anchoring groups such as alkoxysilanes.[63] For instance, both trimethoxysilylpropyl- and triethoxysilylpropyl PEO monomethyl ether [$(RO)_3Si(CH_2)_3$-$(OCH_2CH_2)_n$-OCH_3] have been effectively grafted onto silanol-covered silicone surfaces.[62, 64, 65] Silane (Si-H) enriched silicone surfaces, produced by acid-catalyzed equilibration of silicone in

the presence of polymethylhydrosiloxane, were grafted with allyl PEO monomethyl ether [CH_2=CH_2CH_2-$(OCH_2CH_2)_n$-OCH_3] via Pt-catalyzed hydrosilylation.[66] PEO has also been introduced throughout the bulk of silicone materials via the condensation cure of triethoxysilylpropyl PEO monomethyl ether with α,ω-bis(Si-OH)PDMS and tetraethoxysilane [$Si(OEt)_4$].[67, 68]

PEO's protein resistance has been attributed to its high water content,[35] large excluded volume,[36] steric repulsion,[37, 69] and its blockage of adsorption sites on the underlying surface.[38] The effect of PEO molecular weight (MW) and surface concentration on protein resistance has been widely studied.[41, 54, 70-74] The configurational mobility of PEO produces an entropic penalty of chain compression if protein adsorption were to occur.[55, 69] Thus, enhancement of PEO chain mobility may optimize protein resistance. For instance, surfaces of coatings prepared by crosslinking α,ω-bis(Si-OH)PDMS with *bis*-triethoxysilylpropyl PEO displayed inferior protein resistance compared to surfaces of coatings prepared with triethoxysilylpropyl PEO monomethyl ether.[68] This was attributed to a lack of mobilization of the difunctional PEO to the aqueous interface compared to the monofunctional PEO. Conventional strategies to incorporate PEO into silicones utilize PEO-silanes in which the PEO segment is separated from the grafting or crosslinking site by a short alkane spacer [e.g. propyl as for $(RO)_3Si(CH_2)_3$-$(CH_2CH_2O)_n$-OCH_3)] which may limit PEO mobility.[62, 64-68]

Herein, we propose a synthetic strategy to prepare PEO-modified silicones with enhanced protein resistance by the incorporation of PEO via siloxane tethers. Three

unique ambifunctional molecules **(a-c)** were prepared having the general formula α-$(EtO)_3Si(CH_2)_2$-oligodimethylsiloxane$_n$-*block*-poly(ethylene oxide)$_8$-OCH_3 [n = 0 **(a)**, 4, **(b)** and 13 **(c)**] (Fig. 2.1). Thus, the PEO segment is distanced from the crosslinkable group [$(EtO)_3Si$] by an oligodimethylsiloxane tether. These siloxane tethers are highly flexible due to the wide bond angle (~143 °) and low barrier to linearization (0.3 kcal/mol) of Si-O-Si of dimethylsiloxanes.[75, 76] The dynamic flexibility of Si-O-Si produces polymers with extremely low glass transition temperatures (T_gs) (e.g. PDMS, T_g = -125 °C). Thus, the siloxane tethers of **a-c** should enhance PEO chain mobility so that PEO is more effectively reorganized to film surfaces to improve protein resistance.

To prepare ambifunctional molecules **(a-c)**, we utilized regioselective hydrosilylation reported by Crivello and Bi.[77-80] Rhodium-catatalyzed (Wilkinson's catalyst, $RhCl(Ph_3P)_3$) hydrosilylation of α,ω-bis(Si-H)oligodimethylsiloxanes with vinyl-terminated molecules was shown to proceed in a regioselective fashion. Thus, only one of the two terminal Si-H moieties was added to the vinyl compound. In this study, a series of three commercially available α,ω-bis(Si-H)oligodimethylsiloxanes$_n$ (**ODMS$_0$**, **ODMS$_4$**, and **ODMS$_{13}$**) were utilized. Alternatively, **ODMS$_4$** and **ODMS$_{13}$** may be prepared by the acid-catalyzed equilibration of cyclic siloxanes such a octamethylcyclotetrasilaxane (D_4) or hexamethyltrisiloxane (D_3) with tetramethyl-disiloxane (TMDS) by varying the stoichiometry of the cyclic siloxanes and TMDS.[81, 82] A crosslinkable $(EtO)_3Si$- moiety was introduced to one terminal end of each α,ω-bis(Si-H)oligodimethylsiloxanes (**ODMS$_{0,\ 4,\ 13}$**) by regioselective Rh-catalyzed

hydrosilylation with vinyl triethoxysilane (**VTEOS**) to yield the corresponding α-triethoxysilylethyl-ω-silane-oligodimethylsiloxane$_n$ (**1-3**) (Fig. 2.1). Pt-catalyzed (Karstedt's) hydrosilylation reaction of the regioselective products (**1-3**) each with allyl PEO monomethyl ether (MW = 425 g/mol) yielded the corresponding ambifunctional PEO-silanes **(a-c)**. Although we obtained the allyl PEO monomethyl ether from a commercial source, it may be prepared by reaction of monomethoxy PEO with NaH and allyl bromide.[83]

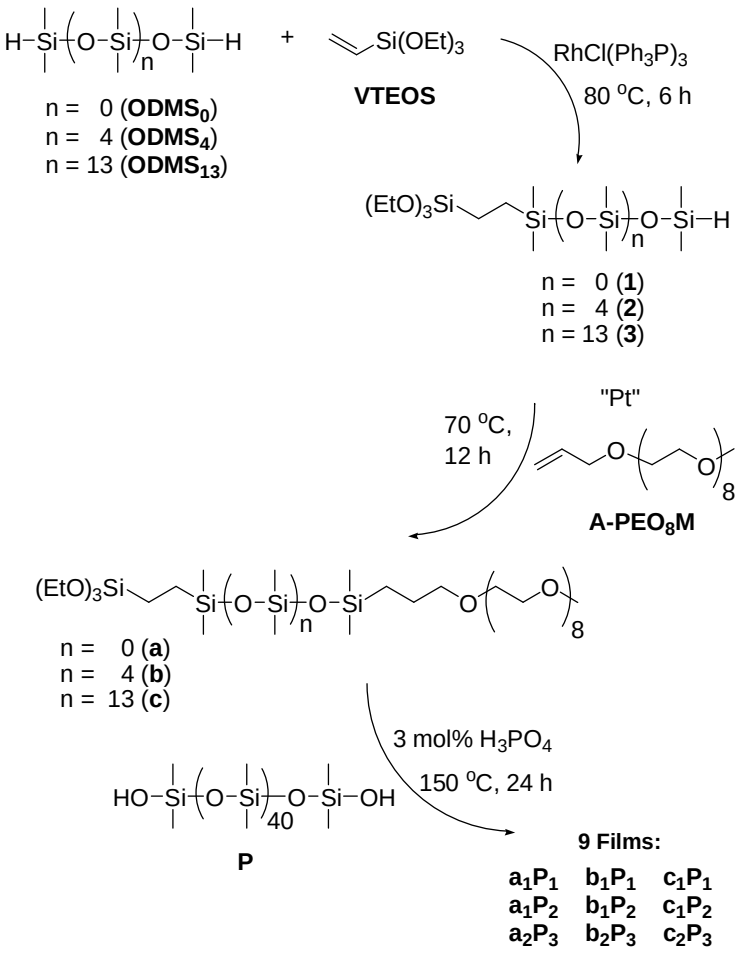

Figure 2.1. Synthesis of **a-c** and subsequent conversion to crosslinked PEO-modified silicone films by the acid-catalyzed sol-gel condensation with α,ω- bis(Si-OH)-polydimethylsiloxane (**P**) at 1:1, 1:2, and 2:3 molar ratios of **a**, **b**, or **c** to **P**.

Finally, **a**-**c** each underwent phosphoric acid (H_3PO_4)-catalyzed sol-gel crosslinking with α,ω-bis(Si-OH)polydimethylsiloxane (**P**, M_n = 3000 g/mol) in varying ratios (1:1, 1:2, and 2:3 molar ratio **a**, **b**, or **c** to **P**) to produce nine compositional unique PEO-modified silicone films.[84]

2.3 Experimental Section

Polymer Characterization

NMR Spectroscopy. ^{1}H spectra were obtained on an Inova-400 MHz and ^{13}C spectra were obtained on an Inova-300 MHz spectrometer both operating in the FT mode. Five percent w/v chloroform-*d* solutions were used to obtain ^{1}H and ^{13}C NMR spectra. Residual $CDCl_3$ was used as an internal standard.

IR Spectroscopy. IR spectra of neat liquids on NaCl plates were recorded using a Bruker TENSOR 27 Fourier transform infrared spectrometer.

Gel Permeation Chromatography (GPC). GPC analysis was performed on a Viscotek GPC system equipped with three detectors in series: refractive index (RI), right angle laser light scattering (RALLS), and viscometer (VP). The ViscoGEL™ HR-Series (7.8 mm x 30 cm) column packed with divinylbenzene crosslinked polystyrene (SDVB) was maintained at 25 °C in a column oven. The eluting solvent was HPLC grade toluene at a flow rate of 1.0 mL/min. The detectors were calibrated with a polystyrene (PS) narrow standard with the following parameters: MW (66K), polydispersity (1.03), intrinsic viscosity (0.845 dL/g), and dn/dc (0.112 mL/g). Data analysis was performed with Viscotek OmniSec software (Version 4.0).

Thermal Gravimetric Analysis (TGA). The thermal stabilities of neat liquid samples (~10 mg) in Pt pans were evaluated with a TA Instruments Q50 under N_2 or air at a flow rate of 40 cc/min. The sample weight was recorded while the temperature was increased 4 ˚C/min from 25 to 800 ˚C.

Film Characterization

Thermal Gravimetric Analysis (TGA). Thermal analyses of free-standing pieces of films (~10 mg) were similarly measured as described above.

Soxhlet Extraction. The amount of uncrosslinked material in a film was determined by Soxhlet extraction. A film cured on a microscope slide was extracted with CH_2Cl_2 in a Soxhlet apparatus for 12 h. The percentage of uncrosslinked material was calculated as the weight difference of the extracted versus unextracted weight divided by the unextracted weight.

Dynamic Mechanical Analysis (DMA). Storage (G') and loss (G") moduli of cured films were measured as a function of temperature on a TA Instruments Q800 dynamic mechanical analyzer. Specimens (length x width = 35 x 5.3 mm) were cut from free-standing films using a clean single-edged razor cutting tool. Electronic calipers were used to measure film thickness (~ 0.5 mm) prior to testing. The DMA was operated using a dual cantilever clamp assembly at a frequency of 5 Hz and a displacement of 4 μm. After equilibration at -140 °C for 3 min, the temperature was increased 4 ˚C/min to 25 ˚C. The T_g was determined from the peak maximum of the measured G".

Contact Angle Measurement. Static (θ_{static}), advancing (θ_{adv}), and receding (θ_{rec}) contact angles of distilled/deionized water droplets at the film-air interface were measured at room temperature (RT) with a CAM-200 (KSV Instruments) contact angle measurement system equipped with an autodispenser, video camera, and drop-shape analysis software. Coated microscope slides were stored in a dessicator for 5 days prior to contact angle measurements. For θ_{static} measurements, a sessile drop of water (5 μL) was measured at 15 sec and 2 min after deposition onto the film surface. The θ_{adv} was measured by the addition of 3 μL (0.25 μL/sec) of water to a 5 μL pendant droplet to advance the contact line. θ_{rec} was measured by the subsequent removal of 4 μL (0.25 μL/sec) from the same droplet to recede the contact line. The reported θ_{static}, θ_{adv}, and θ_{rec} values are an average of three measurements taken on different areas of the same film sample.

Adsorption of BSA Protein. The adhesion of Alexa Fluor 555 dye conjugate of bovine serum albumin (AF-555 BSA; MW = 66 kDa; Molecular Probes, Inc.) onto film surfaces was studied by fluorescence microscopy. To remove residual acid catalyst from the films, all coated microscope slides were first leached in distilled water for 24 h with fresh water changes every 6 h until the pH of the water remained at ~7.2. Coated microscope slides were subsequently dried *in vacuo* (36 in. Hg, 24 h, RT) and stored in a dessicator for 2 days prior to testing. A silicone isolator (20 mm well diameter, 2.5 mm well depth; JTR Press-to-Seal Silicone Isolators) was affixed to each coated microscope slide with clips to prevent leakage of solutions from the well. For each film composition, 2 coated microscopes slides were analyzed. One slide served to test a film surface

exposed to air prior to AF-555 BSA deposition whereas the other served to test a film surface which was first exposed to phosphate buffered saline (PBS, pH = 7.4) for 12 h.

Air Equilibrated Films. The exposed surface of the film inside each isolator well was filled with 1 mL of AF-555 BSA solution (0.1 mg/mL in PBS), equilibrated in the dark at RT for 3 h, and removed. One mL of fresh PBS was then added to each well and removed after 5 min; this process was repeated a total of 3 times. Film surfaces tested in this way are referred to as "air-equilibrated."

PBS Equilibrated Films. On the second set of coated microscope slides, the exposed surface of the film inside each isolator was filled with 1 mL of PBS and removed after 12 h. Exposure to AF-555 BSA solution (3 h) was immediately executed using the same protocol as above. Film surfaces tested in this manner are referred to as "PBS-equilibrated."

A Zeiss Axiovert 200 optical microscope equipped with a A-Plan 5x objective, Axiocam HRC Rev. 2), and filter cube (excitation filter of 546 ± 12 nm [band pass] and emission filter 575-640 nm [band pass]) was used to obtain fluorescent images on 3 randomly selected regions of the surface within each isolator well. The fluorescent light source was permitted to warm up for 30 min prior to image capture. Linear operation of the camera was ensured and constant exposure time used during the image collection to permit quantitative analyses of the observed fluorescent signals. The fluorescence microscopy images were analyzed using the histogram function of PhotoShop, which yielded the mean and standard deviation of the fluorescence intensity within a given image. The fluorescence intensity of each AF-555 BSA exposed region

was subtracted from that of non-exposed region to ensure correction for of any fluorescence signal from the material itself. The background-corrected fluorescence intensities for each film were then used to quantify AF-555 BSA levels adsorbed by comparison against a calibration curve constructed from the measured fluorescence intensities of AF-555 BSA standard slides. Standard slides were prepared by fitting a silicone isolator to uncoated, solvent-cleaned glass slides and adding 1 mL of AF-555 BSA solutions of known concentrations (0, 0.005, 0.01, 0.02, 0.04 mg/mL AF-555 BSA in PBS) to individual wells.

X-ray Photoelectron Spectroscopy (XPS). XPS was used to confirm the chemical grafting of $(EtO)_3Si\text{-}(CH_2)_3\text{-}(OCH_2CH_2)_8\text{-}OCH_3$ onto glass microscope slides which served as the "PEO control". The surface was analyzed using a KRATOS AXIS Ultra Imaging X-Ray Photoelectron Spectrometer with MgK_α non-monochromatic X-ray source. The spot size was 7 x 3 mm. The survey scan (0 to 1100 eV) and C1s high-resolution scan (20 eV scan width) were performed with a take-off angle of 90°. Binding energies were referenced to the C-C peak at 285 eV. The raw data was analyzed using XPS Peak Processing Software.

2.4 Materials

$RhCl(Ph_3P)_3$ (Wilkinson's catalyst) and solvents were obtained from Aldrich. HPLC grade toluene and NMR grade $CDCl_3$ were dried over 4Å molecular sieves. Silastic T-2 (silicone elastomer) was obtained from Dow Corning. Pt-divinyltetra-methyldisiloxane complex (Karstedt's catalyst), triethoxysilane, vinyltriethoxysilane

(**VTEOS**), α,ω-bis(Si-H)oligodimethylsiloxanes (**$ODMS_0$** or tetramethyldisiloxane; **$ODMS_4$**, MW = 400-500 g/mol per manufacturer's specifications; **$ODMS_{13}$**, MW = 1000-1100 g/mol per manufacturer's specifications), α,ω-bis-(Si-OH)polydimethyl-siloxane (**P,** MW = 2000-3500 g/mol per manufacturer's specifications), and monovinyl terminated PDMS (**CH_2=CH-PDMS-*n*Bu**, MW = 62,700 g/mol, essentially 100% monovinyl terminated with the non-functional end *n*-butyl terminated per manufacturer's specifications) were acquired from Gelest. The number average molecular weight (M_n) of **$ODMS_0$**, **$ODMS_4$**, and **$ODMS_{13}$** were determined by ^{1}H NMR end-group analysis: **$ODMS_0$** (134 g/mol), **$ODMS_4$** (430 g/mol), and **$ODMS_{13}$** (1096 g/mol). The MWs of **P** was determined by GPC (M_w/M_n = 5000/3000 g/mol). PEO allyl methyl ether (**A-PEO_8M**) was obtained from Clariant (Polyglykol AM-500) and was dried overnight under high vacuum prior to use. The M_n of **A-PEO_8M** was determined to be 425 g/mol (n = 8) by end group analysis.

2.5 Synthetic Approach

All reactions were run under a N_2 atmosphere with a Teflon-covered stir bar to agitate the reaction mixture.

α-Triethoxysilylethyl-ω-silane-oligodimethylsiloxanes$_n$ (**1-3**) were prepared by the Rh-catalyzed regioselective hydrosilylation of equimolar amounts of **VTEOS** with **$ODMS_0$**, **$ODMS_4$**, or **$ODMS_{13}$**, respectively (Fig. 2.1). **$ODMS_n$** and **VTEOS** (1:1 molar ratio) were combined with Wilkinson's catalyst and toluene into a 350 mL pressure vessel and equipped with a Teflon bushing as a pressure seal. The tube was sealed and

heated to 80 °C. After 6 h, the reaction was cooled to RT and toluene removed under reduced pressure. The residue was purified by flash column chromatography on silica gel with hexanes/ethyl acetate (2/1 v/v) and volatiles removed under reduced pressure.

Triethoxysilylethyl-oligodimethylsiloxane$_n$-*block*-poly(ethylene oxide)$_8$ **(a-c)** were prepared by the Pt-catalyzed hydrosilylation of **A-PEO$_8$M** with **1**, **2**, or **3**, respectively (Fig. 2.1). **1-3** were each combined with **A-PEO$_8$M** (1:1 molar ratio) and toluene in a round-bottom (rb) flask equipped with a rubber septum and heated to 70 °C. The progress of the reaction was monitored with IR spectroscopy by the disappearance of the Si-H (~2125 cm^{-1}) absorbance. After an initial reaction time of ~12 h, an aliquot of the reaction solution was evaporated on a NaCl plate and the IR spectrum obtained. In case of an incomplete reaction, additional Karstedt's catalyst (50% of original volume) was added and the reaction continued for another ~6 h before checking the IR spectrum. This cycle was repeated until no Si-H absorbance was observed in the IR spectrum. Typically, no additional Kartstedt's catalyst was required to complete the reaction. The catalyst was removed from the reaction mixture by refluxing the reaction mixture with activated charcoal for 12 h. After filtration, the volatiles were removed under reduced pressure so that **a-c** were isolated as colorless liquids.

Synthesis of (1)

ODMS$_0$ (20.0 g, 0.15 mol), **VTEOS** (28.4 g, 0.15 mol), and Wilkinson's catalyst (10 mg) in toluene (100 mL) were reacted as above. In this way, **1** (43.4 g, 89% yield) was obtained. ^{1}H NMR (δ, ppm): 0.001-0.02 (m, 6H, SiC*H*$_3$), 0.06-0.12 (m, 6H, SiC*H*$_3$),

0.50 (m, 3H, SiCH_2CH_2), 1.03 (m, 1H, SiCH_2CH_2), 1.18 (m, 9H, SiOCH$_2$CH_3), 3.77 (m, 6H, SiOCH_2CH$_3$), 4.64 (m, 1H, Si*H*). ^{13}C NMR (δ, ppm): -0.44, 1.17, 2.03, 9.30, 9.50, 18.60, 58.62. IR (ν): 2125 (Si-H) cm^{-1}.

Synthesis of (2)

ODMS$_4$ (20.05 g, 0.05 mol), **VTEOS** (8.46 g, 0.05 mol), and Wilkinson's catalyst (10 mg) in toluene (60 mL) were reacted as above. In this way, **2** (28.0 g, 90% yield) was obtained. ^{1}H NMR (δ, ppm): 0.001-0.15 (m, 36H, SiCH_3), 0.52 (m, 3H, SiCH_2CH_2), 1.04 (m, 1H, SiCH_2CH_2), 1.18 (m, 9H, SiOCH$_2$CH_3), 3.77 (m, 6H, SiOCH_2CH$_3$), 4.66 (m, 1H, Si*H*). ^{13}C NMR (δ, ppm): -0.25, 1.02, 1.19, 1.36, 1.51, 2.13, 9.45, 18.67, 58.70. IR (ν): 2125 (Si-H) cm^{-1}.

Synthesis of (3)

ODMS$_{13}$ (20.1 g, 0.02 mol), **VTEOS** (3.5 g, 0.02 mol), and Wilkinson's catalyst (10 mg) in toluene (50 mL) were reacted as above. In this way, **3** (23.2 g, 90% yield) was obtained. ^{1}H NMR (δ, ppm): 0.001-0.17 (m, 78H, SiCH_3), 0.53 (m, 3H, SiCH_2CH_2), 1.05 (m, 1H, SiCH_2CH_2), 1.19 (m, 9H, SiOCH$_2$CH_3), 3.78 (m, 6H, SiOCH_2CH$_3$), 4.68 (m, 1H, Si*H*). ^{13}C NMR (δ, ppm): -0.31, 0.97, 1.13, 1.33, 1.45, 2.08, 9.40, 18.61, 58.67. IR (ν): 2125 (Si-H) cm^{-1}.

Synthesis of (a)

1 (5.1 g, 0.016 mmol), **A-PEO$_8$M** (6.7 g, 0.016 mol), and Karstedt's catalyst (50 μL) in toluene (60 mL) were reacted as above. In this way, **a** (10.6 g, 88% yield) was obtained. ^{1}H NMR (δ, ppm): -0.07 to -0.06 (m, 12H, SiC*H*$_3$), 0.002 (m, 2H, SiC*H*$_2$CH$_2$CH$_2$), 0.43 (m, 3H, SiC*H*$_2$C*H*$_2$), 0.96 (m, 1H, SiC*H*$_2$C*H*$_2$), 1.12 (m, 9H, SiOCH$_2$C*H*$_3$), 1.47 (m, 2H, SiCH$_2$C*H*$_2$CH$_2$), 3.27 (s, 3H, OC*H*$_3$), 3.44 (m, 2H, SiCH$_2$CH$_2$C*H*$_2$), 3.54 (m, 32H, OC*H*$_2$C*H*$_2$), 3.71 (m, 6H, SiOC*H*$_2$CH$_3$). ^{13}C NMR (δ, ppm): -0.39, 0.29, 1.81, 9.21, 14.24, 18.33, 23.44, 58.31, 58.99, 70.03, 70.53-70.63, 71.95, 74.21.IR (ν): no Si-H band.

Synthesis of (b)

2 (5.24 g, 0.008 mol), **A-PEO$_8$M** (3.48 g, 0.008 mmol), and Karstedt's catalyst (50 μL) in dry toluene (45 mL) were reacted as above. In this way, **b** (7.8 g, 91% yield) was obtained. ^{1}H NMR (δ, ppm): -0.02 to 0.01 (m, 36H, SiC*H*$_3$), 0.07 (m, 2H, SiC*H*$_2$CH$_2$CH$_2$), 0.50 (m, 3H, SiC*H*$_2$C*H*$_2$), 1.03 (m, 1H, SiC*H*$_2$C*H*$_2$), 1.16 (m, 9H, SiOCH$_2$C*H*$_3$), 1.53 (m, 2H, SiCH$_2$C*H*$_2$CH$_2$), 3.32 (s, 3H, OC*H*$_3$), 3.47 (m, 2H, SiCH$_2$CH$_2$C*H*$_2$), 3.56 (m, 32H, OC*H*$_2$C*H*$_2$), 3.73 (m, 6H, SiOC*H*$_2$CH$_3$). ^{13}C NMR (δ, ppm): -0.48, 0.21, 1.17, 1.28, 1.87, 9.19, 14.19, 18.43, 23.46, 58.45, 59.13, 70.12, 70.64-70.73, 72.05, 74.33. IR (ν): no Si-H band.

Synthesis of (c)

3 (10.37, 0.008 mol), **A-PEO$_8$M** (3.42, 0.008 mol), and Karstedt's catalyst (50 μL) in toluene (50 mL) were reacted as above. In this way, **c** (12.1 g, 88% yield) was obtained. ^{1}H NMR (δ, ppm): -0.002 to 0.05 (m, 90H, SiC*H*$_3$), 0.09 (m, 2H, SiC*H*$_2$CH$_2$CH$_2$), 0.51 (m, 3H, SiC*H*$_2$C*H*$_2$), 1.05 (m, 1H, SiC*H*$_2$C*H*$_2$), 1.18 (m, 9H, SiOCH$_2$C*H*$_3$), 1.55 (m, 2H, SiCH$_2$C*H*$_2$CH$_2$), 3.34 (s, 3H, OC*H*$_3$), 3.52 (m, 2H, SiCH$_2$CH$_2$C*H*$_2$), 3.60 (m, 32H, OC*H*$_2$C*H*$_2$), 3.78 (m, 6H, SiOC*H*$_2$CH$_3$). ^{13}C NMR (δ, ppm): -0.45, 0.25, 1.21, 1.31, 1.92, 9.24, 14.24, 18.47, 23.51, 58.49, 59.16, 70.17, 70.69-70.79, 72.10, 74.38. IR (ν): no Si-H band.

Synthesis of (EtO)$_3$Si-(CH$_2$)$_3$-(CH$_2$CH$_2$O)$_8$-OCH$_3$

Triethoxysilane (3.07 g, 0.019 mol), **A-PEO$_8$M** (7.94 g, 0.019 mol), and Karstedt's catalyst (50 μL) in toluene (25 mL) were reacted as above to produce triethoxysilylpropyl PEO monomethyl ether (EtO)$_3$Si-(CH$_2$)$_3$-(OCH$_2$CH$_2$)$_8$-OCH$_3$ (9.3 g, 83 % yield).[67] ^{1}H NMR (δ, ppm): 0.59 (m, 2H, SiC*H*$_2$CH$_2$CH$_2$), 1.18 (m, 9H, SiOCH$_2$C*H*$_3$), 1.61 (m, 2H, SiCH$_2$C*H*$_2$CH$_2$), 3.34 (m, 3H, OC*H*$_3$), 3.40 (m, 2H, SiCH$_2$CH$_2$C*H*$_2$), 3.61 (m, 32H, OC*H*$_2$C*H*$_2$), 3.78 (m, 6H, SiOC*H*$_2$CH$_3$). IR (ν): no Si-H band.

Synthesis of (y)

ODMS$_{13}$ (3.06 g, 0.0028 mol), **VTEOS** (1.06 g, 0.0056 mol), and Karstedt's catalyst (50 μL) were combined in toluene in a round-bottom (rb) flask equipped with a

rubber septum and heated to 70 °C for 12 h. The catalyst was removed by refluxing the reaction mixture with activated charcoal for 12 h. The reaction mixture was filtered and the volatiles were removed. In this way, **y** (3.78 g, 91% yield) was obtained.

Synthesis of (z)

$ODMS_{13}$ (0.0215 g, 0.02 mmol), **CH_2=CH-PDMS-*n*Bu** (2.29 g, 0.04 mmol) and Karstedt's catalyst (50 µL) in toluene (50 mL) were reacted as above. In this way, **z** (2.27 g, 93% yield) was obtained.

2.6 Film Preparation

In a scintillation vial equipped with a Teflon-covered stir bar and cap, **a-c** were each combined with α,ω-bis(Si-OH)polydimethylsiloxane (**P**, M_n =3000 g/mol) in varying molar ratios (1:1, 1:2, and 2:3 molar ratio **a**, **b**, or **c** to **P**) and mixed for ~5 min (Table 2.1). Next, 3 mol% of H_3PO_4 (based on total solid weight of the aforementioned mixtures) was added as solution of H_3PO_4/EtOH (10/90 w/w) and the mixture rapidly stirred for 3 h.

Microscope slides (75 x 25 x 1 mm) were sequentially washed with distilled water, CH_2Cl_2/hexane (1/1 v/v), acetone, and finally dried in a 150 °C oven for 24 h prior to use. One mL of each of the aforementioned mixtures was applied to a microscope slide and allowed to level across and coat the entire slide. The slide was then placed in a level 150 °C oven for 24 h. Free-standing films for DMA and TGA testing were obtained by removing films from slides with a clean single-edge razor blade.

Coated microscope slides were used for contact angle measurements and protein adsorption studies.

Table 2.1. Film compositions and percentage weight loss after soxhlet extraction.

film	**a, b,** or **c** (value of *n)*	moles of **a**, **b**, or **c**	moles of **P** (HOSi-$PDMS_{40}$ -SiOH)	% wt loss[a]
a_1P_1	**a** (n = 0)	1	1	1%
b_1P_1	**b** (n = 4)	1	1	3%
c_1P_1	**c** (n = 13)	1	1	2%
a_1P_2	**a** (n = 0)	1	2	9%
b_1P_2	**b** (n = 4)	1	2	8%
c_1P_2	**c** (n = 13)	1	2	4%
a_2P_3	**a** (n = 0)	2	3	0.5%
b_2P_3	**b** (n = 4)	2	3	1%
c_2P_3	**c** (n = 13)	2	3	0.5%

[a]After soxhlet extraction (CH_2CH_2, 12 h), corresponds to percentage of uncrosslinked material. 1:1 molar ratio of **a-c** to **P**, stoichiometric excess of **a-c**; 1:2 molar ratio of **a-c** to **P**, stoichiometric excess of **P**; 2:3 molar ratio of **a-c** to **P**, stoichiometric balance.

Microscope slides (75 x 25 x 1 mm) were sequentially washed with distilled water, CH_2Cl_2/hexane (1/1 v/v), acetone, and finally dried in a 150 °C oven for 24 h prior to use. One mL of each of the aforementioned mixtures was applied to a microscope slide and allowed to level across and coat the entire slide. The slide was then placed in a level 150 °C oven for 24 h. Free-standing films for DMA and TGA testing were obtained by removing films from slides with a clean single-edge razor blade. Coated microscope slides were used for contact angle measurements and protein adsorption studies.

2.7 Preparation of PEO Control Surface

Triethoxysilylpropyl PEO monomethyl ether [$(EtO)_3Si$-$(CH_2)_3$-$(OCH_2CH_2)_8$-OCH_3] was chemically grafted onto microscopes slides with typical procedures.[85] Briefly, clean microscope slides were immersed in HCl (12 M):MeOH (1/1 v/v) for 2 h and then in HCl (12 M) for 2 h. The slides were rinsed thoroughly with DI water and dried under vacuum at 50 °C for 4 h. The glass slides were then immersed in a solution of $(EtO)_3Si$-$(CH_2)_3$-$(OCH_2CH_2)_8$-OCH_3: toluene (5/95 v/v) for 12 h at RT, removed and cured at 180 °C *in vacuo* (36 in. Hg) for 12 h. PEO-grafted microscope slides served as the "PEO control" for contact angle and protein adsorption studies.

2.8 Preparation of Silastic Control Surface

Silastic T-2 (silicone elastomer) was applied to clean microscope slides with a drawdown bar (30 mil) and allowed to cure at RT for over 72 h. The film thickness for cured Silastic T-2 films was ~0.6 mm. A silicone-coated slide served as a "PDMS control" for contact angle and protein adsorption studies.

2.9 Results and Discussion

Synthesis of 1-3

Rh-catalyzed regioselective hydrosilylation reaction of equimolar amounts of **VTEOS** with **$ODMS_0$**, **$ODMS_4$**, or **$ODMS_{13}$** effectively produced **1-3**, respectively, in good yields (≥ 89%) (Fig. 2.1). ^{1}H NMR spectra of **1-3** showed a reduction in the Si-H

peak integration value by one half compared to the starting material. A Si-H (~2125 cm^{-1}) absorbance was noted in the IR spectra of **1-3**.

Verification of the Composition of 1-3

For Rh-catalyzed regioselective hydrosilylation, the enhanced reactivity of one Si-H terminus of α,ω-bis(Si-H) terminated compounds towards vinyl-containing compounds is not well understood. However, the requirement for terminal Si-H groups within an appropriate distance has been suggested. For instance, the rate of regioselective hydrosilylation of bis(dimethylsilyl)alkanes is significantly reduced when the number of methylene units between Si-H groups is increased from 2 to 4.[86] In this study, we utilized α,ω-bis(Si-H)oligodimethylsiloxanes (**$ODMS_0$**, **$ODMS_4$**, and **$ODMS_{13}$**) having 2, 6, and 15 silicon atoms, respectively. Evidence that **1-3** are the pure monosubstituted products of regioselective hydrosilylation cannot be solely based on ^1H NMR analysis because each spectrum represents the average composition of the sample. In other words, a pure monosubstituted product (**1**, **2**, or **3**) would have the same ^1H NMR spectrum as the mixture of three products obtained from the corresponding non-regioselective hydrosilylation: **(i)** α-triethoxysilylethyl- monosubstituted product (**1**, **2**, or **3**), **(ii)** α,ω-triethoxysilylethyl- disubstituted product, and **(iii)** non-substituted product (**$ODMS_0$**, **$ODMS_4$**, or **$ODMS_{13}$**), where the ratio of disubstituted to non-substituted product would be equal (Fig. 2.2). Because **$ODMS_{13}$** is the highest MW α,ω-bis(Si-H)oligodimethylsiloxanes of the series, it is anticipated to most likely to undergo non-regioselective Rh-catalyzed hydrosilylation. Thus, we sought to confirm that **3** was

the pure monosubstituted product of regioselective hydrosilylation of **ODMS$_{13}$** and **VTEOS**. Following Rh-catalyzed hydrosilylation of **ODMS$_{13}$** and **VTEOS** (1:1 molar ratio), the product was reacted with **CH$_2$=CH-PDMS-*n*Bu** (M_w/M_n =83,000/60,000 g/mol) by Pt-catalyzed hydrosilylation such that all Si-H groups were consumed (confirmed by IR) thereby producing **M**. Identifying whether or not **M** was the product of exclusively **3 + CH$_2$=CH-PDMS-*n*Bu** was then determined by GPC. If the initial Rh-catalyzed hydrosilylation reaction was regioselective, the product would be pure, monosubstituted **3** (M_n = 1286 g/mol) which would subsequently react with **CH$_2$=CH-PDMS-*n*Bu** to form single product **(x)** (M_n = 61,286 g/mol). However, *non-regioselective* Rh-catalyzed hydrosilylation would have produced a mixture of **i-iii** which would each subsequently react with **CH$_2$=CH-PDMS-*n*Bu** to yield: **(x)** the product of monosubstituted **3** + **CH$_2$=CH-PDMS-*n*Bu** (M_n = 61,286 g/mol), **(y)** unreacted α,ω-triethoxysilylethyl- disubstituted product (M_n = 1476 g/mol), and **(z)** the product of **ODMS$_{13}$** + **CH$_2$=CH-PDMS-*n*Bu** (1:2 mol) (M_n ~ 121,096 g/mol), where **y** and **z** would be present in equal amounts. Products **y** and **z** were individually synthesized in isolated reactions so that their elution peaks could be identified in the GPC chromatograph of **M** if present. Product **y** was synthesized by Pt-catalyzed hydrosilylation of **ODMS$_{13}$** and **VTEOS** (1:2 molar ratio) whereas **z** was prepared by Pt-catalyzed hydrosilylation of **ODMS$_{13}$** and **CH$_2$=CH-PDMS-*n*Bu** (1:2 molar ratio). In the GPC chromatograph of **M**, the elution peak of **y** is definitively absent (Fig. 2.3). The elution peak of **z** would overlap with the elution peak of **M**, but must absent as well since **y** and **z** would be present in equal amounts. Thus, the composition of **M** may be

identified as that of **x** (i.e. the product of monosubstituted **3** + **CH_2=CH-PDMS-*n*Bu**). **$ODMS_{13}$** + **CH_2=CH-PDMS-*n*Bu** (1:2 mol) (M_n ~ 121,096 g/mol), where **y** and **z** would be present in equal amounts.

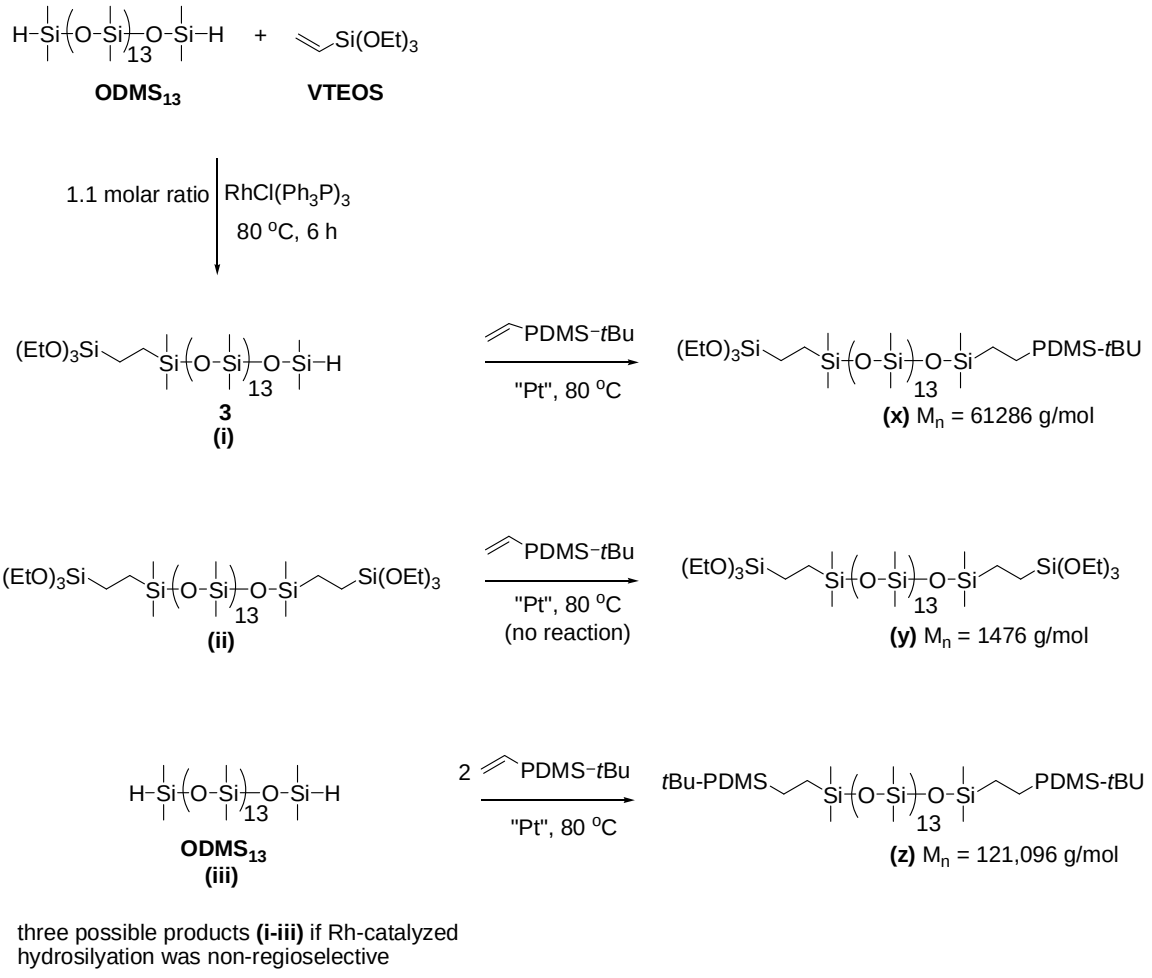

Figure 2.2. If Rh-catalyzed hydrosilylation of **$ODMS_{13}$** and **VTEOS** was non-regioselective, a mixture of 3 species **(i, ii,** and **iii)** would be obtained. Each of these would react with **CH_2=CH-PDMS-*n*Bu** (Mn =60,000 g/mol) via Pt-catalyzed hydrosilylation to produce **x**, **y**, and **z**, respectively. The product of Rh-catalyzed hydrosilylation of **$ODMS_{13}$** and **VTEOS** was subsequently reacted with **CH_2=CH-PDMS-*n*Bu** to produce **M**. The GPC chromatograph of **M** was compared to that of **y** and **z** (Figure 2.4). It was noted that **y** was absent in the GPC of **M**; thus, **z** could be inferred to be absent since **y** and **z** would be present in equal amounts. Thus, the composition of **M** may be identified as that of **x**. This confirms that the Rh-catalyzed hydrosilylation of **$ODMS_{13}$** and **VTEOS** was regioselective and produced only monosubstituted product **3**.

These results confirm that Rh-catalyzed hydrosilylation of reaction of **$ODMS_{13}$** and **VTEOS** was regioselective and produced only monosubstituted **3**. It is assumed that, because of their lower MWs, α,ω-bis(Si-H)oligodimethylsiloxanes **$ODMS_0$** and **$ODMS_4$** similarly underwent regioselective hydrosilylation to produce only monosubstituted **1** and **2**, respectively.The monosubstituted structure of **1-3** is also supported by results of the measured amount of uncrosslinked material in cured films (Table 2.1). If Rh-catalyzed hydrosilylation was non-regioselective and produced the mixture of products **(i-iii)**, **ii** (disubstituted) and **iii** (non-substituted) would be present in equal amounts (Fig. 2.3). Although **ii** would undergo sol-gel crosslinking with **P**, **iii** could not undergo crosslinking and thus would be removed as uncrosslinked material.

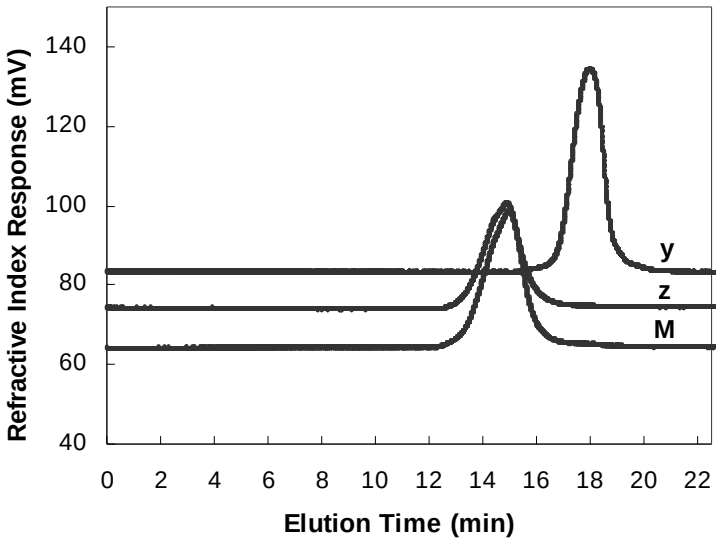

Figure 2.3. GPC chromatographs of **M**, **y**, and **z**. The absence of **y** (and hence **z**) confirms that **M** is the product of the monosubstituted **3** and **CH_2=CH-PDMS-*n*-Bu**.

For films prepared with a stoichiometric balance of $(EtO)_3Si$- **(a-c)** and Si-OH **(P)** (i.e. films $\mathbf{a_2P_3}$, $\mathbf{b_2P_3}$, and $\mathbf{c_2P_3}$), ≤ 1 wt% of uncrosslinked material was extracted. Thus, **ii** and **iii** are not present at greater than 1 wt% each. These results indicate that **1-3** are ≥ 98% monosubstituted.

Synthesis of a-c

Pt-catalyzed hydrosilyation reaction of a 1:1 molar ratio of **1-3** each with **A-PEO$_8$M** produced **a-c,** respectively, in good yields (≥ 88%). Completion of the reaction was confirmed by IR analysis of **a-c** which showed no absorbance at ~2125 cm^{-1} due to unreacted Si-H bonds of **1-3**, respectively. The Si-H peak (~4.7 ppm) of ^1H NMR spectra of **a-c** was also absent. No vinyl peaks were observed in the ^1H or ^{13}C NMR spectra.

Thermal Stability of a-c

As expected, **a-c** began to degrade at lower temperatures in air than in N_2 (Fig. 2.4). Polysiloxanes are known to display exceptional thermal stability compared to many organic polymers.[87] Thus, thermal stability in N_2 and air increased with increasing length of siloxane tether such that **c** was the most stable. Degradation of polysiloxanes in air produces silica residue.[87] Thus, residue weight was highest for **c** (~30 %) because of its relatively higher siloxane content.

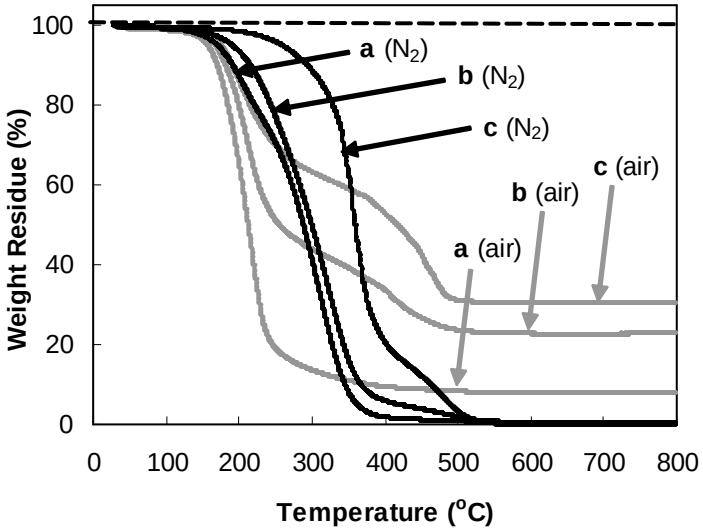

Figure 2.4. Thermal stability of **a-c** in N_2 and in air.

Preparation of Films

The H_3PO_4-catalyzed sol-gel crosslinking of **a-c** each with **P** in varying molar ratios (1:1, 1:2, and 2:3 molar ratio **a**, **b**, or **c** to **P**) produced a series of nine films (Fig. 2.1, Table 2.1). Commonly used tin-based catalysts (e.g. dibutyltin dilaurate) often require long cure schedules and residues may have adverse effects in medical applications.[88-90] H_3PO_4 is an attractive water-soluble catalyst alternative as it may be extracted from the final product. The rate of H_3PO_4-catalyzed sol-gel condensation involving $Si(OEt)_4$ was increased nearly two orders compared to other acids.[91] Gädda et al. reported the H_3PO_4-catalyzed crosslinking of α,ω-bis(Si-OH)polydimethylsiloxane and tetrakis(hydroxyldimethylsiloxane)silane.[84]

The extent of crosslinking was evaluated by Soxhlet extraction. Because there are three EtO- groups (**a-c**) versus two HO-Si groups (**P**) per respective chain, a 2:3

molar ratio of **a**, **b**, or **c** to **P** is stoichiometrically balanced. Thus, for films $\mathbf{a_2P_3}$, $\mathbf{b_2P_3}$, and $\mathbf{c_2P_3}$, ≤ 1 wt% of uncrosslinked material was removed following Soxhlet extraction (Table 2.1). Films prepared with a stoichiometric deficiency of **P** (films $\mathbf{a_1P_1}$, $\mathbf{b_1P_1}$, and $\mathbf{c_1P_1}$) or a stoichiometric excess of **P** ($\mathbf{a_1P_2}$, $\mathbf{b_1P_2}$, and $\mathbf{c_1P_2}$) demonstrated greater weight loss following Soxhlet extraction (1-9 wt%).

XPS of PEO Control

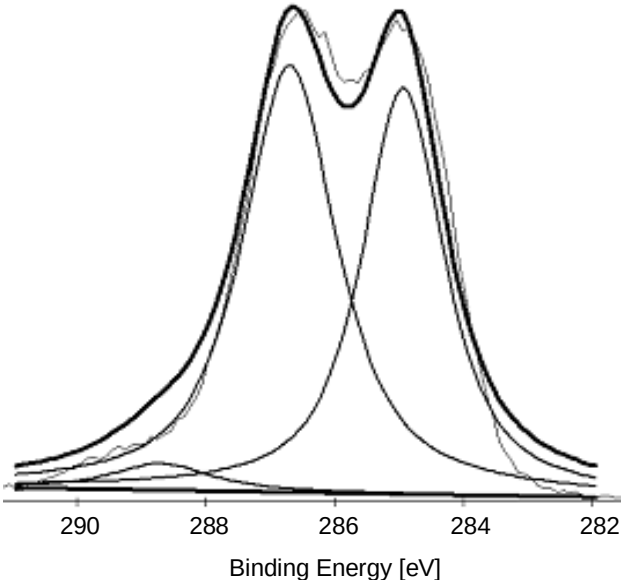

Figure 2.5. High-resolution C1s XPS spectrum of the surface of $(EtO)_3Si\text{-}(CH_2)_3\text{-}(OCH_2CH_2)_8\text{-}OCH_3$ grafted onto a glass microscope slide (i.e. PEO control). The observed C1s peak was fitted with three Gaussian peaks at binding energies of 285.0 eV (C-C), 286.7 eV (C-O), and 288.7 eV (CO_2 contamination). The peak at 286.7 eV is consistent with the ether carbons of the PEO.

The deconvoluted C 1s spectrum of the PEO control surface ($(EtO)_3Si\text{-}(CH_2)_3\text{-}(OCH_2CH_2)_8\text{-}OCH_3$) revealed three peaks: 285.0 eV (C-C), 286.7 eV (C-O), and 288.7 eV (adsorbed CO_2) (Fig. 2.5.). The peak at 286.7 eV is consistent with the ether carbons of PEO.[92]

Thermal Stability of Films

The thermal degradation of films is shown in Fig. 2.6. Films exhibited generally similar degradation profiles. In N_2, films were degraded by ~650 °C whereas in air, films reached their final weight by ~500 °C. In air, ~30-50% of silica residue was produced for all films and is within the expected range. A slight increase in thermal stability is indicated for films $\mathbf{a_2P_3}$, $\mathbf{b_2P_3}$, and $\mathbf{c_2P_3}$ which have the least amount of uncrosslinked material. Acids are known to catalyze chain equilibration of siloxane (Si-O) bonds into low MW cyclics which are volatile at elevated temperatures.[87] However the high thermal stabilities and residue weights (in air) of the films indicate that the presence of catalytic amounts of phosphoric acid do not contribute to the reduction in their thermal stability.

Dynamic Mechanical Analysis

The mechanical properties of the films determined by DMA are summarized in Table 2.2. Each film was cut from the microscope slide and used with typical thickness values ~0.6 mm. The T_g of each film was determined by the maximum of the loss modulus (G").[93] T_gs were generally low for all films and ranged between -117 to -114 °C. Although the films were prepared by sol-gel crosslinking, there was no significant change in the T_g values. There were small amounts of uncrosslinked material that did not alter the T_g values.

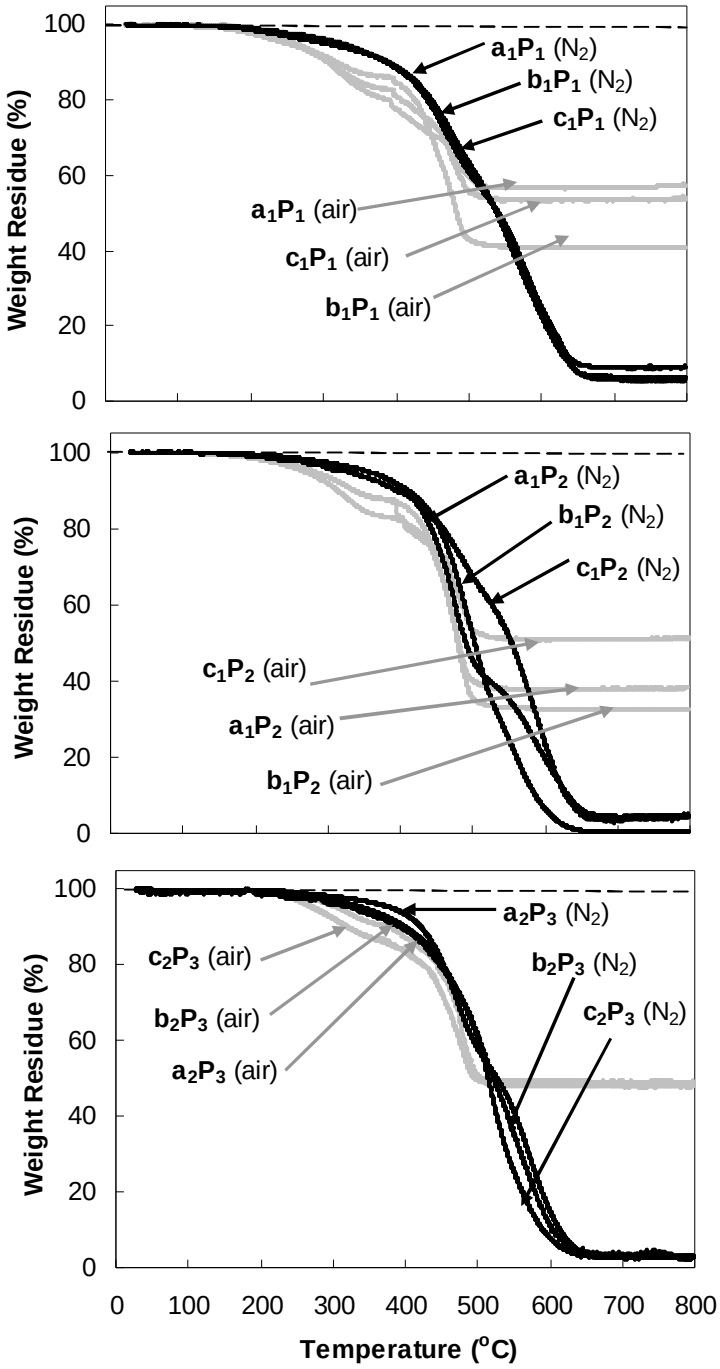

Figure 2.6. Thermal stability of films in N_2 and in air.

Table 2.2. Mechanical and surface properties of films.

Film	DMA	static contact angles		dynamic contact angles	
	T_g (°C)	θ_{static} (°) at 15 sec	θ_{static} (°) at 120 sec	θ_{adv} (°)	θ_{rec} (°)
$\mathbf{a_1P_1}$	-117	93±2	77±3	93±1	85±1
$\mathbf{b_1P_1}$	-116	87±2	71±2	87±1	78±1
$\mathbf{c_1P_1}$	-116	78±1	64±1	89±1	78±1
$\mathbf{a_1P_2}$	-116	96±1	71±1	97±1	81±2
$\mathbf{b_1P_2}$	-116	90±1	62±1	89±1	77±1
$\mathbf{c_1P_2}$	-117	74±2	66±1	94±1	77±2
$\mathbf{a_2P_3}$	-115	97±2	78±1	102±1	86±1
$\mathbf{b_2P_3}$	-114	89±1	63±2	84±1	70±1
$\mathbf{c_2P_3}$	-114	74±2	61±2	81±1	70±1
PEO[*]	--	116±1	115±1	121±1	115±1
PDMS[**]	--	62±6	53±4	61±1	61±1

[a] **PDMS** (control)) Silastic T-2 (silicone elastomer) cured on a glass microscope slide. [b] **PEO** (control) $(EtO)_3Si\text{-}(CH_2)_3\text{-}(OCH_2CH_2)_8\text{-}OCH_3$ grafted onto a glass microscope slide.

Similar T_g values were expected since the distance between crosslinks is maintained at a constant value by the MW of **P**. The presence of small amounts of uncrosslinked **a-c** (films $\mathbf{a_1P_1}$, $\mathbf{b_1P_1}$, and $\mathbf{c_1P_1}$) or **P** (films $\mathbf{a_1P_2}$, $\mathbf{b_1P_2}$, and $\mathbf{c_1P_2}$) did not significantly alter T_g values. Following crosslinking, the PEO segment of **a-c** exists as a "dangling free end". However, due to the low crosslink density of the films, the beta transition temperature (T_β) associated with such free ends is not observed nor is a decrease in T_g with increased siloxane tether length.[93] Lower MW analogues of **P** may be utilized to prepare more densely crosslinked films with higher T_gs which may reveal the aforementioned trends. The storage modulus (G') is related to stiffness or resistance to deformation. For films prepared with the same molar ratio of **a**, **b**, or **c** to **P**, G' increased with decreasing siloxane tether length in the order **c** < **b** < **a** (Fig. 2.7).

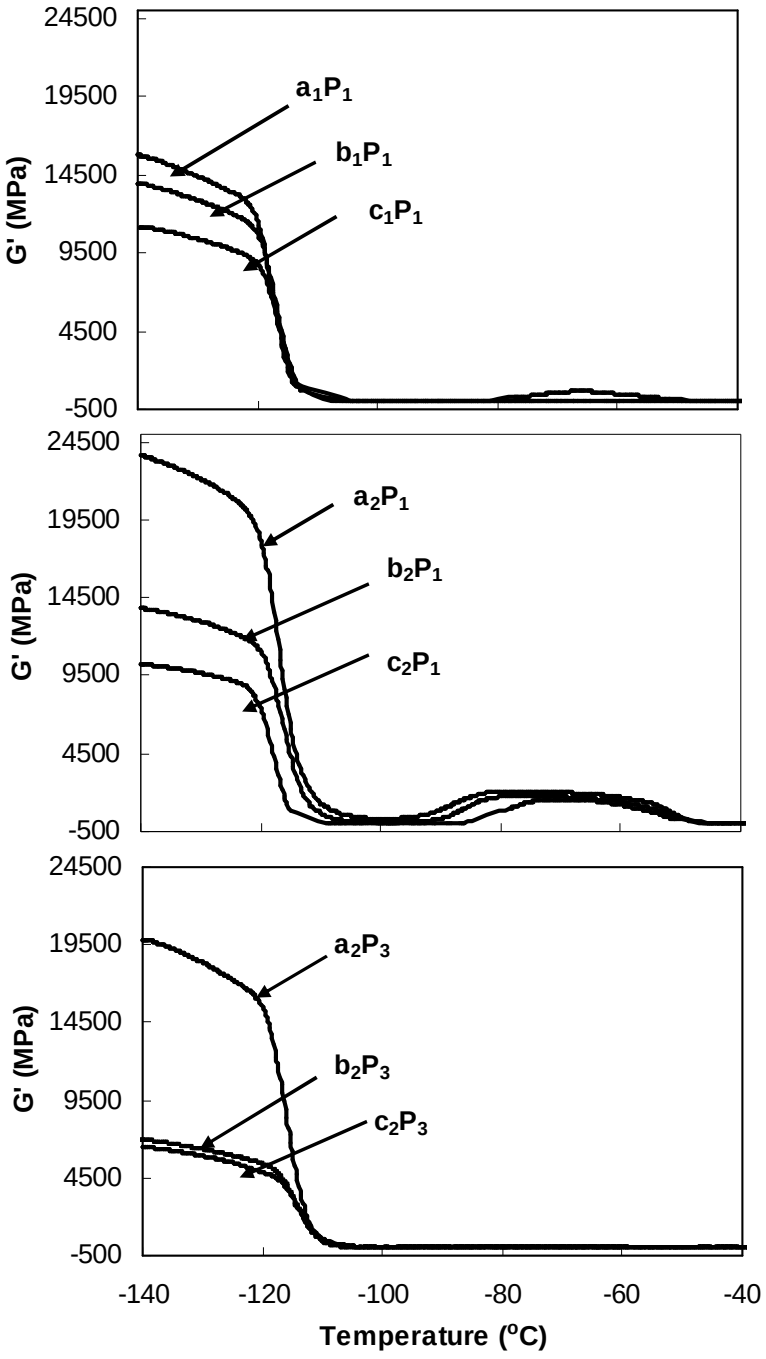

Figure 2.7. Storage moduli (G') of films.

Contact Angle Analysis

Contact angle measurements of water droplets on film surfaces are reported in Table 2.2. The hydrophobic PDMS control produced a high θ_{static} (at 15 sec) (116 °) whereas the θ_{static} (at 15 sec) of the hydrophilic PEO control was low (62 °). For films prepared with the same molar ratio (**a-c** to **P**), θ_{static} (at 15 sec) decreased and surface hydrophilicity increased in the order **a** < **b** < **c**. Furthermore, θ_{static} (at 2 min) was significantly lower than the corresponding θ_{static} (at 15 sec) and hydrophilicity similarly increased in the order **a** < **b** < **c**. The exception to this trend was noted for film $\mathbf{c_1P_2}$ which displayed slightly higher θ_{static} values compared to $\mathbf{b_1P_2}$. Uncrosslinked material may have migrated to the film surface and altered surface properties. Films prepared with a 2:3 molar ratio (**a-c** to **P**) lack significant quantities of uncrosslinked material which may have migrated to the film surface. For these films, increased siloxane tether length **(a-c)** produced surfaces with enhanced hydrophilicity. Thus, longer siloxane tethers more effectively mobilized PEO segments to the surface (Fig. 2.8).

The hydrophobic surface characteristics are obtained from θ_{adv} whereas hydrophilicity is reflected by θ_{rec}.[94] For crosslinked silicones, the presence of Si-CH_3 groups at the film-air interface leads to high θ_{adv}. After a pure silicone surface is wetted, polar groups such as Si-O-Si reorganize to the film-water interface to minimize interfacial tension such that $\theta_{rec} < \theta_{adv}$. For all films, θ_{rec} was significantly reduced versus the corresponding θ_{adv} indicating that PEO reorganized to the surface after exposure to water.[95]

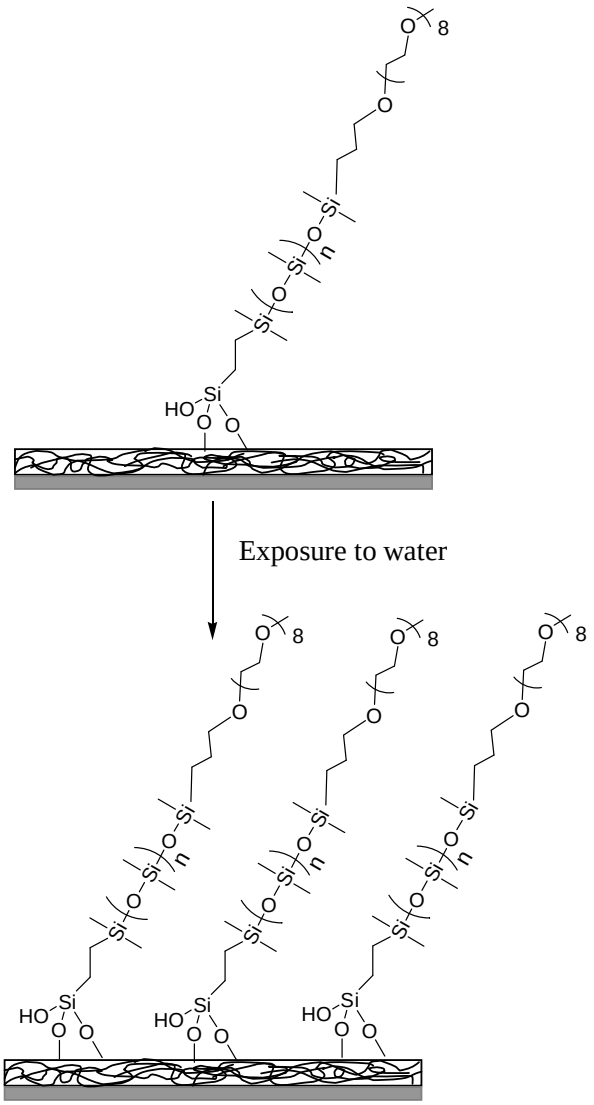

Figure 2.8. Following exposure to an aqueous environment, the PEO segments of **a-c** reorganized to the film-water interface thereby increasing surface hydrophilicity. Surface hydrophilicity increased as the siloxane tether length of **a-c** increased. Thus, longer siloxane tethers enhance reorganization of PEO segments to the surface.

As previously mentioned, surface compositions of films prepared with a 2:3 molar ratio (**a-c** to **P**) are not complicated by the presence of uncrosslinked materials at the surface. For these films, increased siloxane tether length **(a-c)** enhanced

hydrophilicity before and after exposure to an aqueous environment (i.e. lower θ_{adv} and θ_{rec}) in the order of **a** < **b** < **c**. These observations support the conclusion that longer siloxane tethers more effectively mobilize PEO to the surface particularly when exposed to aqueous environments (Fig. 2.8).

Protein Adsorption

The adsorption of BSA protein onto film surfaces and controls are reported in Fig. 2.9. For a given set of films prepared with the same molar ratio (**a-c** to **P**) statistical differences ($p < 0.05$) are noted within that series and compared to the PDMS and PEO controls. BSA adsorption onto the PEO control (air equilibrated) was unusually high possibly due to insufficient PEO hydration produced by the experimental protocol.[35] It was observed that films (air equilibrated) generally adsorbed less BSA compared to the PDMS control (air equilibrated). Films exhibited enhanced surface hydrophilicity compared to the PDMS control as was indicated by their lower θ_{adv} values (Table 2.2).

Thus, PEO is present at film surfaces prior to exposure to an aqueous environment which leads to reduced protein adsorption. There was not a statistical difference in the amount of BSA adsorbed onto film $\mathbf{a_2P_3}$ (air equilibrated) compared to the PDMS control. Its relatively high BSA adsorption may be attributed to the fact that this film was the most hydrophobic (θ_{adv} = 102 °).

For films prepared with 1:1 and 2:3 molar ratio (**a-c** to **P**), equilibration in PBS for 12 h just prior to exposure to BSA significantly reduced BSA adsorption compared to the PDMS control (PBS equilibrated) as well as the PEO control (PBS equilibrated).

These films exhibited lower θ_{static} (2 min) and θ_{rec} values compared to the PDMS control. Also, these values are much lower than the corresponding θ_{static} (15 sec) and θ_{adv} which indicates that additional PEO mobilized to the surface upon exposure to an aqueous environment (Fig. 2.9).

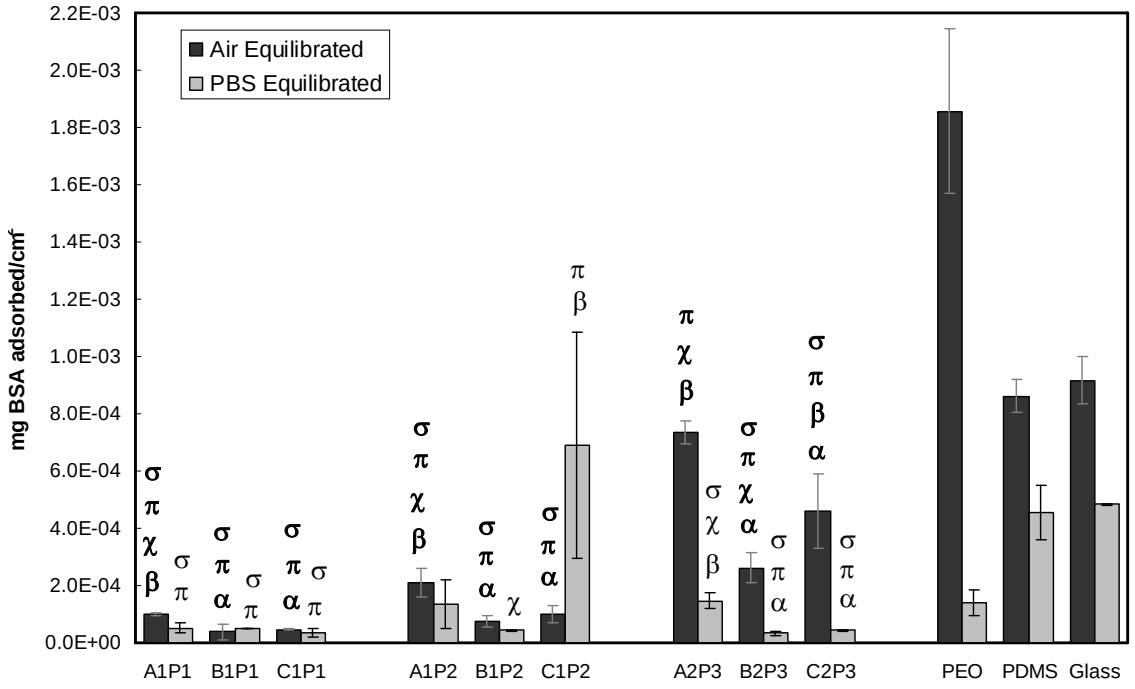

Figure 2.9. Adsorption of BSA protein (3 h) after film surfaces were exposed to air (air-equilibrated) and after first equilibrating in PBS for 12 h (PBS-equilibrated). Error bars represent the standard deviation between the fluorescence measurements of three randomly selected regions. For a set of films prepared at the same molar ratio (i.e., 1:1, 1:2, or 2:3 of **a**, **b**, or **c** to **P**) and with same type of exposure before BSA adsorption (e.g., air- or PBS-equilibrated), statistical significance was determined by one-way analysis of variance (Holm-Sidak method; p) 0.05). Symbol key: R) different than film prepared with **a**; *â*) different than film prepared with **b**; *ø*) different than film prepared with **c**; *ð*) different than PEO control; *ó*) different than PDMS control.

The enhancement of PEO to the surface improves protein repellency. Adsorption of BSA onto film $\mathbf{a_2P_3}$ (PBS equilibrated) versus the PEO control (PBS equilibrated) was not statistically different. It was the least hydrophilic of all films (θ_{rec} = 86 °).

Films prepared with a stoichiometric excess of **P** (1:2 molar ratio **a-c** to **P**; PBS equilibrated) demonstrated different BSA adsorption results. Film $\mathbf{c_1P_2}$ showed higher BSA adsorption after equilibration in PBS; this result was repeated in a second analysis. Also, films $\mathbf{a_1P_2}$ and $\mathbf{b_1P_2}$ (PBS equilibrated) did not adsorb statistically different amounts of BSA compared to the PDMS and PEO controls (PBS equilibrated). The presence of uncrosslinked **P** at these film surfaces may have contributed to these results.

The effect of siloxane tether **(a-c)** length on protein resistance may be evaluated with films prepared with a 2:3 molar ratio (**a-c** to **P**). Films $\mathbf{b_2P_3}$ and $\mathbf{c_2P_3}$ (PBS equilibrated) adsorbed less BSA compared to film $\mathbf{a_2P_3}$ (PBS equilibrated) as well as the PDMS and PEO controls. The amount of BSA adsorbed onto $\mathbf{b_2P_3}$ versus $\mathbf{c_2P_3}$ (PBS equilibrated) was not statistically different. Thus, increased siloxane tether length enhanced mobilization of PEO to the surface following exposure to an aqueous environment leading to improved protein resistance.

2.10 Conclusions

PEO chains were incorporated into silicones via siloxane tethers **(a-c)** of varying lengths to systematically increase PEO mobilization to the film surface and improve protein resistance. Three unique ambifunctional molecules **(a-c)** having the general formula α-$(EtO)_3Si(CH_2)_2$-oligodimethylsiloxane$_n$-*block*-poly(ethylene oxide)$_8$-OCH_3 [n = 0 **(a)**, 4, **(b)** and 13 **(c)**] were prepared via regioselective Rh-catalyzed hydrosilylation. H_3PO_4-catalyzed sol-gel crosslinking of **a-c** each with α,ω-bis(Si-OH)polydimethyl-siloxane (**P**, M_n = 3000 g/mol) in varying ratios (1:1, 1:2, and 2:3 molar ratio **a**, **b**, or **c** to

P) produced nine films. These films exhibited very low T_g and G' values as well as high thermal stability. The effect of siloxane tether length **(a-c)** on surface properties and protein resistance were readily assessed with films prepared with a 2:3 molar ratio (**a-c** to **P**) which are not complicated by the presence of uncrosslinked materials which may migrate to the film surface. For these films, increased length of siloxane tether **(a-c)** produced surfaces with increased hydrophilicity which was further enhanced upon exposure to an aqueous environment. Less BSA protein was adsorbed onto films $\mathbf{b_2P_3}$ and $\mathbf{c_2P_3}$ (PBS equilibrated) compared to film $\mathbf{a_2P_3}$ (PBS equilibrated) as well compared to the PDMS and PEO controls. Films $\mathbf{b_2P_3}$ and $\mathbf{c_2P_3}$ (PBS equilibrated) adsorbed statistically similar amounts of BSA. Thus, increased siloxane tether length of **a-c** enhanced protein resistance of silicone-based films by more effectively mobilizing PEO to the surface particularly after exposure to an aqueous environment.

CHAPTER III

THE INFLUENCE OF POLY(ETHYLENE OXIDE) GRAFTING VIA SILOXANE TETHERS ON PROTEIN ADSORPTION*

3.1 Overview

Amphiphilic PEO-silanes (**a-c**) having siloxane tethers of varying lengths with the general formula α-$(EtO)_3Si$-$(CH_2)_2$-oligodimethylsiloxane$_n$-*block*-poly(ethylene oxide)$_8$-OCH_3 [n = 0 **(a)**, n = 4 **(b)**, and n = 13 **(c)**] were grafted onto silicon wafers and resistance to adsorption of plasma proteins measured. Distancing the PEO segment from the hydrolyzable triethoxysilane [$(EtO)_3Si$] grafting group by a oligodimethylsiloxane tether represents a new method of grafting PEO chains to surfaces. Properties of surfaces grafted with **a-c** were compared to surfaces grafted with a traditional PEO-silane containing a propyl spacer [$(EtO)_3Si$-$(CH_2)_3$-poly(ethylene oxide)$_8$-OCH_3, **PEO control**]. As the siloxane tether length increased, chain density of PEO-silanes grafted onto oxidized silicon wafers decreased and hydrophobicity of the PEO-silane increased which led to a decrease in surface hydrophilicity. Despite decreased surface hydrophilicity, resistance to the adsorption of bovine serum albumin (BSA) increased in the order: **PEO control** < **a** < **b** ≈ **c** and to human fibrinogen (HF) increased in the order: **PEO control** < **a** < **b** < **c**.

---

*Reprinted with permission from "The influence of poly(ethylene oxide) grafting via siloxane tethers on protein adsorption " by Ranjini Murthy, Courtney E. Shell and Melissa A. Grunlan, 2009. *Biomaterials*, 30, 2433-2439, Copyright [2009] by Elsevier.
.

3.2 Introduction

Within minutes of exposure to blood, surfaces of implanted biomaterials adsorb plasma proteins which results in platelet adhesion and activation of coagulation pathways leading to thrombosis and compromising device success. [49, 96] Thus, it is desirable for blood-contacting materials to inhibit the adsorption of blood proteins. Among the polymeric biomaterials which have desirable bulk properties but inadequately resist adhesion of proteins are silicones (e.g. poly(dimethylsiloxane, PDMS), poly(ethylene terephthalate) (PET), polypropylene (PP) and polyethylene (PE). [3-6] Their lack of resistance to protein adsorption is attributed to their hydrophobicity as proteins preferentially adsorb onto hydrophobic, non-polar surfaces.[37, 69] In contrast, poly(ethylene oxide) (PEO; or poly(ethylene glycol) PEG) is a neutral, hydrophilic polymer with particularly high resistance to protein adhesion. [37, 54, 69, 97] The protein-repelling behavior of PEO is attributed to its hydrophilicity[35] as well as its high configurational mobility which leads to a large excluded volume,[36, 98] steric repulsion,[37, 69] blockage of underlying adsorption sites, [38] and an entropic penalty if protein adhesion were to occur. [7, 8, 10]

PEO has been immobilized onto polymer surfaces via self-assembly, [40, 99] physisorption, [42, 100] formation of surface physical interpenetrating networks (SPINs) [4, 43, 44] or by covalent grafting.[22-24] Graft chains can provide long-term chemical stability of new surface functionalities without altering bulk properties of the substrate.[101-103] Thus, covalent grafting of PEO onto activated surfaces is considered to be the most effective method to prepare stable PEO surfaces.[97] Surfaces of

hydrophobic polymers are hydrophilized upon covalent grafting of PEO thereby improving resistance to protein adsorption while maintaining bulk properties. For instance, epoxide and aldehyde end-functionalized PEO chains were covalently grafted onto functionalized PET surfaces [104] and PEO-silanes were grafted onto the surfaces of oxidized silicones. [65, 105]

Functional silanes (i.e. coupling agents) are typically used for the purpose of covalent grafting to achieve surface modification.[63] Silane coupling agents are generally trialkoxysilanes which undergo stepwise hydrolysis and condensation with a hydroxylated surface. For conventional PEO-silanes, the PEO segment is distanced from the alkoxysilane groups by a short alkane spacer (e.g. propyl as for $(RO)_3Si\text{-}(CH_2)_3\text{-}(CH_2CH_2O)_n\text{-}OCH_3$)).[62, 65-68, 106] We have recently reported the preparation of amphiphilic PEO-silanes (**a-c**) with flexible siloxane tethers of varying lengths having the general formula $\alpha\text{-}(EtO)_3Si\text{-}(CH_2)_2$-oligodimethylsiloxane$_n$-*block*-poly(ethylene oxide)$_8$-OCH_3 [n = 0 **(a)**, M_n = 749 g/mol; n = 4 **(b)**, M_n = 1044 g/mol; and n =13 **(c)** M_n = 1710 g/mol].[39] Thus, the PEO segment is distanced from the triethoxysilane group $[(EtO)_3Si]$ by an oligodimethylsiloxane tether. These siloxane tethers are highly flexible due to the wide bond angle (~143 °) and low barrier to linearization (0.3 kcal/mol) of Si-O-Si of dimethylsiloxanes.[75, 76] The dynamic flexibility of Si-O-Si produces polymers with extremely low glass transition temperatures (T_gs) (e.g. PDMS, T_g = -125 °C).

The aforementioned hydrophobic polymeric biomaterials may be oxidized to form a hydroxylated surface with an air or O_2 plasma treatment.[107] However, oxidized

polymeric surfaces, particularly silicones, are physically unstable and reorganize in different environments (e.g. air and water).[56]

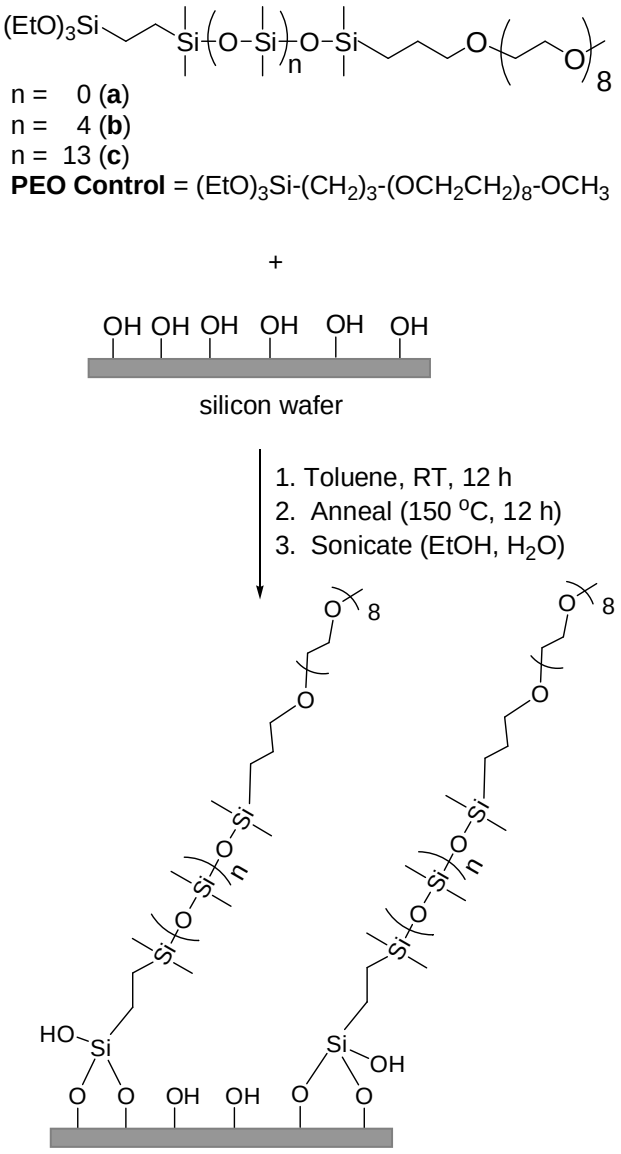

Figure 3.1. Grafting of PEO-silanes onto silicon wafer. Oxidized silicon wafers (SiOX) were exposed to toluene-based grafting solutions of **a-c** and **PEO control**.

Thus, PEO-silanes grafted onto hydroxylated polymer surfaces undergo significant physical reorganization depending on the environment which subsequently alters the surface concentration of PEO.[65] For this present work, we selected oxidized silicon wafer to serve as a model hydroxylated biomaterial surface.

Because a silicon wafer is physically stable, the surface concentration of covalently grafted PEO-silanes is conveniently maintained which allows the effect of PEO-silane structure to be evaluated. Thus, amphiphilic PEO-silanes **(a-c)** were grafted onto oxidized silicon wafers (Fig. 3.1). A conventional PEO-silane $(EtO)_3Si$-$(CH_2)_3$-poly(ethylene oxide)$_8$-OCH_3 (M_n = 588 g/mol) (no siloxane tether but the same PEO length) was grafted onto wafer to serve as the **PEO control**.

3.3 Experimental Section

Surface Characterization

Ellipsometry. Ellipsometry measurements were performed by null ellipsometry using a Nanofilm EP3SE Spectroscopic Imaging Ellipsometer, with an incident angle of 54° and at 532 nm. For grafted surfaces, the thickness values were determined using a three-layer air-(PEO-silane)-silicon model.[108] The index of refraction (n) of **PEO control** and **a-c** were assumed to be that of crystalline PEO (n = 1.450). Because PEO chains may be slightly hydrated, even under dry conditions, the true value is not precisely known. However, the index of refraction (n) of crystalline PEO is a good estimate commonly employed for ellipsometry measurements of PEO-grafted surfaces.[92, 109] The assumed value of n = 1.450 for **a-c** grafted films is reasonable

because the index of refraction of dimethylsiloxane tether component is considered to be that of PDMS (n = 1.406).[110, 111] Moreover, it has been shown that variation of 0.05 in the refractive index produces only a 0.1 nm change in thickness.[112] Data was collected in air at a temperature of 20 °C. Thickness values were calculated using the software provided by the manufacturer. From the obtained thickness values, we subtracted the average thickness of the underlying oxide layer to obtain a final thickness (h) of the grafted film (Table 3.1). The average thickness of the oxide layer was determined by ellipsometry measurements on three different regions of five individual wafers. The obtained average oxide layer thickness of 1.7 ± 0.2 nm is in agreement with literature values.[113]

XPS Spectroscopy. Surface composition analysis of PEO-silane grafted silicon wafers were performed using a KRATOS AXIS Ultra Imaging X-Ray Photoelectron Spectrometer with a monochromatised Mg K_α source and operating at a base pressure of ~2% 10^{-9} mbar. The spot size used in all analyses was 7 X 3 mm. Elemental atomic percent compositions were obtained from survey spectra, which were performed from 0 to 1100 eV. High-resolution analyses with pass energy of 40 eV were performed at a take-off angle of 90°. The binding energies were referenced to C 1s peak at 285.0 eV. The raw data was quantified and analyzed using XPS Peak Processing software.

Contact Angle Measurements. Static (θ_{static}), advancing (θ_{adv}), and receding (θ_{rec}) contact angles of distilled/DI water at the surface-air interface were measured at room temperature (RT) with a CAM-200 (KSV Instruments) contact angle measurement system equipped with an autodispenser, video camera, and drop-shape analysis software.

θ_{static} of a sessile drop of water (5 μL) was measured at 15 sec and 2 min after deposition onto the silicon surface. The θ_{adv} was measured by the addition of 3 μL (0.25 μL/sec) of water to a 5 μL pendant droplet to advance the contact line. θ_{rec} was measured by the subsequent removal of 4 μL (0.25 μL/sec) from the same droplet to recede the contact line. The reported θ_{static}, θ_{adv}, and θ_{rec} values are an average of three measurements taken on different areas of the same sample.

Protein Adsorption. Adsorption of bovine serum albumin (AF-555 BSA) and human fibrinogen (AF-546 HF) onto grafted surfaces was evaluated using a Zeiss Axiovert 200 optical microscope equipped with a A-Plan 5x objective, Axiocam (HRC Rev. 2), and filter cube (excitation filter of 546 ± 12 nm [band pass] and emission filter 575-640 nm [band pass]) to obtain fluorescent images on 3 randomly selected regions of the surface. A silicone isolator (20 mm well diameter, 2.5 mm well depth; JTR Press-to-Seal Silicone Isolators) was affixed with adhesive to prevent leakage of solutions from the well. Immediately prior to protein deposition, the wafers were thoroughly washed with phosphate buffered saline (PBS, pH = 7.4) and dried under a stream of N_2. The exposed surface inside each isolator well was filled with 1 mL of AF-555 BSA solution (0.1 mg/mL in PBS) or 1 mL of AF-546 HF solution (0.1 mg/mL in PBS), equilibrated in the dark at RT for 3 h, and removed. One mL of fresh PBS was then added to each well and removed after 5 min; this process was repeated a total of three times. The samples were then dried under a stream of N_2 and imaged. For all samples, the reported protein adsorption value is an average of three measurements taken on different areas of the same sample.

The fluorescent light source was permitted to warm up for 30 min prior to image capture. Linear operation of the camera was ensured and constant exposure time used during the image collection to permit quantitative analyses of the observed fluorescent signals. The fluorescence microscopy images were analyzed using the histogram function of PhotoShop, which yielded the mean and standard deviation of the fluorescence intensity of the whole image. The fluorescence intensity of each AF-555 BSA and AF-546 HF exposed region was subtracted from that of non-exposed region to ensure correction for any fluorescence signal from the material itself. The background-corrected fluorescence intensities for each film were then used to quantify AF-555 BSA and AF-546 HF levels adsorbed by comparison against a calibration curve constructed from the measured fluorescence intensities of AF-555 BSA and AF-546 HF standard samples. The obtained value was converted to mg/cm^2 by dividing by the area inside silicone isolator. Standard samples were prepared by fitting a silicone isolator to unmodified solvent-cleaned silicon wafers (not oxidized) and adding 1 mL of AF-555 BSA or 1 mL of AF-546 HF solutions of known concentrations (0, 0.005, 0.01, 0.02, 0.04 mg/mL AF-555 BSA or AF-546 HF in PBS) to individual wells.

3.4 Materials

Silicon wafers (111) were obtained from University Wafers, Inc. (Boston, MA). All solvents were obtained from Sigma-Aldrich (St. Louis, MO) and thoroughly dried over 4Å molecular sieves prior to use. Sulfuric acid (H_2SO_4) and hydrogen peroxide (H_2O_2) were obtained from Sigma-Aldrich and was used as received. Alexa Fluor 555-

dye conjugate of bovine serum albumin (AF-555 BSA; MW = 66 kDa; lyophilized powder; >96% BSA) and Alexa Fluor 546-dye conjugate of human fibrinogen (AF-546 HF; MW = 340 kDa; lyophilized powder; 95% clottable protein) were purchased from Molecular Probes, Inc. (Eugene, OR) and used as received. PEO-silanes **(a-c)** and **PEO control** were synthesized according to procedures previously reported [39]. Silastic T-2 (silicone elastomer) was obtained from Dow Corning (Midland, MI).

3.5 Grafting PEO-silanes onto Oxidized Silicon Wafers

Silicon wafers (1" X 1") were first ultrasonically cleaned in acetone (10 min) and washed with deionized (DI) water. Next, wafers were placed in a 7:3 (v/v) concentrated H_2SO_4/30% H_2O_2 (Piranha) solution for 30 min, thoroughly washed with DI water and dried under a stream of nitrogen (N_2). The resulting oxidized wafers (Si$_{OX}$) were then placed in a sealed jar containing the grafting solution comprised of the designated PEO-silane (**a-c** or **PEO control**) at a specified concentration in toluene, placed on a rocker table for 12 h, removed and annealed in a vacuum oven (36 mm Hg) at 150 ºC for 12 h.

To remove unbound PEO-silane, the wafers were subjected to sequential soaking (1 h), sonication (3 min), and rinsing with ethanol, the sequence repeated with DI water and lastly dried under a stream of N_2.

3.6 Preparation of Silastic Control Surface

Silastic T-2 (silicone elastomer) was applied to a solvent-cleaned microscope slide with a drawdown bar (30 mil) and allowed to cure at RT for over 72 h. The film

thickness for cured Silastic T-2 films was ~0.6 mm. A silicone-coated slide served as a hydrophobic "silicone control" for its well-known low resistance to protein adhesion.[47, 48] An oxidized wafer (Si^{OX}) served as a hydrophilic control.

3.7 Results and Discussion

Ellipsometry

PEO-silanes were grafted with different molar concentrations of grafting solutions. Several parameters were evaluated to characterize the grafted surfaces. The dry thickness of the graft layer (h) was used to estimate the chain density (σ) of PEO-silanes on the surface:[97, 114-116]

$$\sigma = \frac{h\rho N_A}{M_n}$$

where h is the grafted layer thickness measured by ellipsometry, ρ is the density of the dry grafted layer (i.e. the density of the PEO-silane), N_A is Avogadro's number and M_n is the number-average molecular weight of the PEO-silane.

Chain density is known to impart a particular conformation to an end-tethered polymer chain.[117] A random coil conformation (mushroom regime) occurs when grafting distance (D) is greater than $2R_f$ (the Flory radius; $D > 2R_f$) and a more extended conformation (brush regime) is observed when $D < 2R_f$.[108] The distance between grafting sites, D (nm), was calculated using the following equation:[115]

$$D = (4/\pi\sigma)^{1/2}$$

The Flory radius (R_f) for an unperturbed surface-anchored random polymer chain in a good solvent (e.g. PEO in water) can be calculated by the Flory eqn:[108, 118]

$$R_f = aN^{3/5}$$

where N is the degree of polymerization (i.e. number of monomers) and a is the length of one monomer, taken to be 0.35 nm for PEO.[119]

For all PEO-silanes (**a-c** and **PEO control**), N = 8 and $2R_f$ = 2.44 nm for the PEO segment. The chain density values (σ) for all surface-grafted layers correspond to those required for the onset of the brush regime (i.e. $D < 2R_f$) (Table 3.1). All chain densities are lower than the estimated upper limit of 5.8 chains/nm^2 for fully extended PEO chains.[108, 120]

For a given PEO-silane, increased grafting solution concentration generally produced increased chain density (σ) in the order: **c** < **b** < **a** < **PEO control**. However, the magnitude of this increase diminished as the siloxane tether length increased (Table 3.1). Thus, higher chain densities (σ) were obtained with the **PEO control** and **a** at lower grafting solution concentrations (0.005-0.02 M) than for **b** and **c** at higher grafting solution concentrations (0.012-0.075 M). To obtain surfaces with thickness values (h) similar to **PEO control** and **a** grafted surfaces, a minimum grafting solution concentration of 0.0120 M was required for grafting of **b** and **c** (Table 3.1).

The observed dependence of chain density (σ) on grafting solution concentration may be attributed to the M_n of the PEO-silane as well as its solubility in the grafting solvent (toluene). The observed decrease in chain density (σ) with increased M_n of PEO-silanes is attributed to the ability of higher molecular weight chains to more effectively

block grafting of subsequent chains. In other words, already grafted longer chains present a greater steric barrier to inhibit further grafting.[108, 121] Similarly, it has been observed that PEO chains which are in poor solubility conditions graft at higher chain densities due to their collapsed structure in the grafting solvent.[122] In this study, the solubility of the PEO-silanes increases with increased siloxane tether length since toluene is a good solvent for dimethysiloxane tether but a poor solvent for the PEO segment. Hence, **a** and **PEO control** are less soluble and are more collapsed than **b** and **c** which results in a somewhat higher chain density for the former.

Table 3.1. Ellipsometry data for grafted surfaces.

Surface (**a, b, c** or **PEO control)**	**Grafting Solution Molarity** [mol/L]	**Ellipsometry Thickness** h [nm]	**Surface Coverage** $\Gamma = h \times \rho$ [mg/m^2]	**Chain Density** $\sigma = (6.023\Gamma)/M_n$ [chains/nm^2]	**Graft Distance** $D = (4/\pi\sigma)^{1/2}$ [nm]
PEO control	**0.0050**	**3.75 ± 0.7**	**4.15**	**4.25**	**0.55**
PEO control	0.0075	4.37 ± 0.4	4.83	4.95	0.51
PEO control	0.0150	3.63 ± 0.1	4.01	4.11	0.56
PEO control	0.0200	3.55 ± 0.2	3.93	4.02	0.56
A	0.0050	1.79 ± 0.2	1.92	1.54	0.91
A	0.0075	2.15 ± 0.3	2.30	1.85	0.83
A	**0.0150**	**3.75 ± 1.0**	**4.02**	**3.23**	**0.63**
A	0.0200	2.41 ± 0.4	2.58	2.08	0.78
B	0.0120	2.08 ± 0.3	2.26	1.30	0.99
B	0.0240	3.17 ± 0.3	3.43	1.98	0.80
B	0.0480	3.42 ± 0.2	3.71	2.14	0.77
B	**0.0750**	**4.11 ± 0.2**	**4.45**	**2.57**	**0.70**
C	0.0120	3.22 ± 0.3	3.51	1.24	1.02
C	0.0240	3.32 ± 0.5	3.62	1.27	1.00
C	**0.0480**	**4.25 ± 0.3**	**4.63**	**1.63**	**0.88**
C	0.0750	3.06 ± 0.5	3.32	1.17	1.04

ρ = density (g/cm^3), M_n = number average molecular weight (g/mol). **PEO Control** = $(EtO)_3Si$-$(CH_2)_3$-$(OCH_2CH_2)_8$-OCH_3 (M_n = 588 g/mol; ρ = 1.16 cm^3); **a**: M_n = 749 g/mol; ρ = 1.07 g/cm^3; **b**: M_n = 1044 g/mol; ρ = 1.08 g/cm^3**;** and **c**: M_n = 1710 g/mol; ρ = 1.09 g/cm^3. Compositions in **boldface** were used in XPS, contact angle analysis and protein studies.

A series of PEO-silane grafted surfaces with similar thickness (h) and surface coverage (Γ) values were used to evaluate surface properties and protein adsorption (Table 3.1, compositions selected for XPS, contact angle analysis and protein studies in boldface). For these selected grafted surfaces, the PEO segments of all of the grafted chains (**a-c** and **PEO control**) were determined to be in the brush regime [D < 2Rf (where $2R_f$ = 2.44 nm)] and all chain densities are lower than the estimated upper limit of 5.8 chains/nm^2 for fully extended PEO chains. Thus, although chain density (σ) decreases somewhat with siloxane tether length, comparison of these grafted surfaces with similar h and Γ values and having brush conformations should provide insight into the effect of siloxane tether length on surface properties and resistance to protein adsorption.

X-Ray Photoelectron Spectroscopy

XPS was used to confirm successful grafting of PEO-silanes onto silicon wafers. The elemental compositions of these surfaces are reported in Table 3.2.

Table 3.2. XPS elemental analysis.

Surface	C 1s	C-C	C-O	Contamination	O 1s	Si 2p
	Total	284.0-284. 9	285.8-286.5	286.9-288.5		
Wafer	27.6	91.3	8.7		28.2	44.2
PEO control	31.7	54.3	36.3	9.4	36.9	31.4
a (n =0)	37.4	51.0	44.4	4.6	29.2	33.4
b (n = 4)	38.9	67.2	26.6	6.2	27.3	33.8
c (n = 13)	43.6	73.7	21.0	5.3	26.7	29.7

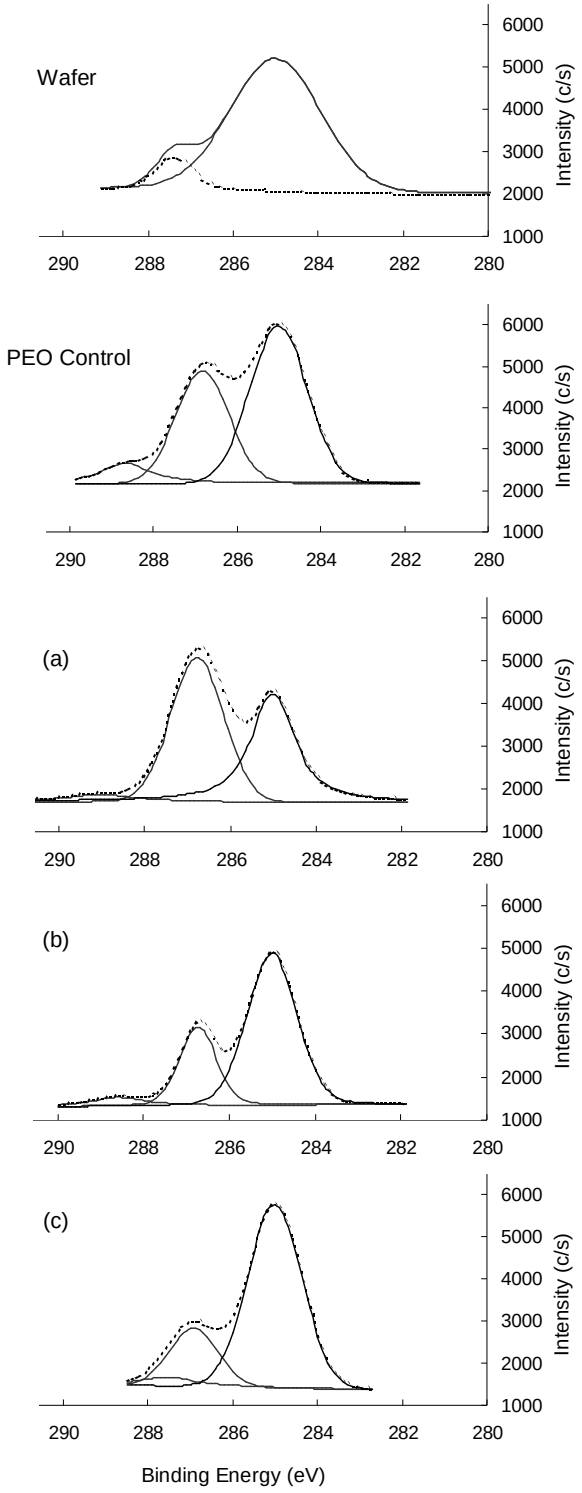

Figure 3.2. High-resolution C 1s spectra of unmodified silicon wafer, **PEO control** and wafers grafted with PEO-silanes **(a-c)**. The increase in C-O is evidence of PEO present at the surface.

Carbon present on the surface of unmodified silicon wafer was probably adsorbed contamination from the atmosphere.[92, 123] The O 1s and Si 2p peaks corresponds to the wafer composition.

As expected, following grafting, the Si 2p decreased and the C 1s content increased. The observed C 1 s peak was fitted with three Gaussian peaks at binding energies: (**i)** 284 eV – 285 eV corresponding to the C-C in the PEO, **(ii)** 285.8 eV – 286.5 eV corresponding to the C-O in PEO and **(iii)** 286.9 eV – 288.5 eV is likely contamination (Fig. 3.2). Thus, the increased C-O peak intensity of grafted surfaces versus the unmodified silicon wafer confirmed the presence of PEO.

Contact Angle Analysis

θ_{static}, θ_{adv}, and θ_{rec} of DI water droplets on grafted surfaces are reported in Table 3.3. A crosslinked silicone elastomer served as a hydrophobic control. The θ_{static} and observed θ_{adv} values for the PEO-control grafted surface are similar to those of PEO-grafted silicon surfaces reported in the literature.[92, 95] For surfaces grafted with PEO-silanes, θ_{static} decreased and surface hydrophilicity increased in the order: **c** < **b** < **a** < **PEO control**. This trend reflects the increase in chain density (σ) or the surface concentration of PEO which similarly increased in the order: **c** < **b** < **a** < **PEO control** (Table 3.3). Also, since the siloxane tether is hydrophobic, an increase in tether length contributed to a decrease in hydrophilicity for **b** and **c** grafted surfaces. The observed decrease in θ_{static} (15 sec) versus θ_{static} (2 min) for all grafted surfaces may be attributed to the hydration of the PEO segments.

Table 3.3. Contact angle measurements of wafers grafted with PEO-silanes.

surface grafted with:	static contact angles		dynamic contact angles	
	θ_{static} @ 15 sec	θ_{static} @ 2 min	θ_{adv}	θ_{rec}
Si^{OX}	21 ± 2.0	16 ± 4.0	24 ± 2.0	23 ± 2.0
PEO-control	55 ± 1.0	51 ± 1.0	50 ± 1.0	45 ± 2.0
a (n = 0)	57 ± 1.0	52 ± 0.1	62 ± 0.3	59 ± 1.0
b (n = 4)	79 ± 0.5	75 ± 0.8	85 ± 1.0	83 ± 1.0
c (n = 13)	86 ± 2.0	81 ± 2.0	90 ± 1.0	87 ± 1.0
Silicone	116 ± 1.0	115 ± 1.0	121 ± 1.0	115 ± 1.0

An oxidized silicon wafer (Si^{OX}) was used as a model hydroxylated biomaterial surface because it is physically stable, unlike silicone elastomer surfaces, for instance, which undergo reorganization in different environments.[56] Thus, the surface concentration of covalently grafted PEO-silanes may be conveniently maintained on silicon surfaces which permits evaluation of the effect of PEO-silane structure (i.e. siloxane tether length). Hysteresis ($\theta_{\Delta} = \theta_{adv} - \theta_{rec}$) is typically used as an indicator of surface reorganization.[95] For instance, after a pure silicone surface is wetted, polar Si-O-Si groups reorganize to the film-water interface to minimize interfacial surface tension such that $\theta_{rec} < \theta_{adv}$.[56] Delamarche et al. observed significant hysteresis (~ 15 °) for surfaces prepared by grafting of $(EtO)_3Si\text{-}(CH_2)_3\text{-poly(ethylene oxide)}_7\text{-}OCH_3$ onto silicone due to the ability of siloxane and PEO segments to reorganize.[65] The physical stability or absence of surface reorganization of the silicon wafer (Si^{OX}) surface was confirmed by its lack of significant hysteresis. Similarly, PEO-silane grafted surfaces did not exhibit significant hysteresis. In other words, the surface concentration of the grafted PEO-silanes remains constant since the underlying silicon wafer is physically stable. Hence, the observed surface properties may be related to chain density (σ) and the chemical structure of PEO-silanes as stated above.

Protein Adsorption

Albumin is the most abundant plasma protein (60 %) and fibrinogen (4 %), also a plasma protein, plays an important role in the process of thrombosis as it is converted by thrombin to insoluble fibrin.[124] Thus the amounts of BSA and HF proteins adsorbed onto PEO-silane grafted surfaces were analyzed to determine plasma protein adsorption (Fig. 3.3). Protein adsorption of BSA and HF conjugated with a fluorescent dye was measured via fluorescence microscopy.[27, 64-66]

As was observed in this study, silicone exhibits high protein adsorption as a result of its extreme hydrophobicity.[47, 48] For every surface, higher amounts of HF were adsorbed compared to BSA which is consistent with previous observations.[124, 125] The enhanced adhesion of HF compared to BSA is attributed to the former's greater hydrophobicity [126] as well as HF's rod-like geometry which facilitates reorientation on the adsorbing surface to increase protein-protein interaction and surface concentration. [124] The amount of protein adsorbed by grafted surfaces is substantially lower than that adsorbed by the silicone control.

If protein adhesion was controlled by only surface hydrophilicity, one would predict that the **PEO control** grafted surface would be the most resistant to protein adsorption since it is most hydrophilic. This trend, however, was not observed. For surfaces grafted with **a-c**, adsorption of BSA and HF was less compared to a surface grafted with the **PEO control**. Resistance to BSA adsorption increased with siloxane tether length in the order: **PEO control** < **a** < **b** ≈ **c**. Adsorption onto **b** and **c** grafted surfaces were not statistically different from each other.

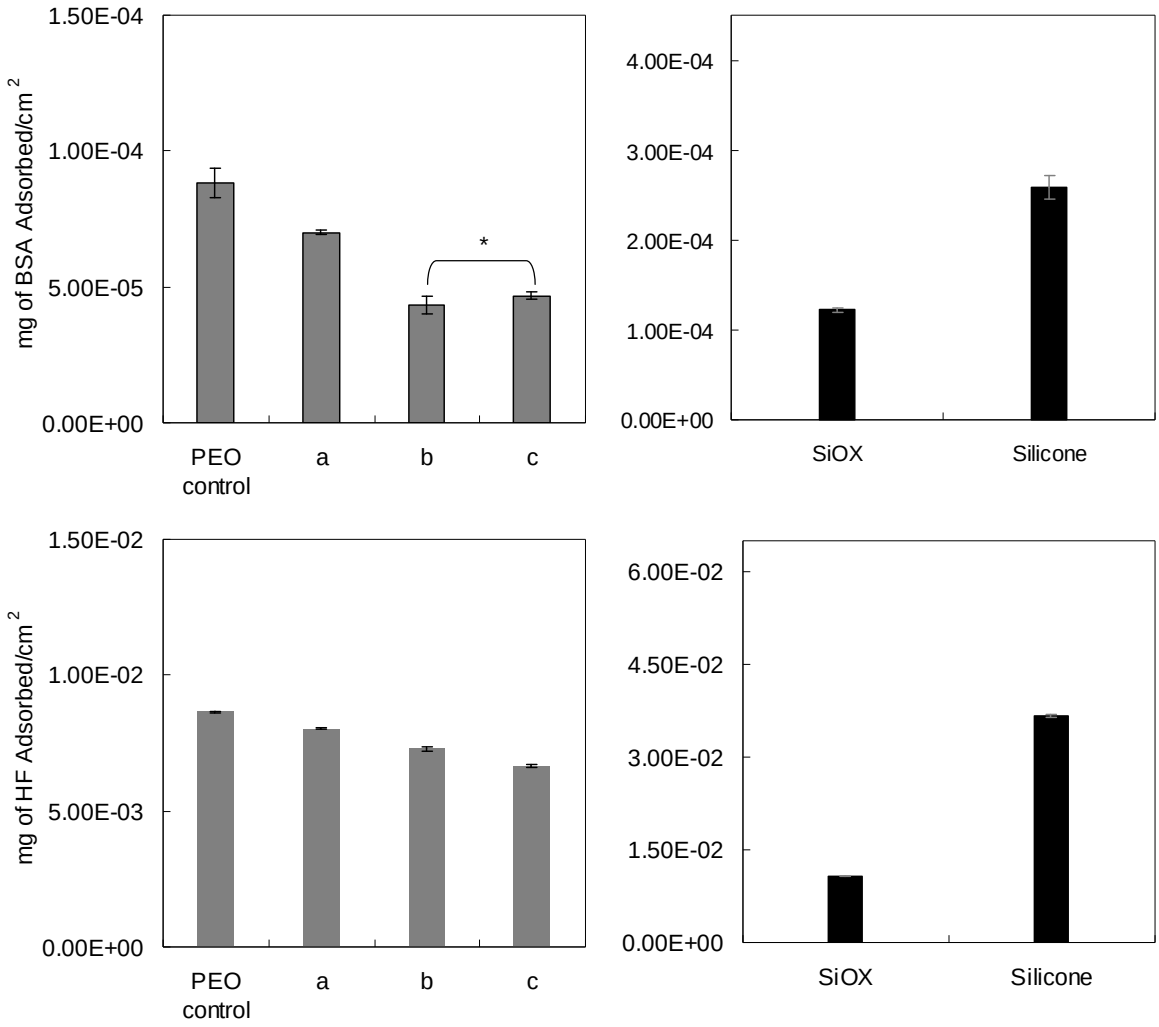

Figure. 3.3. Adsorption of [Top] BSA and [Bottom] HF onto PEO-silane grafted wafers. Error bars represent the standard deviation between the fluorescence measurements of 3 randomly selected regions. Statistical significance was determined by one-way analysis of variance (Holm-Sidak Method where $p = 0.05$ unless other wise noted. * indicates $p > 0.05$.). **SiOX** = oxidized wafer and **Silicone** = Dow Corning Silastic T-2 cured on a glass microscope slide.

Similarly, resistance to HF adsorption increased in the order: **PEO control < a < b < c.** In this case, adsorption onto **b** and **c** grafted surfaces were statistically different from each other. Thus, despite the highest surface hydrophobicity due to the lowest chain density (σ) as well as longest hydrophobic siloxane tether, **c** grafted surfaces exhibited the least protein adsorption. In the absence of surface hydrophilicity to explain

the superior protein resistance of surfaces prepared by grafting PEO via longer siloxane tethers, enhanced configurational mobility of the PEO segment may be considered. Although the PEO segments of all of the grafted chains (**a-c** and **PEO control**) were determined to be in the brush regime, the chain density (σ) decreased with siloxane tether length. Thus, any enhanced configurational mobility may be attributed not only to the longer siloxane tether, but also to the somewhat lower chain density. Thus, future studies are required to probe the mechanism by which grafting of PEO segments via longer siloxane tethers diminishes protein adsorption. In future studies, we will attempt to prepare silicon surfaces grafted with PEO-silanes (**a-c** and **PEO control**) using different solvent and temperature conditions to obtain more similar chain densities.[122] This would allow us to eliminate any enhanced PEO configurational mobility due to lower chain density and thus examine the contribution of longer siloxane tether towards increased PEO configurational mobility and subsequent enhanced resistance to protein adsorption. In addition to their configurational mobility, the increasing amphiphilic nature of the PEO-silanes **(a-c)** with longer siloxane tether length may also be considered as a source of their resistance to protein adsorption. Their amphiphilic nature should result in thermodynamically driven phase segregation of the siloxane and PEO segments due to their difference in surface energy. Such phase-segregation on surfaces has been previously shown to generate complex surface topographies which resist the adsorption of proteins.[11, 12]

3.8 Conclusions

Distancing the PEO segment from the grafting site via a siloxane tether represents a new method of grafting PEO chains to surfaces. PEO-silanes containing siloxane tethers of varying lengths **(a-c)** were grafted onto the surfaces of oxidized silicon wafers. As the siloxane tether length increased, chain density (σ) decreased due the greater steric barrier presented by already grafted longer chains and enhanced solubility of PEO-silanes in the grafting solvent. Surface properties and resistance to protein adsorption were measured using a series of PEO-silane grafted surfaces with similar thickness (h) and surface coverage (Γ) values and in which the PEO segments of all of the grafted PEO-silanes were determined to be in the brush regime and all chain densities were lower than the estimated upper limit of 5.8 chains/nm^2 for fully extended PEO chains. As a result of decreased chain density (σ) (i.e. decreased PEO surface concentration) and increased length of the hydrophobic siloxane tether, surface hydrophilicity increased in the order: **c** < **b** < **a** < **PEO control**. However, despite lower chain density (σ) and higher surface hydrophobicity, resistance to BSA adsorption increased in the order of **PEO control** < **a** < **b** ≈ **c** and resistance to HF adsorption increased in the order of **PEO control** < **a** < **b** < **c.** In other words, longer siloxane tethers contributed to resistance to protein adsorption of the PEO-silane. Because hydrophilicity is not enhanced, it is postulated that the improved protein resistance may be due to enhanced configurational mobility of the PEO segment with longer siloxane tethers. The grafting of amphiphilic PEO-silanes (**a-c**) onto the surfaces of common

polymeric biomaterials may provide enhanced blood-compatibility while maintaining desirable bulk properties.

CHAPTER IV

SILICONES WITH ENHANCED PROTEIN RESISTANCE: INTRODUCTION OF BRANCHED PEO-SILANES WITH SILOXANE TETHERS

4.1 Overview

Adsorption of proteins onto silicones was reduced by incorporation of branched polyethylene oxide (PEO)-silanes having siloxane tethers. Six novel amphiphilic branched PEO-silanes were prepared with varying siloxane tether lengths as well as PEO molecular weight (M_n) with the general formula: α-$(EtO)_3Si(CH_2)_2$-oligodimethyl-siloxane$_n$-*block*-$[PEO_m$-$OCH_3]_2$ where n = 0, m = 6 **(1a)**; n = 4, m = 6 **(2a)**; n = 13, m = 6 **(3a)** (i.e. the lower M_n PEO series) and n = 0, m = 12 **(1b)**; n = 4, m = 12 **(2b)**; n = 13, m = 12 **(3b)** (i.e. the higher M_n PEO). Each PEO-silane **(1a-3a and 1b-3b)** were crosslinked via H_3PO_4-catalyzed sol-gel condensation with α,ω-bis(Si-OH)PDMS (**P**, M_n = 3000 g/mol) in a 2:3 molar ratio of PEO-silane to **P** to yield six unique PEO-modified silicone films **(1a-P-3a-P** and **1b-P-3b-P)**. Film surface hydrophilicity increased with siloxane tether length, particularly after exposure to an aqueous environment, indicating that the PEO segments were more readily driven to the surface. This effect was more pronounced for films prepared with PEO-silanes based on the lower M_n PEO segment **(1a-P-3a-P).** Adsorption of bovine serum albumin (BSA) and human fibrinogen (HF) proteins decreased with siloxane tether length, particularly after first exposing to an aqueous environment. For a given siloxane tether length, relatively

more BSA adsorbed onto films prepared with PEO-silanes based on the higher M_n PEO segment **(1a-P-3a-P)** whereas more HF adsorbed onto films prepared with PEO-silanes on the lower M_n PEO segment **(1a-P-3a-P)**.

4.2 Introduction

Surface induced thrombosis is a major problem associated with blood-contacting medical devices.[121, 127] Within the first few minutes of exposure to blood, plasma proteins adsorb onto implant surfaces which results in platelet adhesion and activation of coagulation pathways leading to thrombosis.[49, 96] Thus, minimizing adsorption of proteins on surfaces is desirable to prevent thrombosis. Silicones, (e.g. polydimethylsiloxane (PDMS)) have been used in many biomedical applications due to its excellent bulk properties such as thermal and oxidative stability, chemical and physiological inertness, low modulus, flexibility and gas permeability.[45, 46, 128] Unfortunately, because proteins preferentially adsorb onto hydrophobic surfaces, the extreme hydrophobicity of silicones causes poor resistance to blood proteins. Thus, silicones have been hydrophilized by various chemical or physical treatments or a combination of both to reduce protein adsorption. [47, 51, 52, 129]

Polyethylene oxide (PEO or polyethylene glycol; PEG) is a neutral, hydrophilic polymer with exceptional resistance to protein adhesion.[54, 97] Thus, to improve protein resistance of silicones, PEO has been introduced via bulk crosslinking,[39] physisorption,[42] or surface grafting.[70] These processes often employ PEO-silanes such as trialkoxysilanes which undergo stepwise hydrolysis and condensation with either

hydroxylated precursor molecules (bulk crosslinking) or with hydroxylated surfaces (surface grafting). For instance, PEO-modified silicones have been formed by crosslinking triethoxysilylpropyl PEO monomethyl ether with α,ω-bis(Si-OH)PDMS and tetraethoxysilane $(SiOEt)_4$.[67, 68] The surfaces of silicones may also be modified with PEO-silanes as well.[56-60, 62] For instance, following surface oxidation, triethoxysilylpropyl PEO monomethyl ethers have been covalently grafted.[63] Allyl PEO monomethylethers [CH_2=$CHCH_2$-$(OCH_2CH_2)_n$-OCH_3] have also been covalently grafted onto silane-enriched silicone surfaces. The surface concentration of PEO-silanes introduced into silicones, whether bulk crosslinked or surface grafted, will vary with environment (e.g. air and aqueous) because of the significant reorganization of silicones in different environments.[56, 65]

The exceptional protein resistance of PEO is attributed to its high water content, conformational flexibility and high chain mobility.[35] These properties lead to the "exclusion effect" or "steric stabilization effect" by which proteins are repelled from the surface. In addition, the high chain mobility of PEO produces an entropic penalty of chain compression if protein adsorption were to occur. Thus, enhancement of PEO's chain mobility onto surfaces should increase its resistance to proteins. For instance, protein resistance was decreased for silicones prepared by crosslinking α,ω-bis(Si-OH)-PDMS with *bis*-triethoxysilylpropyl PEO versus those prepared with triethoxysilylpropyl PEO monomethyl ether.[68] This was attributed to a lack of mobilization of the difunctional PEO to the aqueous interface compared to the monofunctional PEO.

Conventional PEO-silanes used to introduce PEO into silicones consist of a PEO segment separated from the reactive group by a short alkane spacer [e.g. propyl as for $(RO)_3Si\text{-}(CH_2)_3\text{-}(CH_2CH_2O)_n\text{-}OCH_3$)] which may limit PEO mobility. We have previously reported the synthesis of novel amphiphilic *linear* PEO-silanes with the general formula: α-$(EtO)_3Si(CH_2)_2$-oligodimethylsiloxane$_n$-*block*-poly(ethylene oxide)$_8$-OCH_3 [n = 0, 4, and 13].[53] Thus, the PEO segment is separated from the reactive ethoxysilane group by siloxane tethers of varying lengths. The siloxane tethers are highly flexible due to the wide bond angle (~ 145°) and low barrier to linearization (~0.3 kcal/mol) of Si-O-Si of dimethylsiloxanes. The dynamic flexibility of the Si-O-Si backbone produces polymers with low glass transition temperatures (T_gs) (e.g. PDMS, T_g = -125 °C). These PEO-silanes were subsequently crosslinked with α,ω-bis(Si-OH)-PDMS to produce PEO-modified silicone coatings whose surface hydrophilicity and resistance to proteins increased as the length of the siloxane tether increased. Thus, longer flexible siloxane tethers of PEO-silanes more effectively mobilized PEO segments to the aqueous interface to diminish adsorption of proteins.

It has been predicted that branched polymer architectures should be superior for prevention of nonspecific protein adsorption.[130, 131] Therefore, branched PEO-silanes bearing siloxane tethers are interesting alternative to prepare crosslinked PEO-modified silicones. Herein, we report the synthesis of six amphiphilic branched PEO-silanes with siloxane tethers **(1a-3a** and **1b-3b)** having the general formula α-$(EtO)_3Si(CH_2)_2$-oligodimethylsiloxane$_n$-*block*-$[PEO_m\text{-}OCH_3]_2$ [n = 0; m = 6 **(1a)**, n = 4, m = 6 **(2a)**, n = 13, m = 6 **(3a)** and n = 0; m = 12 **(1b)**, n = 4, m = 12 **(2b)**, n = 13, m =

12 **(3b)**] (Fig. 4.1). A siloxane tether may aide in the reorganization of the PEO segments to the film-water interface to improve protein resistance.

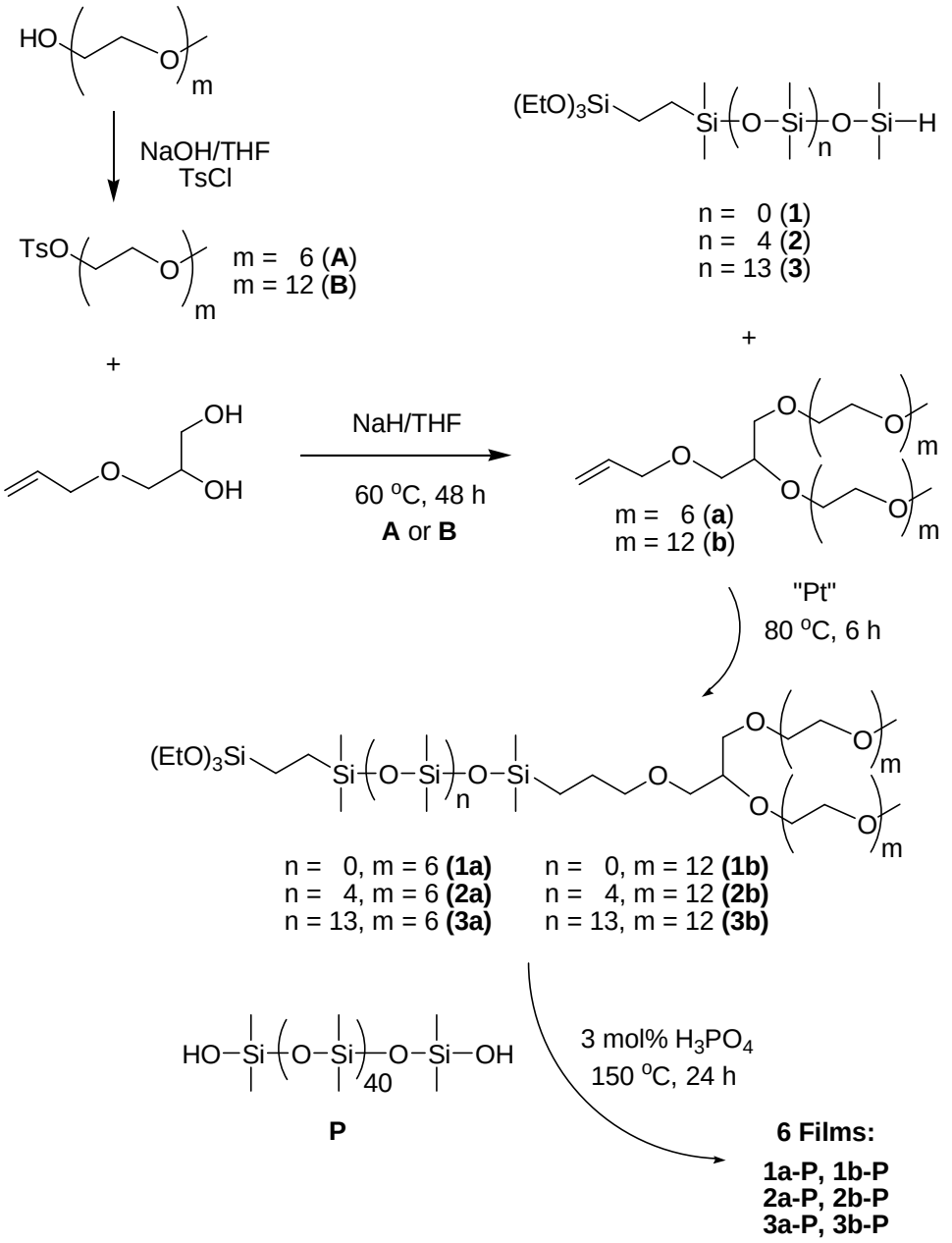

Figure 4.1. Synthesis of crosslinkable α-$(EtO)_3$Si-oligodimethylsiloxane$_n$-*block*-[oligo(oxyethylene oxide)$_m$]$_2$ and subsequent conversion to crosslinked films by acid-catalyzed sol-gel condensation with α,ω-bis(Si-OH)polydimethylsiloxanes **(P)** at 2:3 molar ratios of **(1a-3a)** and **(1b-3b)** to **P.**

The effect of PEO MW and surface concentration on protein resistance has been widely studied.[72] Thus, for a given siloxane tether length, each branched PEO-silane was prepared with two different PEO M_n's. To prepare the branched PEO-silanes, three α-triethoxysilylethyl-ω-silane-oligodimethylsiloxanes$_n$ [n= 0 (**1**), n = 4 (**2**), and n = 13 (**3**)] each underwent Rh-catalyzed hydrosilylation with allyl-branched-PEO_6 (**a**) and allyl-branced-PEO_{12} (**b**), respectively, to yield the corresponding branched PEO-silanes **(1a-3a** and **1b-3b)**. Six compositionally unique PEO-modified silicone coatings **(1a-P-3a-P** and **1b-P-3b-P)** were subsequently prepared by phosphoric acid (H_3PO_4)-catalyzed sol-gel condensation crosslinking of **1a-3a** and **1b-3b** each with α,ω-bis(Si-OH)PDMS (**P**, M_n = 3000 g/mol) in a 2:3 molar ratio, respectively.

4.3 Experimental Section

Polymer Characterization

NMR. ^{1}H spectra were obtained on a Mercury 300-MHz spectrometer operating in the Fourier transform mode. Five percent (w/v) $CDCl_3$ solutions were used to obtain spectra. Residual $CDCl_3$ was used as an internal standard.

IR Spectroscopy. IR spectra of neat liquids on NaCl plates were recorded using a Bruker TENSOR 27 FT-IR spectrometer.

Thermal Gravimetric Analysis (TGA). The thermal stabilities of ~ 10 mg neat liquid samples in Pt pans were evaluated with a TA Instruments Q50 under N_2 and air at a flow rate of 40 cc/min. The sample weight was recorded while the temperature was increased 4 ˚C/min from 25 to 800 ˚C.

Gel Permeation Chromatography (GPC). GPC analysis was performed on a Viscotek GPC system equipped with three detectors in series: refractive index (RI), right angle laser light scattering (RALLS), and viscometer (VP). The ViscoGEL™ HR-Series (7.8 mm x 30 cm) column packed with divinylbenzene crosslinked polystyrene (SDVB) was maintained at 25 °C in a column oven. The eluting solvent was HPLC grade toluene at a flow rate of 1.0 mL/min. The detectors were calibrated with a polystyrene (PS) narrow standard with the following parameters: MW (66K), polydispersity (1.03), intrinsic viscosity (0.845 dL/g), and dn/dc (0.112 mL/g). Data analysis was performed with Viscotek OmniSec software (Version 4.0).

Film Characterization

Thermal Gravimetric Analysis (TGA). Thermal analyses of free-standing pieces of films (~10 mg) were similarly measured as described above.

Soxhlet Extraction. The amount of uncrosslinked material in a film was determined by Soxhlet extraction. A film cured on a microscope slide was extracted with CH_2Cl_2 in a Soxhlet apparatus for 12 h. The percentage of uncrosslinked material was calculated as the weight difference of the extracted versus unextracted weight divided by the unextracted weight.

Dynamic Mechanical Analysis (DMA). Storage (G') and loss (G") moduli of films were measured as a function of temperature on a TA Instruments Q800 dynamic mechanical analyzer. Specimens (length x width = 35 x 5.3 mm) were cut from free-standing films using a clean single-edged razor cutting tool. Electronic calipers were

used to measure film thickness (~ 0.5 mm) prior to testing. The dynamic mechanical analyzer was operated using a dual cantilever clamp assembly at a frequency of 5 Hz and a displacement of 4 μm. After equilibration at -140 °C for 3 min, the temperature was increased 4 ˚C/min to 25 ˚C. The T_g was determined from the peak maximum of the measured G".

Contact Angle Measurement. Static (θ_{static}), advancing (θ_{adv}), and receding (θ_{rec}) contact angles of distilled/deionized (DI) water droplets at the film-air interface were measured with a CAM-200 (KSV Instruments) contact angle measurement system equipped with an autodispenser, video camera, and drop-shape analysis software. Following cure, coated microscope slides were stored in a dessicator for 5 days prior to contact angle measurements. For θ_{static} measurements, a sessile drop of water (5 μL) was measured at 15 sec and 2 min after deposition onto the film surface. The θ_{adv} was measured by the addition of 3 μL (0.25 μL/sec) of water to a 5 μL pendant droplet to advance the contact line. θ_{rec} was measured by the subsequent removal of 4 μL (0.25 μL/sec) from the same droplet to recede the contact line. The reported θ_{static}, θ_{adv}, and θ_{rec} values are an average of three measurements taken on different areas of the same film sample. For each film composition, 2 coated microscopes slides were analyzed. One slide served to test a film surface exposed to only to air ("air-equilibrated") prior to contact angle measurements. The other served to test a film surface which was first equilibrated in DI water for 36 h and immediately dried under a stream of N_2 just prior to contact angle measurements ("water equilibrated").

Adsorption of Proteins. The adhesion of Alexa Fluor 555 dye conjugate of bovine serum albumin (AF-555 BSA; MW = 66 kDa; Molecular Probes, Inc.) and Alexa Fluor 546 dye conjugate of human fibrinogen (AF-546 BSA; MW = 340 kDa; Molecular Probes, Inc) onto film surfaces was studied by fluorescence microscopy. To remove residual acid catalyst from the films, all coated microscope slides were first leached in distilled water for 3 days with fresh water changes every 12 h until the pH of the water remained at ~7.2. Coated microscope slides were subsequently dried *in vacuo* (36 in. Hg, 24 h, RT) and stored in a dessicator for 2 days prior to testing. A silicone isolator (20 mm well diameter, 2.5 mm well depth; JTR Press-to-Seal Silicone Isolators) was affixed with adhesive to prevent leakage of solutions from the well. For each film composition, 2 coated microscopes slides were analyzed. One slide served to test a film surface exposed to air ("air-equlibrated") prior to exposure to protein whereas the other served to test a film surface which was first exposed to phosphate buffered saline (PBS, pH = 7.4; "PBS equilibrated") for 36 h prior to exposure to protein.

Air Equilibrated Films. The exposed surface of the film inside each isolator well was filled with 1 mL of AF-555 BSA solution (0.1 mg/mL in PBS) or 1 mL of AF-546 HF solution (0.1 mg/mL in PBS), equilibrated in the dark at RT for 3 h, and removed. One mL of fresh PBS was then added to each well and removed after 5 min; this process was repeated a total of three times. The samples were then dried under a stream of nitrogen (N_2) and imaged. Film surfaces tested in this way are referred to as "air-equilibrated."

PBS Equilibrated Films. On the second set of coated microscope slides, the exposed surface of the film inside each isolator was filled with 1 mL of PBS and removed after 36 h. Exposure to AF-555 BSA solution (3 h) or 1 mL of AF-546 HF solution was immediately executed using the same protocol as above. Film surfaces tested in this manner are referred to as "PBS-equilibrated."

A Zeiss Axiovert 200 optical microscope equipped with a A-Plan 5x objective, Axiocam HRC Rev. 2), and filter cube (excitation filter of 546 ± 12 nm [band pass] and emission filter 575-640 nm [band pass]) was used to obtain fluorescent images on 3 randomly selected regions of the surface within each isolator well. The fluorescent light source was permitted to warm up for 30 min prior to image capture. Linear operation of the camera was ensured and constant exposure time used during the image collection to permit quantitative analyses of the observed fluorescent signals. The fluorescence microscopy images were analyzed using the histogram function of PhotoShop, which yielded the mean and standard deviation of the fluorescence intensity within a given image. The fluorescence intensity of each protein-exposed region was subtracted from that of non-exposed region to ensure correction for of any fluorescence signal from the material itself. The background-corrected fluorescence intensities for each film were then used to quantify AF-555 BSA or AF-546 HF levels adsorbed by comparison against a calibration curve constructed from the measured fluorescence intensities of AF-555 BSA or AF-546 HF standard slides, respectively. The obtained value was converted to mg/cm^2 by dividing by the area inside silicone isolator. Standard slides were prepared by fitting a silicone isolator to uncoated, solvent-cleaned glass slides and adding 1 mL of

AF-555 BSA or AF-546 HF solutions of known concentrations (0, 0.005, 0.01, 0.02, 0.04 mg/mL AF-555 BSA or AF-546 HF in PBS) to individual wells.

X-ray Photoelectron Spectroscopy (XPS). XPS was used to confirm the chemical grafting of $(EtO)_3Si\text{-}(CH_2)_3\text{-}(OCH_2CH_2)_8\text{-}OCH_3$ onto glass microscope slides which served as the "PEO control". The surface was analyzed using a KRATOS AXIS Ultra Imaging X-Ray Photoelectron Spectrometer with MgK_α non-monochromatic X-ray source. The spot size was 7 x 3 mm. The survey scan (0 to 1100 eV) and C1s high-resolution scan (20 eV scan width) were performed with a take-off angle of 90°. Binding energies were referenced to the C-C peak at 285 eV. The raw data was analyzed using XPS Peak Processing Software.

4.4 Materials

$RhCl(Ph_3P)_3$ (Wilkinson's catalyst), glycerol-1-allyl-ether, sodium hydride (NaH), sodium hydroxide (NaOH), *p*-toluene sulfonyl chloride (tosyl chloride, TsCl), and solvents were obtained from Aldrich. Magnesium sulfate ($MgSO_4$) was obtained from Fisher Scientific. HPLC grade toluene, tetrahydrofuran (THF), dichloromethane (CH_2Cl_2), chloroform ($CHCl_3$) and NMR grade $CDCl_3$ were dried over 4Å molecular sieves. α,ω-bis(Si-H)oligodimethylsiloxanes (**$ODMS_0$** or tetramethyldisiloxane; **$ODMS_4$**, MW = 400-500 g/mol per manufacturer's specifications; **$ODMS_{13}$**, MW = 1000-1100 g/mol per manufacturer's specifications), vinyltriethoxysilane (**VTEOS**), α,ω-bis-(Si-OH)polydimethylsiloxane (**P,** MW = 2000-3500 g/mol per manufacturer's specifications), triethoxysilane, and Pt-divinyltetramethyldisiloxane complex (Karstedt's

catalyst) were acquired from Gelest. The number average molecular weight (M_n) of **ODMS$_0$**, **ODMS$_4$**, and **ODMS$_{13}$** were determined by ^{1}H NMR end-group analysis: **ODMS$_0$** (134 g/mol), **ODMS$_4$** (430 g/mol), and **ODMS$_{13}$** (1096 g/mol). The MWs of **P** was determined by GPC (M_w/M_n = 5000/3000 g/mol). PEO hydroxyl methyl ether (**HO-PEO$_6$M** and **HO-PEO$_{12}$M**) was obtained from Clariant (Polyglykol M-500 and Polyglykol M-250) and was dried overnight under high vacuum prior to use. The M_n of **HO-PEO$_6$M** and **HO-PEO$_{12}$M** was determined to be 290 g/mol and 560 g/mol, respectively, by end group analysis: ^{1}H NMR (δ, ppm, **HO-PEO$_6$M**): 3.26 (s, 3H, OC*H*$_3$) and 3.41 – 3.61 (m, 24H, OC*H*$_2$C*H*$_2$). ^{1}H NMR (δ, ppm; **HO-PEO$_{12}$M**): 3.28 (s, 3H, OC*H*$_3$) and 3.43 – 3.59 (m, 46H, OC*H*$_2$C*H*$_2$). PEO allyl methyl ether (**A-PEO$_8$M**) was obtained from Clariant (Polyglykol AM-500) and was dried overnight under high vacuum prior to use. The M_n of **A-PEO$_8$M** was determined to be 425 g/mol (n = 8) by end group analysis: ^{1}H NMR (δ, ppm): 3.26 (s, 3H, OC*H*$_3$), 3.51 (m, 32H, OC*H*$_2$C*H*$_2$), 3.90 (d, 2H, *J* = 5.7 Hz, CH_2=CHC*H*$_2$O), 5.11 (m, 2H, C*H*$_2$=CHCH$_2$O), and 5.79 (m, 1H, CH_2=C*H*CH$_2$O).

4.5 Synthetic Approach

All reactions were conducted in oven-dried (100 °C) glassware with Teflon covered magnetic stir bars to agitate reaction mixtures.

Synthesis of 1-3

α-Triethoxysilylethyl-ω-silane-oligodimethylsiloxanes$_n$ (**1-3**) were prepared by

the Rh-catalyzed regioselective hydrosilylation of equimolar amounts of **VTEOS** with **$ODMS_0$**, **$ODMS_4$**, or **$ODMS_{13}$**, respectively, as previously reported.[39]

Synthesis of A

Tosylated PEO monomethyl ether (**$TsO\text{-}PEO_6\text{-}M$; A**) was synthesized by the reaction of **$HO\text{-}PEO_6M$** and TsCl in the presence of NaOH according to procedures previously reported.[83, 132] **$HO\text{-}PEO_6M$** (30.0 g, 103.5 mmol) in 120 mL of THF was added dropwise to a solution of NaOH (5.7 g, 142.0 mmol) in 180 mL of water and 135 mL of THF at 0 ºC. This mixture was allowed to stir for 30 min and then TsCl (23.8 g, 125.0 mmol) in 280 mL of THF was added dropwise and allowed to stir for 4 h at RT. The mixture was then poured onto ice (200 mL) and extracted three times with CH_2Cl_2 and subsequently dried with $MgSO_4$. All volatiles were removed under reduced pressure to isolate the final product. In this way, **A** (31.84 g, 68% yield) was obtained. ^{1}H NMR (δ, ppm): 2.39 – 2.45 (m, 3H, O*CH*$_3$), 3.32 (s, 3H, C_6H_4-*CH*$_3$), 3.48 – 3.66 (m, 24H, O*CH*$_2$*CH*$_2$), 7.29 – 7.39 (m, 2H, C_6*H*$_4$), 7.74 – 7.89 (m, 2H, C_6*H*$_4$).

Synthesis of B

$HO\text{-}PEO_{12}M$ (40.0 g, 71.4 mmol) in 160 mL of THF was reacted with NaOH (4.0 g, 100.1 mmol) in 130 mL of water and 95 mL of THF and TsCl (16.3 g, 85.7 mmol) in 195 mL of THF. In this way, **$TsO\text{-}PEO_{12}\text{-}M$ (B)** (39.36 g, 77% yield) was obtained. ^{1}H NMR (δ, ppm): 2.38 – 2.43 (m, 3H, O*CH*$_3$), 3.31 (s, 3H, C_6H_4-*CH*$_3$), 3.48 – 3.64 (m, 46H, O*CH*$_2$*CH*$_2$), 7.29 – 7.37 (m, 2H, C_6*H*$_4$), 7.71 – 7.87 (m, 2H, C_6*H*$_4$).

Synthesis of a

a was prepared by the reaction of glycerol-1-allyl ether and **A** in the presence of NaH according to procedures previously reported.[83, 132, 133] Glycerol-1-allyl ether (1.47 g, 11.16 mmol) in 20 mL of THF was added dropwise to a suspension of NaH (60 % dispersion in mineral oil) (1.11 g, 27.80 mmol) in 30 mL of THF at 0 °C in a round-bottomed flask (rb) under an atmosphere of N_2. After addition of the diol, the mixture was stirred until no bubbling of H_2 gas was observed. Next, a solution of **A** (10.01 g, 22.20 mmol) in 30 mL of THF was slowly added dropwise. This mixture was then heated to 60 °C and stirred for 48 h. Next, the reaction mixture was allowed to cool and a mixture of 100 mL of diethyl ether and 70 mL of THF was added to completely precipitate sodium tosylate salts. The salts were then filtered and all volatiles removed under reduced pressure. The resulting yellow oil was dissolved in 75 mL of toluene and the organic layer was extracted with 3 x 50 mL of water. Next, the aqueous layer was extracted with 3 x 50 mL of $CHCl_3$. The organic layers were combined, dried with $MgSO_4$, and the solvent was removed under reduced pressure to isolate the final product. In this way, **4** (4.11 g, 54% yield) was obtained. ^{1}H NMR (δ, ppm): 3.35 (m, 6H, O*CH*$_3$), 3.51 – 3.54 (m, 4H, C*H*$_2$O(CH_2CH_2O)CH_3 and C*H*$_2$CHO(CH_2CH_2O)CH_3), 3.62 – 3.64 (m, 48H, C*H*$_2$C*H*$_2$O), 3.82 – 3.87 (m, 1H, CH_2OCH_2CH) 3.96 – 4.01 (m, 2H, CH_2=CHC*H*$_2$OCH_2), 5.12 – 5.29 (m, 2H, C*H*$_2$=CHCH_2OCH_2), 5.82 – 5.95 (m, 1H, CH_2=C*H*CH_2OCH_2).

Synthesis of b

Glycerol-1-allyl ether (0.92 g, 7.00 mmol) in 10 mL of THF was reacted with **B** (10.00 g, 14.00 mmol) in 30 mL of THF in the presence of NaH in 30 mL of THF (0.70, 17.50 mmol) as above. In this way, **b** (4.81 g, 57% yield) was obtained. ^{1}H NMR (δ, ppm): 3.32 (m, 6H, O*CH*$_3$), 3.47 – 3.52 (m, 4H, C*H*$_2$O(CH$_2$CH$_2$O)CH$_3$ and C*H*$_2$CHO(CH$_2$CH$_2$O)CH$_3$, 3.58 – 3.66 (m, 92H, *CH*$_2$*CH*$_2$O), 3.80 – 3.84 (m, 1H, CH$_2$OCH$_2$C*H*) 3.93 – 4.00 (m, 2H, CH$_2$=CHC*H*$_2$OCH$_2$), 5.12 – 5.18 (m, 1H, C*H*$_2$=CHCH$_2$OCH$_2$), 5.80 – 5.86 (m, 1H, CH$_2$=C*H*CH$_2$OCH$_2$).

Synthesis of 1a-3a and **1b-3b**

α-(EtO)$_3$Si(CH$_2$)$_2$-oligodimethylsiloxane$_n$-*block*-[PEO$_m$-OCH$_3$]$_2$ [**1a-3a** and **1b-3b**] were prepared by the Pt-catalyzed hydrosilylation of equimolar amounts of **a** or **b** with **1-3**, respectively (Fig. 4.1). **1, 2,** or **3** were each combined with **a** or **b,** then combined with Karstedt's catalyst and toluene in a 250 mL rb flask equipped with a septum and heated to 80 °C. The progress of the reaction was monitored with IR spectroscopy by the disappearance of the Si-H (~2125 cm^{-1}) absorbance peak. After an initial reaction time of ~12 h, an aliquot of the reaction solution was evaporated on a NaCl plate and the IR spectrum obtained. In case of an incomplete reaction, additional Karstedt's catalyst (50% of original volume) was added and the reaction continued for another ~6 h before checking the IR spectrum. This cycle was repeated until no Si-H absorbance was observed in the IR spectrum. Typically, no additional Kartstedt's catalyst was required to complete the reaction. The catalyst was removed from the

reaction mixture by refluxing with activated charcoal for 12 h. After filtration, the volatiles were removed under reduced pressure so that **1a-3a** and **1b-3b** were isolated as colorless liquids.

Synthesis of 1a

1 (0.71 g, 2.18 mmol), **a** (1.50 g, 2.18 mmol), and Karstedt's catalyst (50 µL) were reacted as above. In this way, **1a** (1.79 g, 81 % yield) was obtained. ^{1}H NMR (δ, ppm): 0.017 – 0.046 (m, 12H, Si*CH*$_3$), 0.064 – 0.088 (m, 2H, SiC*H*$_2$CH$_2$CH$_2$), 0.51 (m, 3H, SiC*H*$_2$C*H*$_2$), 1.03 – 1.06 (m, 1H, SiC*H*$_2$C*H*$_2$), 1.17 – 1.23 (m, 9H, SiOCH$_2$C*H*$_3$), 1.42 -1.59 (m, 2H, SiCH$_2$C*H*$_2$CH$_2$), 3.36 (s, 6H, OC*H*$_3$), 3.51 – 3.56 (m, 6H, SiCH$_2$CH$_2$C*H*$_2$O, C*H*$_2$O(CH$_2$CH$_2$O)CH$_3$ and C*H*$_2$CHO(CH$_2$CH$_2$O)CH$_3$), 3.61 – 3.64 (48H, C*H*$_2$C*H*$_2$O), 3.76 – 3.84 (7H, SiOC*H*$_2$CH$_3$ and CH$_2$C*H*O(CH$_2$CH$_2$O)CH$_3$.

Synthesis of 2a

2 (1.13 g, 1.82 mmol), **a** (1.25 g, 1.82 mmol), and Karstedt's catalyst (50 µL) were reacted as above. In this way, **2a** (1.96 g, 83 % yield) was obtained. ^{1}H NMR (δ, ppm): ^{1}H NMR (δ, ppm): 0.024 – 0.052 (m, 36H, Si*CH*$_3$), 0.108 – 0.13 (m, 2H, SiC*H*$_2$CH$_2$CH$_2$), 0.52 – 0.54 (m, 3H, SiC*H*$_2$C*H*$_2$), 1.08 (m, 1H, SiC*H*$_2$C*H*$_2$), 1.17 – 1.23 (m, 9H, SiOCH$_2$C*H*$_3$), 1.44 -1.63 (m, 2H, SiCH$_2$C*H*$_2$CH$_2$), 3.36 (s, 6H, OC*H*$_3$), 3.52 – 3.56 (m, 6H, SiCH$_2$CH$_2$C*H*$_2$O, C*H*$_2$O(CH$_2$CH$_2$O)CH$_3$ and C*H*$_2$CHO(CH$_2$CH$_2$O)CH$_3$, 3.56 – 3.64 (48H, C*H*$_2$C*H*$_2$O), 3.77 – 3.84 (m, 7H, SiOC*H*$_2$CH$_3$ and CH$_2$*CH*O(CH$_2$CH$_2$O)CH$_3$.

Synthesis of 3a

3 (1.87 g, 1.45 mmol), **a** (1.00 g, 1.45 mmol), and Karstedt's catalyst (50 µL) were reacted as above. In this way, **3a** (2.29 g, 80 % yield) was obtained. ^{1}H NMR (δ, ppm): 0.027 – 0.084 (m, 90H, Si*CH*$_3$), 0.11 – 0.12 (m, 2H, SiC*H*$_2$CH$_2$CH$_2$), 0.54 (m, 3H, SiC*H*$_2$C*H*$_2$), 1.07 (m, 1H, SiC*H*$_2$C*H*$_2$), 1.20 – 1.25 (m, 9H, SiOCH$_2$C*H*$_3$), 1.53 – 1.59 (m, 2H, SiCH$_2$C*H*$_2$CH$_2$), 3.36 (s, 6H, OC*H*$_3$), 3.53 – 3.55 (m, 6H, SiCH$_2$CH$_2$C*H*$_2$O, C*H*$_2$O(CH$_2$CH$_2$O)CH$_3$ and C*H*$_2$CHO(CH$_2$CH$_2$O)CH$_3$, 3.62 – 3.75 (m, 48H, C*H*$_2$C*H*$_2$O), 3.79 – 3.84 (7H, SiOC*H*$_2$CH$_3$ and CH$_2$C*H*O(CH$_2$CH$_2$O)CH$_3$.

Synthesis of 1b

1 (0.54g, 1.66 mmol), **b** (2.00 g, 1.66 mmol), and Karstedt's catalyst (50 µL) were reacted as above. In this way, **1b** (1.94 g, 77 % yield) was obtained. ^{1}H NMR (δ, ppm): ^{1}H NMR (δ, ppm): 0.018 – 0.066 (m, 12H, Si*CH*$_3$), 0.077 – 0.10 (m, 2H, SiC*H*$_2$CH$_2$CH$_2$), 0.52 (m, 3H, SiC*H*$_2$C*H*$_2$), 1.03 – 1.06 (m, 1H, SiC*H*$_2$C*H*$_2$), 1.15 – 1.26 (m, 9H, SiOCH$_2$C*H*$_3$), 1.49 -1.64 (m, 2H, SiCH$_2$C*H*$_2$CH$_2$), 3.36 (s, 6H, OC*H*$_3$), 3.51 – 3.56 (m, 6H, SiCH$_2$CH$_2$C*H*$_2$O, C*H*$_2$O(CH$_2$CH$_2$O)CH$_3$ and C*H*$_2$CHO(CH$_2$CH$_2$O)CH$_3$), 3.60 – 3.63 (92H, C*H*$_2$C*H*$_2$O), 3.77 – 3.83 (m, 7H, SiOC*H*$_2$CH$_3$ and CH$_2$C*H*O(CH$_2$CH$_2$O)CH$_3$.

Synthesis of 2b

2 (0.81g, 1.31 mmol), **b** (1.60 g, 1.31 mmol), and Karstedt's catalyst (50 µL) were reacted as above. In this way, **2b** (2.00 g, 83 % yield) was obtained. ^{1}H NMR (δ,

ppm): 0.006 – 0.05 (m, 36H, SiCH_3), 0.11 – 0.13 (m, 2H, Si$CH_2CH_2CH_2$), 0.54 (m, 3H, SiCH_2CH_2), 1.06 – 1.09 (m, 1H, SiCH_2CH_2), 1.16 – 1.24 (m, 9H, $SiOCH_2CH_3$), 1.50 - 1.61 (m, 2H, $SiCH_2CH_2CH_2$), 3.37 (s, 6H, OCH_3), 3.53 – 3.56 (m, 6H, $SiCH_2CH_2CH_2O$, $CH_2O(CH_2CH_2O)CH_3$ and $CH_2CHO(CH_2CH_2O)CH_3$), 3.58 – 3.70 (m, 92H, CH_2CH_2O), 3.77 – 3.84 (m, 7H, $SiOCH_2CH_3$ and $CH_2CHO(CH_2CH_2O)CH_3$).

Synthesis of (3b)

3 (1.63 g, 1.27 mmol), **b** (1.53 g, 1.26 mmol), and Karstedt's catalyst (50 µL) were reacted as above. In this way, **3b** (2.61 g, 83 % yield) was obtained. ^{1}H NMR (δ, ppm): 0.028 – 0.076 (m, 90H, SiCH_3), 0.10 – 0.13 (m, 2H, Si$CH_2CH_2CH_2$), 0.54 (m, 3H, SiCH_2CH_2), 1.06 – 1.09 (m, 1H, SiCH_2CH_2), 1.19 – 1.24 (m, 9H, $SiOCH_2CH_3$), 1.48 - 1.61 (m, 2H, $SiCH_2CH_2CH_2$), 3.37 (s, 6H, OCH_3), 3.52 – 3.55 (m, 6H, $SiCH_2CH_2CH_2O$, $CH_2O(CH_2CH_2O)CH_3$ and $CH_2CHO(CH_2CH_2O)CH_3$), 3.63 – 3.65 (m, 92H, $CH_2CH_2OCH_2CH_2O$), 3.77 – 3.82 (m, 7H, $SiOCH_2CH_3$ and $CH_2CHO(CH_2CH_2O)CH_3$).

Synthesis of $(EtO)_3Si$-$(CH_2)_3$-$(OCH_2CH_2)_8$-OCH_3

The PEO-silane was prepared by the Pt-catalyzed regioselective hydrosilylation of equimolar amounts triethoxysilane and **A-PEO$_8$M** as previously reported.[67]

4.6 Film Preparation

In a scintillation vial equipped with a Teflon-covered stir bar and cap, **1a-3a** and **1b-3b** were each combined with α,ω-bis(Si-OH)PDMS (**P**, M_n =3000 g/mol)

in a 2:3 molar ratio which corresponds to a stoichiometric balance of reactive ethoxysilane and silanol groups (Table 4.1). After mixing for 5 min, 3 mol% of H_3PO_4 (based on total solid weight of the aforementioned mixtures) was added as solution of H_3PO_4/EtOH (10/90 w/w) and the mixture rapidly stirred for 3 h.

Table 4.1. Film compositions and percentage weight loss after soxhlet extraction.

Film[a]	Branched PEO-silane	"siloxane tether" value of n (**1a-3a** or **1b-3b**)	"PEO segment" value of m (**1a-3a** or **1b-3b**)	% wt loss[b]
1a-P	**1a**	n = 0	m = 6	2 %
2a-P	**2a**	n = 4	m = 6	1%
3a-P	**3a**	n = 13	m = 6	2%
1b-P	**1b**	n = 0	m = 12	3 %
2b-P	**2b**	n = 4	m= 12	4 %
3b-P	**3b**	n = 13	m = 12	3 %

[a]Each film prepared with a 2:3 molar ratio of branched PEO-silane (**1a-3a** and **1b-3b**) to **P** [α,ω-bis(Si-OH)PDMS, M_n =3000 g/mol]. [b]After Soxhlet extraction (CH_2Cl_2, 12 h); corresponds to percentage of uncrosslinked material of 2:3 molar ratio of **1a-3a** or **1b-3b** to P, respectively.

Microscope slides (75 x 25 x 1 mm) were sequentially washed with distilled water, CH_2Cl_2/hexane (1/1 v/v), acetone, and finally dried in a 150 °C oven for 24 h prior to use. One mL of each of the aforementioned mixtures was applied to a microscope slide and allowed to level across and coat the entire slide. The slide was then placed in a level 150 °C oven for 24 h. Free-standing films for DMA and TGA testing were obtained by removing films from slides with a clean single-edge razor blade. Coated microscope slides were used for contact angle measurements and protein adsorption studies.

4.7 Preparation of PEO Control Surface

Triethoxysilylpropyl PEO monomethyl ether [**$(EtO)_3Si\text{-}(CH_2)_3\text{-}(OCH_2CH_2)_8\text{-}OCH_3$**] was chemically grafted onto microscopes slides with typical procedures.[85] Briefly, clean microscope slides were immersed in HCl (12 M):MeOH (1/1 v/v) for 2 h and then in HCl (12 M) for 2 h. The slides were rinsed thoroughly with DI water and dried under vacuum at 50 °C for 4 h. The glass slides were then immersed in a solution of $(EtO)_3Si\text{-}(CH_2)_3\text{-}(OCH_2CH_2)_6\text{-}OCH_3$ or $[(EtO)_3Si\text{-}(CH_2)_3\text{-}(OCH_2CH_2)_{12}\text{-}OCH_3$: toluene (5/95 v/v) for 12 h at RT. The slides were removed from the solution and cured at 180 °C *in vacuo* (36 in. Hg) for 12 h. PEO-grafted To remove unbound polymer chains, the microscope slides rinsed with ethanol thoroughly dried under a stream of N_2 prior to use. The microscope slides served as the "**PEO**" control for contact angle and protein adsorption studies.

4.8 Preparation of Silastic Control Surface

Silastic T-2 (silicone elastomer) was applied to clean microscope slides with a drawdown bar (30 mil) and allowed to cure at RT for over 72 h. The film thickness for cured Silastic T-2 films was ~0.6 mm. A silicone-coated slide served as a "**silicone"** control for contact angle and protein adsorption studies.

4.9 Results and Discussion

Synthesis of A and B

Synthesis of **A** and **B.** Tosylation of **HO-PEO$_6$M** and **HO-PEO$_{12}$M** produced **TsO-PEO$_6$-M (A)** and **TsO-PEO$_{12}$-M (B),** respectively, (yields ≥ 68%). ^{1}H NMR spectra of **A** and **B** verified the presence of tosyl peaks at roughly 7.2 to 7.8 ppm.

Synthesis of a and b

A and **B** were each reacted with glycerol-1-allyl ether to produce **a** or **b**, respectively, (yields ~ 55%). ^{1}H NMR spectra of **a** and **b** showed an increase in the C*H*$_2$C*H*$_2$O peak integration value by two times compared to the corresponding starting material.

Synthesis of 1a-3a and 1b-3b

Pt-catalyzed hydrosilyation of **a** or **b** each with **1-3** effectively produced **1a-3a** and **1b-3b** (yields ≥ 80%). Completion of the reaction was confirmed by IR analysis of **1a-3a** and **1b-3b**, which showed no absorbance peak at ~2125 cm^{-1} due to unreacted Si-H bonds of **1-3**, respectively. ^{1}H NMR spectra of **1a-3a** and **1b-3b** showed the absence of both the Si-H peak (~4.7 ppm) and the vinyl peaks (5.1 – 5.3 ppm) from unreacted **1-3** and **a-b**, respectively.

Thermal Stability of 1a-3a and 1b-3b

The thermal stability of **1a-3a** and **1b-3b** was evaluated in both air and N_2 (Fig. 4.2). As expected, degradation occurred at lower temperatures in air than in N_2.

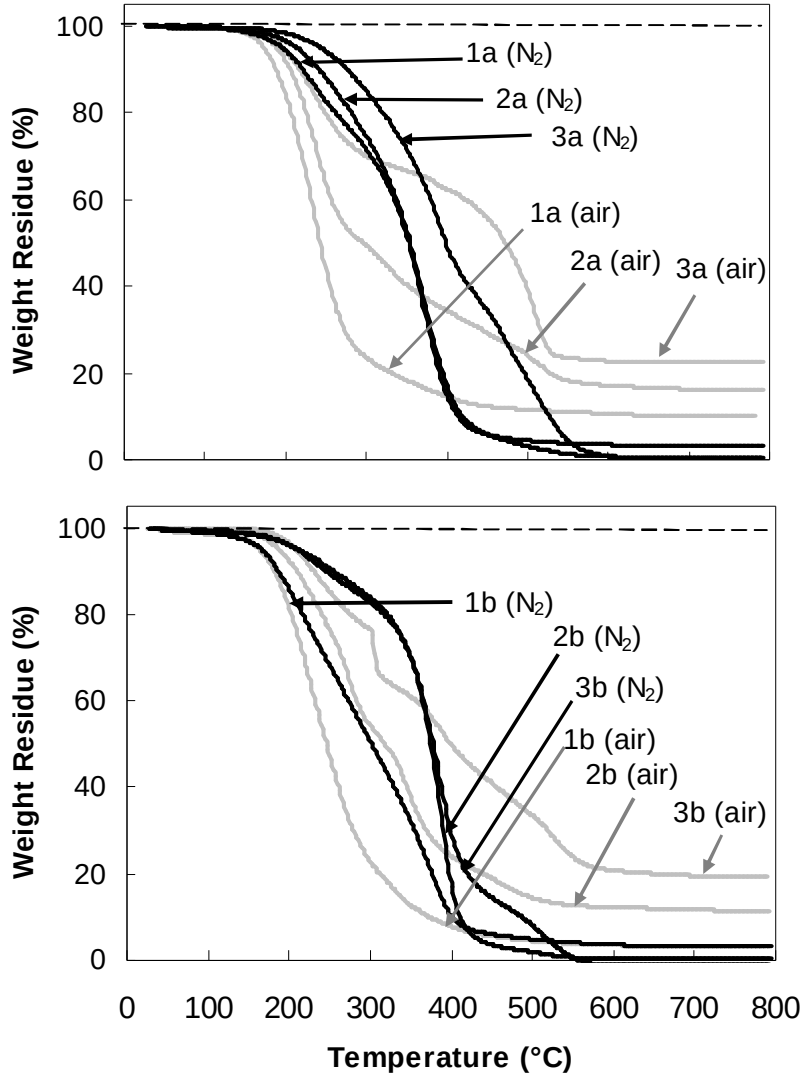

Figure 4.2. Thermal stability of [Top] **1a-3a** and [Bottom] **1b-3b** in N_2 and in air.

The exceptional thermal stability of polysiloxanes compared to other organic polymers is well-known.[134] Thus, thermal stability in both N_2 and air increased with increased siloxane tether length. For a given siloxane tether length, the thermal stability did not significantly vary with PEO segment M_n. Because silica residue is produced

during degradation of siloxanes in air, residue weight was the highest (~25%) for **3a** and **3b** due to the relatively higher siloxane content of the tether.

Preparation of Films

PEO-modified silicone films were prepared by the sol-gel crosslinking of **1a-3a** and **1b-3b** each with **P** in a 2:3 molar ratio to produce a series of 6 films (Fig. 4.1, Table 4.1). Phosphoric acid (H_3PO_4) has been shown to effectively catalyze the sol-gel crosslinking of α,ω-bis(Si-OH)-polydimethylsiloxanes and tetrakis (hydroxyldimethyl siloxane)silane.[84] This is an attractive alternative to the commonly used tin-based catalysts which require long cure schedules and residues which may cause adverse effects in medical applications.

Soxhlet Extraction

Soxhlet extraction was used to measure unreacted sol content or the extent of crosslinking. For these films, ≤ 4 wt% of uncrosslinked material was removed following Soxhlet extraction (Table 4.1). A 2:3 molar ratio of **1a-3a** or **1b-3b** to **P** is stoichiometrically balanced because there are three EtO- groups **(1a-3a and 1b-3b)** and two HO-Si groups (**P**) per respective chain. Thus, the balanced stoichiometry as well as efficacy of the catalyst system and cure schedule produced films with minimal uncrosslinked material.

X-Ray Photoelectron Spectroscopy

The deconvoluted C1s XPS of the surface of the $(EtO)_3Si\text{-}(CH_2)_3\text{-}(OCH_2CH_2)_8\text{-}OCH_3$ grafted microscope slide revealed two peaks: 285.0 eV (C-C) and 286.7 eV (C-O (Fig. 4.3). The peak at 286.7 eV is consistent with the ether carbons of PEO.[92]

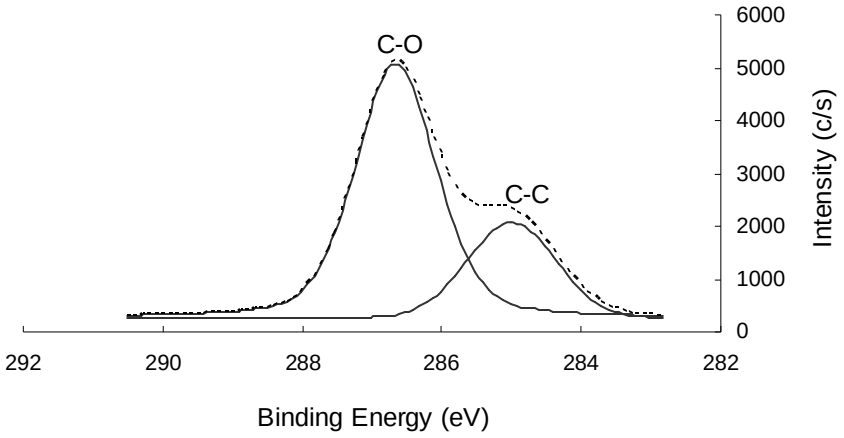

Figure 4.3. High-resolution C1s XPS spectrum of the surface of $(EtO)_3Si\text{-}(CH_2)_3\text{-}(OCH_2CH_2)_8\text{-}OCH_3$ grafted onto a glass microscope slide (**PEO control**). The observed C1s peak was fitted with two Gaussian peaks at binding energies of 285.0 eV (C-C) and 286.7 eV (C-O). The peak at 286.7 eV is consistent with the ether carbons of the PEO.

Thermal Stability of Films

Thermal degradation of films **1a-P-3a-P** and **1b-P-3b-P** was evaluated in air and N_2 (Fig. 4.4). Films generally exhibited similar degradation profiles. In N_2, films degraded by ~ 700 °C whereas films degraded in air by ~550 °C. In air, ~30 – 50% silica residue was produced in all films. Acids are known to catalyze chain equilibration of siloxane (Si-O) bonds into low MW cyclics which are volatile at elevated temperatures.[134] However, the high thermal stabilities and residue weights (in air) of

the films indicate that the presence of catalytic amounts of H_3PO_4 do not contribute to a reduction in their thermal stability.

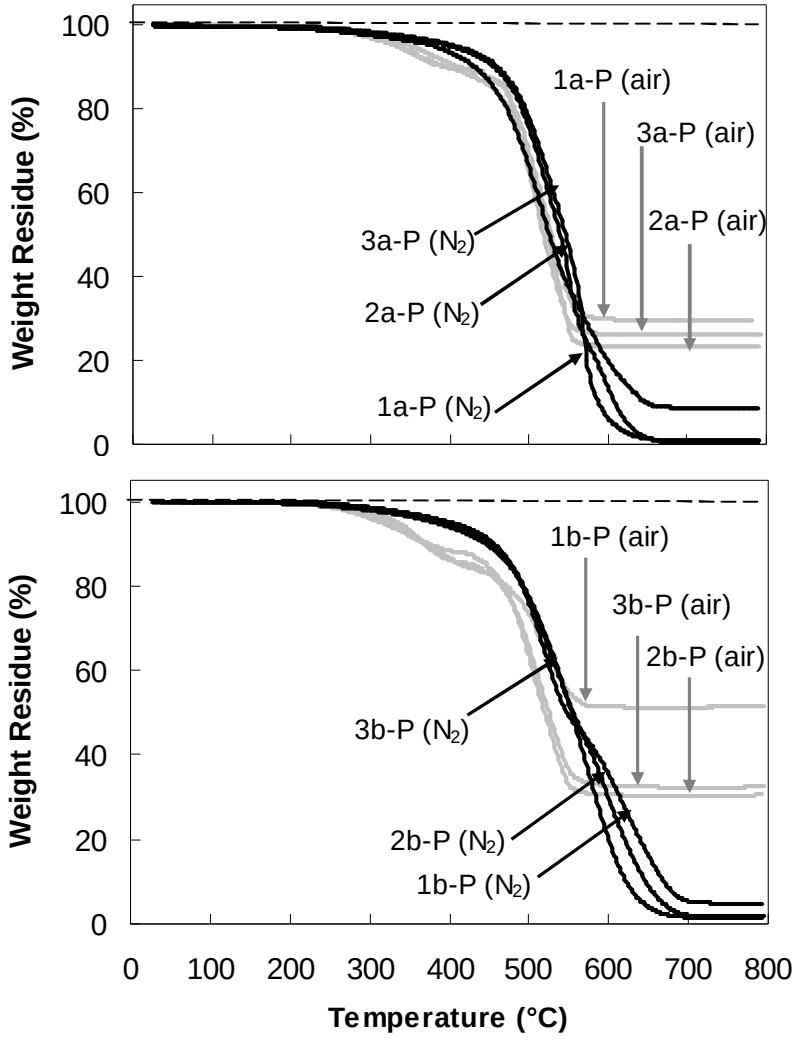

Figure 4.4. Thermal stability of films in N_2 and in air. [Top] **1a-P-3a-P** and [Bottom] **1b-P-3b-P**.

Dynamic Mechanical Analysis

The mechanical properties of all films are summarized in Table 4.2. Films were removed from the microscope slide with a razor blade and use with thickness ~0.6 mm.

The T_g of each film was determined by the maximum of the loss modulus (G").[93] T_gs were low for all films and ranged between -116 to -108 °C. Although A change in T_g was not expected since the distance between crosslinks is maintained at a constant value by the MW of **P**.

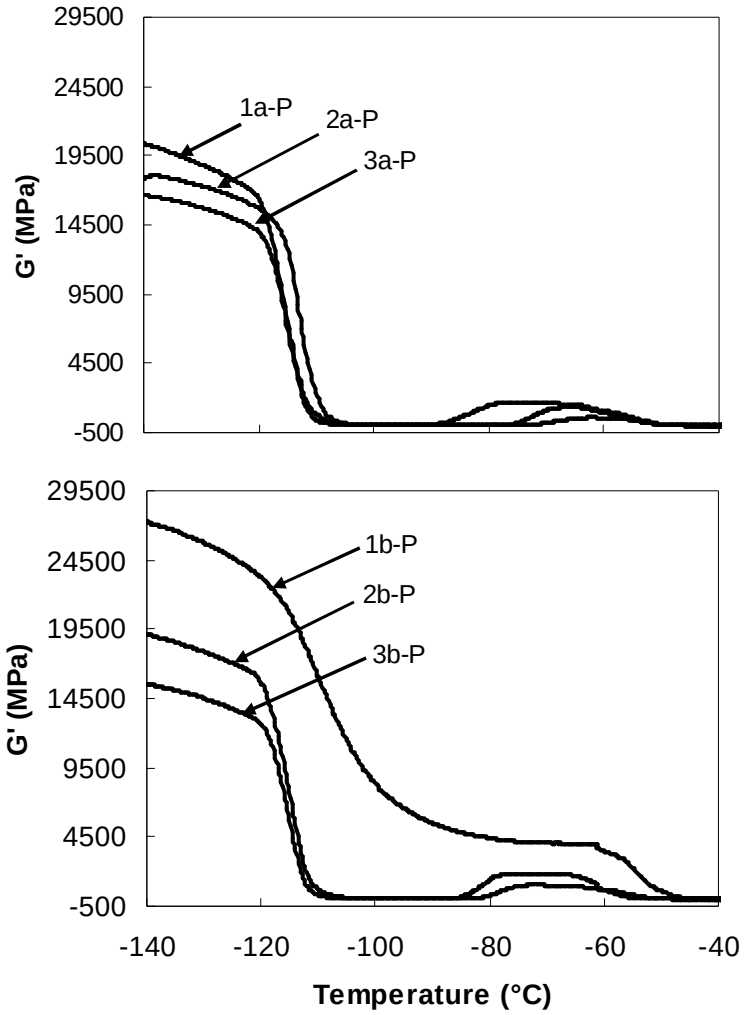

Figure 4.5. Storage moduli (G') of films. [Top] **1a-P**-**3a-P** and [Bottom] **1b-P**-**3b-P**.

Following crosslinking, the PEO segment in all films exists as "dangling free ends". However, due to the low crosslink density of the films, the beta transition temperature (T_β) associated with such free ends is not observed nor is a decrease in T_g with increased siloxane tether length.[135] Lower MW analogues of **P** may be utilized to prepare more densely crosslinked films with higher T_gs which may reveal the aforementioned trends. The storage modulus (G') is related to stiffness or resistance to deformation. For all films, G' increased with decreasing siloxane tether length in the order **PDMS** < **c** < **b** < **a** (Fig.4.5).

Contact Angle Analysis

Contact angle measurements of water droplets on film surfaces are reported in Table 4.2. The hydrophobic silicone control produced a high θ_{static} (at 15 secs) (110°) whereas the θ_{static} (at 15 secs) of the hydrophilic PEO control was low (55°).

For "air equilibrated" films, θ_{static} (at 15 secs) was higher than θ_{static} (at 2 min) which indicates PEO mobilization to the film-water interface (Fig. 4.6). For a given PEO M_n, surface hydrophilicity increased (i.e. θ_{static} decreased) with increased siloxane tether length. θ_{static} (at 2 min) of **1a-P-3-P** (i.e. lower M_n PEO) was lower than that of **1b-P-3b-P** (i.e. higher M_n PEO). Thus, lower M_n PEO segments were more readily driven to the film-water interface. Therefore, longer siloxane tethers and lower PEO M_n favor reorganization of PEO to the film-water interface such that **3a-P** was the most hydrophilic film.

Films were exposed to water for 36 h ("water equilibrated") in order to allow complete equilibration of PEO chains to the film-water interface. As above, for a given PEO M_n, surface hydrophilicity increased (i.e. θ_{static} decreased) with increased siloxane tether length. θ_{static} (at 2 min) of **1a-P-3-P** (i.e. lower M_n PEO) was similarly lower than that of **1b-P-3b-P** (i.e. higher M_n PEO). Thus, lower M_n PEO segments were more readily driven to the film-water interface. Even after equilibrating the films in water, the θ_{static} (at 15 secs) was higher than θ_{static} (at 2 min). This indicates that, from the time it took to remove the film from water and begin contact angle analysis, some PEO chains reorganized below the surface but began reorganizing to the surface after 2 min exposure to water (i.e. while θ_{static} (at 2 min) was measured).

Table 4.2. Mechanical and surface properties of films.

Film	DMA	static contact angles				dynamic contact angles			
		"air equilibrated"		"water equilibrated" 36 h		"air equilibrated"		"water equilibrated" 36 h	
	T_g (°C)	θ_{static} (°) (15 s)	θ_{static} (°) (120 s)	θ_{static} (°) (15 s)	θ_{static} (°) (120 s)	θ_{adv} (°)	θ_{rec} (°)	θ_{adv} (°)	θ_{rec} (°)
1a-P	-115	99 ± 1	92 ± 1	95 ± 1	89 ± 1	99 ± 1	98 ± 1	91 ± 1	89 ± 1
2a-P	-116	92 ± 1	77 ± 1	88 ± 1	78 ± 1	96 ± 1	93 ± 1	87 ± 1	82 ± 1
3a-P	-116	90 ± 1	73 ± 1	86 ± 1	73 ± 1	95 ± 1	93 ± 1	87 ± 1	81 ± 2
1b-P	-109	97 ± 2	94 ± 1	93 ± 2	89 ± 1	98 ± 1	97 ± 1	95 ± 1	93 ± 1
2b-P	-113	95 ± 2	92 ± 1	89 ± 1	87 ± 1	95 ± 1	95 ± 1	90 ± 1	89 ± 1
3b-P	-114	92 ± 1	87 ± 1	88 ± 1	81 ± 1	96 ± 1	92 ± 1	89 ± 1	85 ± 1
PEO*	--	55 ± 1	52 ± 1	--	--	62 ± 1	61 ± 1	--	--
Silicone**	-115	110 ± 1	106 ± 2	110 ± 1	107 ± 1	111 ± 1	108 ± 1	110 ± 1	108 ± 1

** **Silicone** (control) = Dow Silastic T-2 (silicone elastomer) cured on a glass microscope slide. * **PEO** (control) = $(EtO)_3Si\text{-}(CH_2)_3(OCH_2CH_2)_8\text{-}OCH_3$ grafted onto glass.

The change in θ_{static} (at 15 secs) versus θ_{static} (at 2 min) was greatest as the siloxane tether length increased and PEO M_n decreased (i.e. for film **3a-P**). Thus,

reorganization *to* the film-water interface and away from the film-air interface is more favorable with longer siloxane tethers and low PEO M_n.

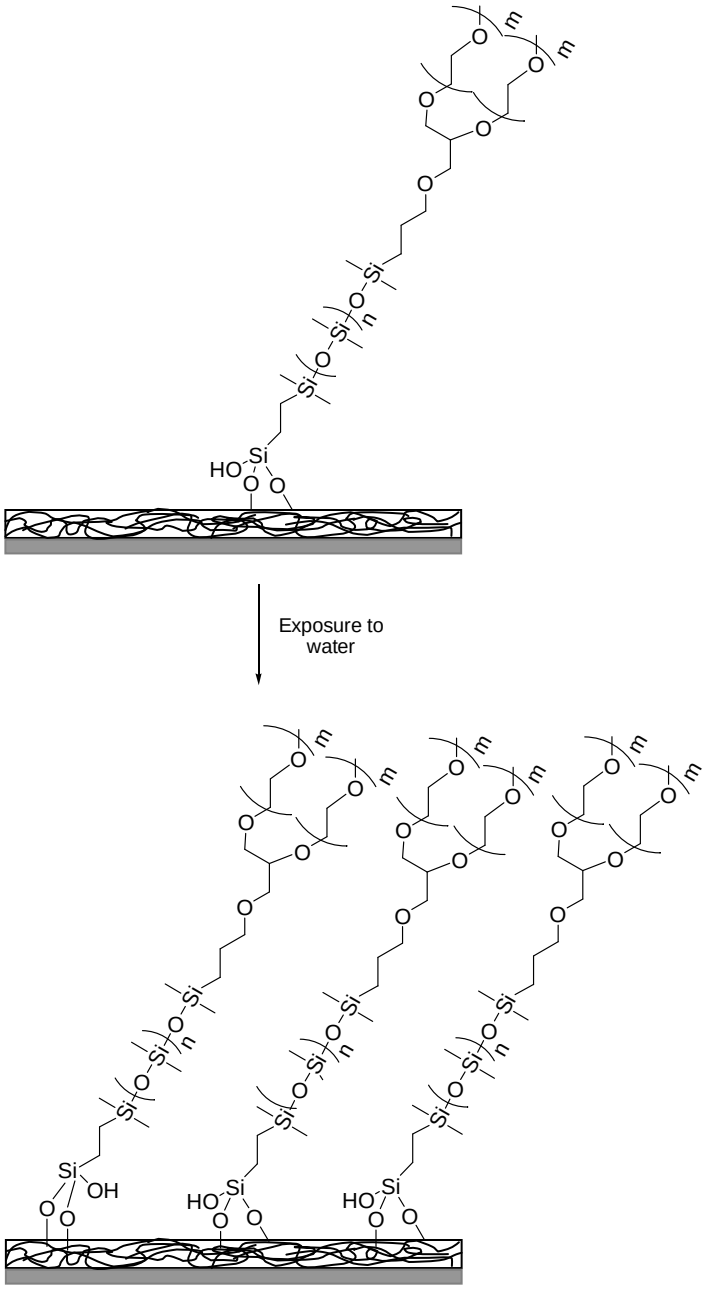

Figure 4.6. Films exposed to an aqueous environment showed reorganization of PEO segments to the surface, thus increasing hydrophilicity. An increase in surface hydrophilicity was observed with increased siloxane tether length. Thus, longer siloxane tethers enhance reorganization of PEO segments to the surface.

Comparison of "water equilibrated" θ_{static} values to those of "air equilibrated" films will indicate how quickly PEO surface equilibration occurs. Notably, θ_{static} (at 2 min) of **1a-P-3a-P** ("air equilibrated") were similar to θ_{static} (at 2 min) ("water equilibrated"). This indicates that the lower M_n PEO could rapidly reorganize to the film water-interface. On the other hand, θ_{static} (at 2 min) of **1b-P-3b-P** ("air equilibrated") were higher than the corresponding θ_{static} (at 2 min) ("water equilibrated"). This similarly confirms that PEO reorganization to the film-water interface increases with siloxane tether length and PEO M_n.

Surface reorganization may also be characterized via dynamic contact angle analysis. θ_{adv} represents the hydrophobic surface characteristics whereas hydrophilicity is reflected by θ_{rec}.[94] Hysteresis ($\theta_{\Delta} = \theta_{adv} - \theta_{rec}$) is typically used as an indicator of surface reorganization. For instance, crosslinked silicone surfaces undergo reorganization in different environments.[56] The presence of Si-CH_3 groups at the film-air interface leads to high θ_{adv}. However, after wetting, polar groups such as Si-O-Si reorganize to the film-water interface to minimize interfacial tension such that $\theta_{rec} < \theta_{adv}$.[56] Generally, θ_{adv} and θ_{rec} decreased with siloxane tether length. However, for all "air-equilibrated" and "water-equilibrated" films, θ_{rec} was not significantly reduced versus the corresponding θ_{adv}. This indicates that PEO segments were unable to reorganize to the film-water interface during the θ_{rec} measurement. The time of exposure to water during the measurement of θ_{rec} was only 15 sec. Thus, this is not sufficient time to allow for PEO reorganization to the surface. Thus, measurement of θ_{static} at 15 sec

versus 2 min and for both “air equilibrated” and “water equilibrated” films better captures the extent of PEO surface reorganization over longer time periods.

Protein Adsorption

Albumin (60%) is the most abundant plasma protein and fibrinogen (4%), also a plasma protein, plays an important role in the process of surface-induced thrombosis. Thus the amounts of BSA and HF proteins adsorbed onto films were analyzed to determine plasma protein resistance (Figs. 4.7 and 4.8, respectively).

Films **1a-P-3a-P** (“air equilibrated”) adsorbed less BSA compared to the silicone control (“air equilibrated”). For films **1b-P-3b-P** (“air equilibrated”), BSA adsorption was similar for all films and the PEO control. For each film, exposing first to PBS for 36 hours (“PBS equilibrated”) reduced the amount of BSA adsorbed. Films **1a-P-3a-P** (“PBS equilibrated”) similarly adsorbed less BSA compared to the silicone control (“PBS equilibrated”). These films (“water equilibrated) exhibited lower θ_{static} (at 2 min) and θ_{rec} values compared to the silicone control. Similar amounts of BSA adsorbed onto films **2a-P** and **3a-P** (“PBS equilibrated”). For films **1b-P-3b-P** (“PBS equilibrated”), BSA adsorption was less compared to the silicone control (“PBS equilibrated”). BSA adsorption was higher for **1b-P** compared to **2b-P**, **3b-P**, and PEO control. BSA adsorption onto **2b-P** and **3b-P** were similar. Thus, BSA adsorption was reduced with increased siloxane tether length, lower PEO M_n, and exposure first to an aqueous environment. These promote reorganization of PEO to the surface (as confirmed by contact angle analysis) to prevent protein adhesion.

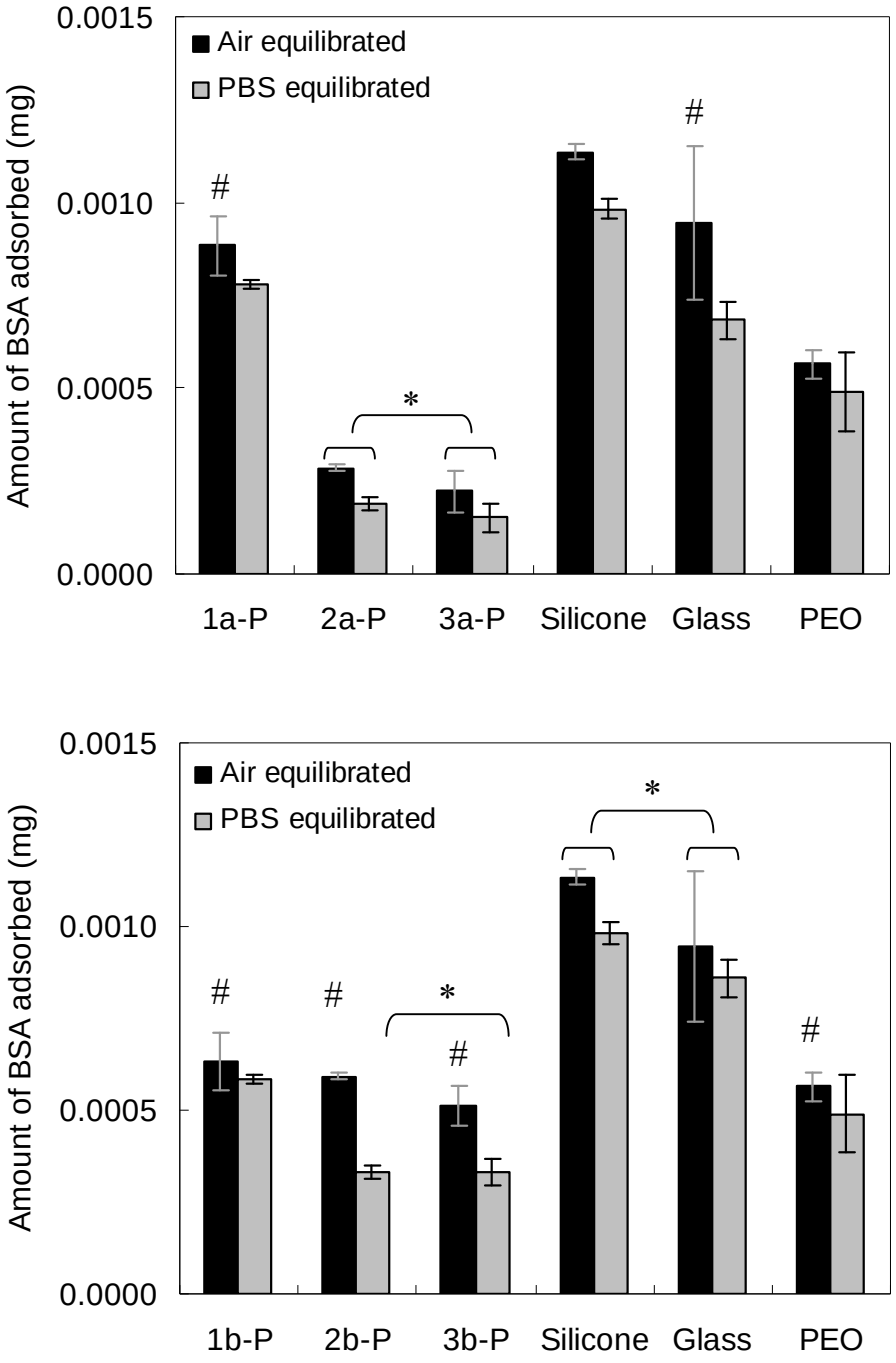

Figure 4.7. Adsorption of BSA protein (3 h) onto [Top] **1a-P-3a-P** and [Bottom] **1b-P-3b-P** after film surfaces were exposed to air (air-equilibrated) and after first equilibrating in PBS for 36 h (PBS-equilibrated). Error bars represent the standard deviation between the fluorescence measurements of three randomly selected regions. For all films, statistical significance was determined by one-way analysis of variance (Holm-Sidak method; $p = 0.05$ unless otherwise noted). * indicates $p < 0.05$ and # indicates $p > 0.05$.

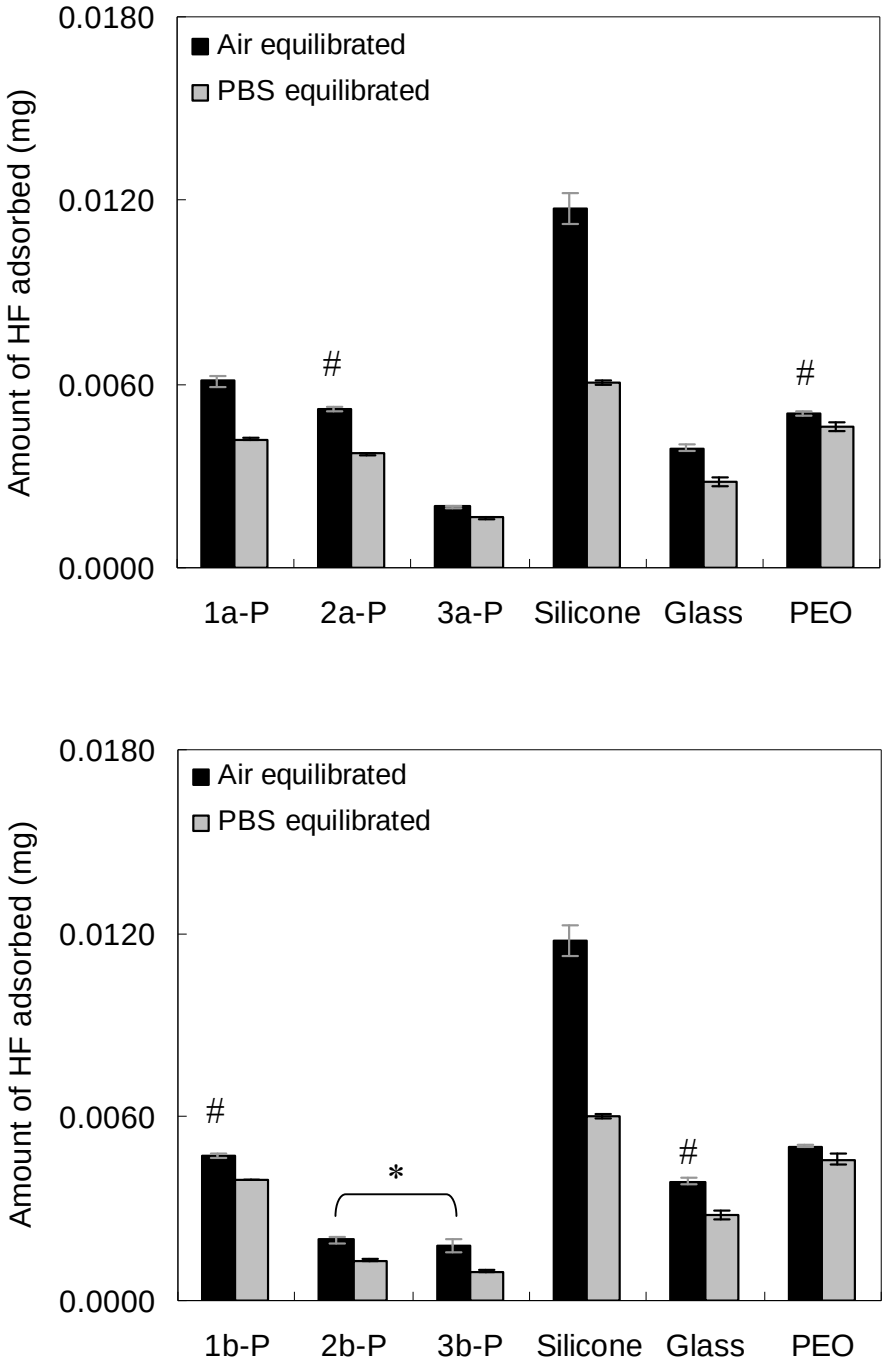

Figure 4.8. Adsorption of HF protein (3 h) onto [Top] **1a-P-3a-P**; and [Bottom] **1b-P-3b-P** after film surfaces were exposed to air (air-equilibrated) and after first equilibrating in PBS for 36 h (PBS-equilibrated). Error bars represent the standard deviation between the fluorescence measurements of three randomly selected regions. For all films, statistical significance was determined by one-way analysis of variance (Holm-Sidak method; $p = 0.05$ unless otherwise noted). * indicates $p < 0.05$ and # indicates $p > 0.05$.

Films **1a-P-3a-P** (“air equilibrated”) adsorbed less HF than silicone and PEO controls (“air equilibrated”) with the exception of film **1a-P** which is the most hydrophobic (θ_{static} at 2 min = 92°). Films **1b-P-3b-P** (“air equilibrated”) also adsorbed less HF than silicone and PEO controls. Films **2b-P** (“air equilibrated”) and **3b-P** (“air equilibrated”) adsorbed similar amounts of HF. For each film, exposing to PBS for 36 hours (“PBS equilibrated”) reduced the amount of HF adsorbed. All films **(1a-P-3a-P** and **1b-P-3b-P)** (“PBS equilibrated”) adsorbed less HF than silicone and PEO controls. For every film, higher amounts of HF was adsorbed compared to BSA which is consistent with previous observations [124, 125]. The enhanced adhesion of HF compared to BSA is attributed to the former’s greater hydrophobicity as well as HF’s rod-like geometry which facilitates reorientation on the adsorbing surface to increase protein-protein interaction and surface concentration. For each film, exposing first to PBS for 36 hours (“PBS equilibrated”) reduced the amount of HF adsorbed. Thus, HF adsorption was reduced with increased siloxane tether length, higher PEO M_n, and exposure first to an aqueous environment. The PEO M_n trend is opposite to that observed for BSA in which, for a given siloxane tether length, more BSA adsorbed onto films based on lower PEO M_n.

4.10 Conclusions

PEO chains were incorporated into silicones via siloxane tethers **(1a-3a** and **1b-3b)** of varying lengths to systematically increase PEO mobilization to the film surface and improve protein resistance. Six unique amphiphilic branched PEO-silanes were

prepared with varying siloxane tether lengths as well as PEO M_n with the general formula α-$(EtO)_3Si(CH_2)_2$-oligodimethylsiloxane$_n$-*block*-$[PEO_m$-$OCH_3]_2$ where n = 0, m = 6 **(1a)**; n = 4, m = 6 **(2a)**; n = 13, m = 6 **(3a)** (i.e. the lower M_n PEO series) and n = 0, m = 12 **(1b)**; n = 4, m = 12 **(2b)**; n = 13, m = 12 **(3b)** (i.e. the higher M_n PEO). H_3PO_4-catalyzed crosslinking of **1a-3a** and **1b-3b** each with α,ω-bis(Si-OH)PDMS (**P**, M_n = 3000 g/mol) in a 2:3 molar ratio of PEO-silane to **P** produced six unique PEO-modified silicone films **(1a-P-3a-P** and **1b-P-3b-P)**. These films exhibited very low T_g and G' values as well as high thermal stability. Film surface hydrophilicity increased with siloxane tether length and decreased PEO M_n particularly after exposure to an aqueous environment as PEO segments were more readily driven to the surface. Adsorption of BSA and HF proteins were similarly reduced if the film was first equilibrated in an aqueous environment (PBS). All PEO-modified films adsorbed less protein than the pure silicone control and resistance to protein adhesion generally increased with siloxane tether length. Thus, adsorption of BSA was reduced with increased siloxane tether length, prior exposure to PBS, and also lower PEO M_n. The first two trends were similarly observed for HF adsorption but the PEO M_n trend is opposite: for given siloxane tether length, more HF adsorbed onto films based on lower PEO M_n. Films based on lower PEO Mn were more hydrophilic and would be expected to adsorb less HF as well. Differences in surface topography of surfaces based on higher versus lower PEO M_n may be the source of this unexpected observation. Coatings constructed with polymer components which undergo phase-segregation have been used to generate complex surface topographies with non-fouling behavior.

CHAPTER V

CONCLUSIONS AND FUTURE DIRECTIONS

5.1 Conclusions

In these studies, crosslinked silicone coatings and surface-grafted coatings were prepared with amphiphilic *linear* PEO-silanes **(a-c)**. Crosslinked silicone coatings were also prepared with *branched* PEO-silanes **(1a-3a** and **1b-3b).** All coatings showed improved resistance to common plasma proteins compared to silicone coatings. Furthermore, protein adsorption generally decreased with siloxane tether length.

For crosslinked PEO-modified silicone coating system based on *linear* PEO-silanes **(a-c)**, longer tethers clearly enhanced PEO reorganization to the film-water interface such that protein adsorption was reduced. Surface reorganization effects were eliminated for surface grafted coatings (on silicon wafer) prepared with *linear* PEO-silanes. Despite a moderate decrease in graft density (σ) and decrease in surface hydrophilicity, surfaces prepared with PEO-silanes having longer siloxane tethers better inhibited protein adsorption. This indicates that longer siloxane tethers enhance the configurational mobility of the PEO segments to better repel proteins.

5.2 Future Directions

In the future studies, in order to obtain more precisely similar graft densities for better comparison, *linear* PEO-silanes (**a-c**) may be grafted with variations to temperature and solvent type. In addition, amphiphilic *branched* PEO-silanes **(1a-3a** and

1b-3b) may be grafted onto oxidized silicon wafers at similar graft densities (Fig. 5.1) and resistance to protein adhesion measured. One may similarly examine the effect of grafting solution concentration, temperature, and solvent type on graft density.

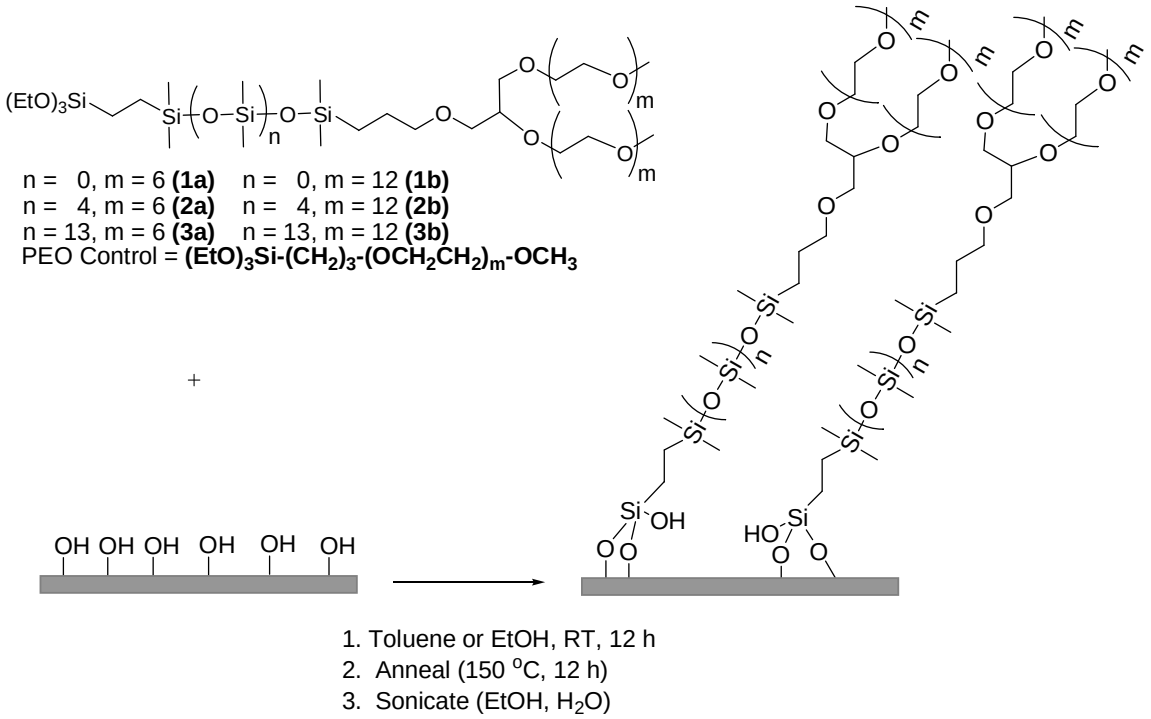

Figure 5.1. Proposed strategy to graft branched amphiphilic PEO-silanes **(1a-3a** and **1b-3b)** onto silicon wafers.

Given the promising in vitro protein adhesion results, one may move forward with additional in vitro experiments to examine platelet adhesion onto both crosslinked PEO-modified silicone coatings and surface grafted coatings prepared with *linear* **(a-c)** and branched **(1a-3a** and **1b-3b)** PEO-silanes**.** Evaluating platelet adhesion may better predict the overall thromboresistance of these materials when used for actual blood-contacting biomedical devices. For static experiments, surfaces may be exposed to

freshly drawn whole blood and the time for thrombus formation will be measured. In dynamic testing, if formed into a tubular geometry in which whole blood can be flowed through, the time it takes for thrombus formation on the surface could also be measured. Finally, in vivo assessment may be performed consisting of placement of both crosslinked and surface-grafted coatings in an animal model (e.g. mouse) to determine hemocompatibility and extent of thrombus formation.

REFERENCES

1. Park K, Kim HS, Dewanjee MK, Eigler NL. In vitro and in vivo studies of PEO-grafted blood-contacting cardiovascular prostheses. J Biomater Sci Polym Ed 2000;11(11):1121-1134.

2. Baier RE. Intial events in interactions of blood with foreign surface. J Biomed Mater Res 1969;3:191-206.

3. Jo S, Park K. Surface modification using silanated poly(ethylene glycol)s. Biomaterials 2000;21:605-616.

4. Ikada Y. Surface modification of polymers for medical applications. Biomaterials 1994;15(10):725-736.

5. Michel R, Pasche S, Textor M, Castner DG. Influence of PEG architecture on protein adsorption and conformation. Langmuir 2005;21:12327-12332.

6. Brash JL. Exploiting the current paradigm of blood-material interactions for the rational design of blood-compatible materials. J Biomater Sci Polym Ed 2000;11(11):1135-1146.

7. Baglin TP. Heparin induced thrombocytopenia thrombosis (HIT/T) syndrome: diagnosis and treatment. J Clin Pathol 2001;54:272-274.

8. Ratner BD. The catastrophe revisited: blood compatibility in the 21st century. Biomaterials 2007;28:5144-5147.

9. Tami C, Puig M, Reepmeyer JC, Ye H, D'Avignon DA, Buhse L, et al. Inhibition of Taq polymerase as a method for screening heparin for oversulfated contaminants. Biomaterials 2008;29:4808-4814.

10. Sarkar S, Sales KM, Hamilton G, Seifalian AM. Addressing thromobogenicity in vascular graft reconstruction. J Biomed Mater Res Part B: Appl Biomat 2006:100-108.

11. Hester J, Banerjee P, Won Y, Akthakul A, Acar M, Mayes A. Preparation of protein-resistant surfaces on poly(vinylidene fluoride) membranes via surface segregation. Macromolecules 2000;32:1643-1650.

12. Gudapati SC, Finlay JA, Callow JA, Callow ME, Wooley KL. Hyperbranched fluoropolymer and linear poly(ethylene glycol) based amphiphilic crosslinked networks as efficient antifouling coatings: an insight into the surface

compositions, topographies, and morphologies. PolySci Part A: Polym Chem 2004;42:6193-8207.

13. Rosenman JE, Kempezinski RF, Pearce WH. Kinetics of endothelial cell seeding. J Vasc Surg 1985;2:778-785.

14. Conklin BS, Richter ER, Kreutziger KL, Zhong D-S, Chen C. Development and evaluation of a novel decellularized vascular xenograft. Med Eng and Phys 2002;24:173-183.

15. Knetsch MLW, Aldenhoff YBJ, Hanssen HHL, Koole LH. A novel synthetic vascular prosthesis: effect of plasma protein adsorption on blood-and cyto-compatibility. Mat-wiss u Werkstofftech 2006;37(6):509-515.

16. Szilagi DE, Smith RF, Elliott JP, Allen HM. Long term behavior of a Dacron arterial substrate. Annals of Surgery 1965;162:453-477.

17. Sofia SJ, Premnath V, Merrill EW. Poly(ethylene oxide) grafted onto silicone surfaces: grafting density and protein adsorption. Macromolecules 1998;31:5059-5070.

18. Sjalander A, Jansson JH, Bergqvist D, Eriksson H, Carlberg B, Svensson P. Efficacy and safety of anticoagulant prophylaxis to prevent venous thromboembolism in acutely ill medical inpatients: a meta analysis. J Intern Med 2008;263:52-60.

19. Chen M-C, Tsai H-W, Lai W-Y, Mi F-L, Liu C-T, Wong H-S, et al. Rapidly self-expandable polymeric stents with shape-memory property. Biomacromolecules 2007;8:2774-2780.

20. Giessen WJ, Lincoff MA, Schwartz RS, Beusekom HM, Serruys PW, Holmes DR, et al. Marked inflammatory sequelae to implantation of biodegradable and nondegradable polymers in porcine coronary arteries. Amer Heart Assc 1996;94:1690-1697.

21. Kukreja N, Onuma Y, Deamen J, Serruys PW. The future of drug-eluting stents. Pharmacological Research 2008;57:171-180.

22. Mani G, Feldman MD, Patel D, Agrawal CM. Coronary stents: a materials perspective. Biomaterials 2007;28:1689-1710.

23. Giessen WJvd, A ML, Schwartz RS, Beusekom HMMv, Serruys PW, Holmes DR, et al. Marked inflammatory sequelae to implantation of biodegradable and nondegradable polymers in porcine coronary arteries. Amer Heart Assc 1996;94:1690-1697.

24. Cooper SL, Visser SA, Hergenrother RW, Lamba NMK. Biomaterials science: an introduction to materials in medicine. San Diego, CA: Elsevier Academic Press,2004.

25. Murphy JG, Schwartz RS, Edwards WD, Camrud AR, Vlietstra RE, Holmer DR. Percutaneous polymeric stents in porcine coronary artery initial experience with polyethylene terephthalate stents. Circulation 1992;86(5):1596-1604.

26. Burke SE, Kuntz RE, Schwartz LB. Zotarolimus (ABT-578) eluting stents. Adv Drug Delivery Rev 2006;58:437-446.

27. Kheriaklan GM, Roedersheimer LR, Arbaugh JJ, Newmark KJ, King LR. Comparison of autogenous fistula versus expanded polytetrafluoroethylene graft fistula for angioaccess in hemodialysis. Am J Surg 1986;152:238-243.

28. Ascher E, Prasad G, Hingorani A. Changes in the practice of angioaccess surgery: impact of dialysis outcome and quality initiative recommendations. J Vasc Surg 2000;31:84-92.

29. Dolmatch BL, Castaneda F, McNamara TO, Zemel G, Lieber M, Cragg AH. Synthetic dialysis shunts: thromobolysis with the cragg thrombolytic brush catheter. Radiology 1999;213(1):180-184.

30. Smits HFM, Van PPR, Isselt JWV, Mali W, Koomans HA, Blankestijn PJ. Pulmonary embolism after thrombolysis of hemodialysis grafts. J Am Soc Nephrol 1997;8:1458-1461.

31. Beathard GA. Percutaneous therapy of vascular access dysfunction: optimal management of access stenosis and thrombosis. Seminars in Dialysis 1994;7(3):165-167.

32. Asif A. Reducing the morbidity of tunneled hemodialysis catheters: a symposium. Seminars in Dialysis 2008;21(6).

33. Ash SR. Advances in tunneled central venous catheters for dialysis: design and performance. Seminars in Dialysis 2008;21(6):504-515.

34. Dwyer A. Surface-treated catheters: a review. Seminars in Dialysis 2008;21(6):542-546.

35. Elbert DL, Hubbel JA. Surface treatments of polymers for biocompatibility. Annu Rev Mater Sci 1996;26:365-394.

36. Knoll D, Hermans J. Polymer-protein interactions. J Biol Chem 1983;258:5710-5715.

37. Jeon SI, Andrade JD. Protein-surface interactions in the presence of polyethylene oxide. J Colloid Interface Sci 1991;142:159-166.

38. McPherson T, Kidane A, Szleifer I, Park K. Prevention of protein adsorption by tethered poly(ethylene oxide) layers: experiments and single-chain mean-field analysis. Langmuir 1998;14:176-186.

39. Murthy R, Cox CD, Hahn MS, Grunlan MA. Protein-resistant silicones: incorporation of poly(ethylene glycol) via siloxane tethers. Biomacromolecules 2007;8:3244-3252.

40. Pale-Grosdemange C, Simon ES, Prime KL, Whitesides GM. Formation of self-assembled monolayers of chemisorption of derivatives of oligo(ethylene glycol) of structure $HS(CH_2)_{11}(OCH_2CH_2)_mOH$. J Am Chem Soc 1991;113:12-20.

41. Prime KL, Whitesides GM. Adsorption of proteins onto surfaces containing end-attached oligo(ethylene oxide): a model system using self-assembled monolayers. J Am Chem Soc 1993;115:10714-10721.

42. Huang Y-W, Gupta VK. Influence of polymer flux and chain length on adsorption of poly(ethylene oxide) on physically heterogeneous surfaces. Langmuir 2002;18:2280-2287.

43. Desai NP, Hubbell JA. Solution technique to incorporate poly(ethylene oxide) and other water-soluble polymers into surfaces of polymeric biomaterials. Biomaterials 1991;12:144-153.

44. Desai NP, Hubbell JA. Surface physical interpenetrating networks of poly(ethylene terephthalate) and poly(ethylene oxide) with biomedical applications. Macromolecules 1992;25:226-332.

45. Dyke MEV, Clarson SJ, Arshady R. Silicone biomaterials. An introduction to polymeric biomaterials: London: Citus Books,2003.

46. Curtis J, Colas A. Medical applications of silicones in biomaterials science. San Diego, CA: Elsevier Academic Press,2004.

47. Hron P. Hydrophilisation of silicone rubber for medical applications. Polym Int 2003;52:1531-1539.

48. Bartzoka V, McDermott MR, Brook MA. Protein-silicone interactions. Adv Mater 1999;11:257-259.

49. Pitt WG, Park K, Cooper SL. Sequential protein adsorption and thrombus deposition on polymeric biomaterials. J Colloid Interface Sci 1986;111:343-362.

50. Sharma CP. Blood-compatible materials: a perspective. J Biomaterials Appl 2001;15:359-381.

51. Zhang H, Annich GM, Miskulin J, Osterholzer K, Merz SI, Bartlett RH, et al. Nitric oxide releasing silicone rubbers with improved blood compatibility: preparation, characterization, and in vivo evaluation. Biomaterials 2002;23:1485-1494.

52. Yao K, Huang X-D, Huang X-J, Xu Z-K. Improvement of the surface biocompatibility of silicone intraocular lens by the plasma-induced tethering of phospholipid moieties. J Biomed Mater Res 2006;78A:684-692.

53. Abbasi F, Mirzadeh H, Katbab A-A. Modification of polysiloxane polymers for biomedical applications: a review. Polym Int 2001;50:1279-1287.

54. Gombotz WR, Guanghui W, Horbett TA, Hoffman AS. Protein adsorption to poly(ethylene oxide) surfaces. J Biomed Mater Res 1991;25:1547-1562.

55. Lee JH, Lee HB, Andrade JD. Blood compatiblity of polyethylene oxide surfaces. Prog Polym Sci 1995;20:1043-1079.

56. Owen MJ, Smith PJ. Plasma treatment of polydimethylsiloxanes. J Adhes Sci Technol 1994;8:1063-1075.

57. Kuznetsov AY, Bagryansky VA, Perov AK. The surface relaxation of glow discharge-treated silicone polymer. J Appl Poly Sci 1995;57:201-207.

58. Xia Y, Whitesides GM. Soft lithography. Angew Chem Int Ed 1998;37:550-575.

59. Graubner V-M, Jordan R, Nuyken O, Schnyder B, Lippert T, Kotz R, et al. Photochemical modification of cross-linked poly(dimethylsiloxane) by irradiation at 172 nm. Macromolecules 2004;37:5936-5943.

60. Efimenko K, Wallace WE, Genzer J. Surface modification of Sylguard-184 poly(dimethylsiloxane) networks by ultraviolet and ultraviolet/ozone treatment. J Colloid Interface Sci 2002;254:306-315.

61. Efimenko K, Crowe JA, Manias E, Schwark DW, Fischer DA, Genzer J. Rapid formation of soft hydrophilic silicone elastomers. Polymer 2005;46:9329-9341.

62. Sui G, Wang J, Lee C-C, Lu W, Lee SP, Leyton JV, et al. Solution-phase surface modification in intact poly(dimethylsiloxane) microfluidic channels. Anal Chem 2006;78:5543-5551.

63. Brook MA. Silicon in organic, organometallic, and polymer chemistry. New York, NY: John Wiley & Sons, Inc.,2000.

64. Papra A, Bernard A, Juncker D, Larsen NB, Michel B, Delamarche E. Microfluidic networks made of poly(dimethylsiloxane), Si, and Au coated with polyethylene glycol for patterning proteins onto the surface. Langmuir 2001;17:4090-4095.

65. Delamarche E, Donzel C, Kamounah FS, Wolf H, Geissler M, Stutz R, et al. Microcontact printing using poly(dimethylsiloxane) stamps hydrophilized by poly(ethylene oxide) silanes. Langmuir 2003;19:8749-8758.

66. Chen H, Zhang Z, Chen Y, Brook MA, Sheardown H. Protein repellant silicone surfaces by covalent immobilization of poly(ethylene oxide). Biomaterials 2005;26:2391-2399.

67. Chen H, Brook MA, Sheardown H. Silicone elastomers for reduced protein adsorption. Biomaterials 2004;25:2273-2282.

68. Chen H, Brook MA, Chen Y, Sheardown H. Surface properties of PEO-silicone composites: Reducing protein adsorption. J Biomater Sci Polym Ed 2005;16:531-548.

69. Jeon SI, Lee JH, Andrade JD, DeGennes PG. Protein-surface interactions in the presence of polyethylene oxide. J Colloid Interface Sci 1991;142:149-158.

70. Osterberg E, Bergstrom K, Holmberg K, Riggs JA, Alstine JMV, Schuman TP, et al. Comparison of polysaccharide and poly(ethylene glycol) coatings for reduction of protein adsorption on polystyrene surfaces. Coll Surf A: Phys Eng Aspects 1993;77:159-169.

71. Desai NP, Hubbel JA. Solution technique to incorporate polyethylene oxide and other water soluble polymers into surfaces of polymeric biomaterial. Biomaterials 1991;12:144-153.

72. Berstrom K, Holmber K, Safranj A, Hoffman AS, Edgell MJ, Kozlowski A, et al. Reduction of fibrinogen adsorption on PEG-coated polystyrene surfaces. J Biomed Mater Res 1992;26:779-790.

73. Desai NP, Hubbell JA. Biological responses to polyethylene oxide modified polyethylene terephthalate surfaces. J Biomed Mater Res 1991;25:829-843.

74. Prime KL, Whitesides GM. Self-assembled organic monolayers: model systems for studying protein adsorption of proteins at surfaces. Science 1991;252:1164-1166.

75. Mark JE. Silicon-containing polymers. Washington DC, American Chemical Society,1990.

76. Lane TH, Burns SA. Silica, silicon and silicones...unraveling the mystery: Berlin: Springer,1996.

77. Crivello JV, Bi D. Regioselective hydrosilylations. I. The hydrosilylation of a,w-dihydrogen functional oligopolydimethylsiloxanes with 3-vinyl-7-oxabicyclo[4.1.0]heptane J Polym Sci Part A: Polym Chem 1993;31:2563-2572.

78. Crivello JV, Bi D. Regioselective hydrosilylations. II. The synthesis of silicon-hydrogen functional compounds. J Polym Sci Part A: Polym Chem 1993;31:2729-2737.

79. Crivello JV, Bi D. Regioselective hydrosilylations. III. The synthesis and polymerization of ambifunctional silicon-containing epoxy-monomers. J Polym Sci Part A: Polym Chem 1993;31:3109-3119.

80. Crivello JV, Bi D. Regioselective hydrosilylations. IV. The synthesis and polymerization of monomers containing epoxy and alkoxysilane groups. J Polym Sci Part A: Polym Chem 1993;31:3121-3132.

81. Grubb WT, Osthoff RO. The mechanism of acid- and base-catalyzed equilibration of siloxanes. J Am Chem Soc 1954;76:5190-5197.

82. Mabry JM, Paulasaari JK, Weber WP. Synthesis of poly(silyl ethers) by Ru-catalyzed hydrosilylation. Polymer 2000;41:4423-4428.

83. Hooper R, Lyons LJ, Mapes MK, Schumacher D. Highly conductive siloxane polymers. Macromolecules 2001;34:931-936.

84. Gadda TM, Kus E, Mansfeld F, Finlay JA, Callow JA, Callow ME, et al. Synthesis and properties of Q-silicon crosslinked siloxane networks: H_3PO_4-catalyzed sol-gel dehydration/crosslinking of a,w-bis(hydroxy)oligodimethylsiloxanes with tetrakis(hydroxydimethyl)silane. J Polym Sci Part A: Polym Chem 2006;44:2237-2247.

85. Gudipati CS, Finlay JA, Callow JA, Callow ME, Wooley KL. The antifouling and fouling-release performance of hyperbranched fluoropolymer (HBFP)-poly(ethylene glycol) (PEG) composite coatings evaluated by adsorption of biomacromolecules and the green fouling alga Ulva. Langmuir 2005;21:3044-3053.

86. Nagashima H, Tatebe K, Ishibashi T, Sakaklbara J, Itoh K. (PPH3)3RhCl-catalyzed hydrosilylation of unsaturated molecules by 1,2-bis(dimethylsilyl)ethane: unprecedented rate differences between two Si-H bonds. Organometallics 1989;8:2495-2496.

87. Dvornic PR. Thermal properties of polysiloxanes. Dordrecht: Kluwer Academic Publishers,2000.

88. Johnston E, Bullock S, Uilk J, Gatenholm P, Wynne KJ. Networks from alpha, omega-dihydroxypoly(dimethylsiloxane) and tridedecafluoro-1,1,2,2-tetrahydrooctyl)triethoxysilane:surface microstructures and surface characterization. Macromolecules 1999;32:8173-8182.

89. Uilk J, Bullock S, Johnston E, Meyers SA, Merwin L, Wynne KJ. Surface science of elastomeric coatings prepared from alpha, omega-dihydroxy poly(dimethylsiloxane) and (tridecafluoro-1,1,2,2-etrahydrooctyl)triethoxysilane: surface microstructures and surface characterization. Macromolecules 2000;33:8791-8801.

90. Alam MS, Hussain R, Seth PK, Srivastava SP. Age and sex related behavior changes induced by dibutyltin-dilaurate in rats. Bull Environ Contam Toxicol 1993;50:286-292.

91. Cihlar J. Hydrolysis and polycondensation of ethyl silicates. 2. Hydrolysis and polycondensation of ETS40 (ethyl silicate 40). Coll Surf A: Phys Eng Aspects 1993;70:253-268.

92. Moreau O, Portella C, Massicot F, Herry JM, Riquet AM. Adhesion of polyethylene glycol and quaternary ammonium salt-grafted silicon surfaces: influences of physiochemical properties. Surf Coat Tech 2007;201:5994-6004.

93. Sperling LH. Introduction to physical polymer science. New York, NY: John Wiley & Sons,2001.

94. Davies J, Nunnerley CS, Brisley AC, Edwards JC, Finalyson SD. Use of dynamic contact angle profile analysis in studying the kinetics of protein removal from steel, glass, polytetrafluoroethylene, polypropylene, ethylenepropylene rubber, and silicone surfaces. J Colloid Interface Sci 1996;182:437-443.

95. Johnson RE, Dettre RH. Contact angle hysteresis III: Study of an idealized heterogeneous surface. J Phys Chem 1964;68:1744-1750.

96. Kenausis GL, Voros J, Elbert DL, Huang N, Hofer R, Ruiz-Taylor L, et al. Poly(L-lysine)-G-poly(ethylene glycol) layers on metal oxide surfaces: attachment mechanism and effect of architecture on resistance of protein adsorption. J Phys Chem B 2000;104:3298-3309.

97. Lee JH, Lee HB, Andrade JD. Blood compatibility of polyethylene oxide surfaces. Prog Polym Sci 1995;20:1043-1079.

98. Oesterberg E, Bergstrom K, Holmberg K, Riggs JA, Alstine JMV, Schuman TP, et al. Comparison of polysaccharide and poly(ethylene glycol) coatings for reduction of protein adsorption on polystyrene surfaces. Coll Surf A: Phys Eng Aspects 1993;77:159-169.

99. Prime KL, Whitesides GM. Adsorption of proteins onto surfaces containing end-attached oligo(ethylene oxide): a model system using self-assembled monolayers. J Am Chem Soc 1993;115:10714.

100. Ruiz-Taylor LA, Martin TL, Zaugg GG, Witte K, Indermuhle P, Nock S, et al. Monolayers of derivatived poly(L-lysine)-grafted poly(ethylene glycol) on metal oxides as a class of biomolecular interfaces. Proceedings of the National Academy of Sciences of the United States of America 2001;3:852-857.

101. Kato K, Uchida E, Kang E-T, Uyama Y, Ikada Y. Polymer surfaces with graft chains. Prog Polym Sci 2003;28:209-259.

102. Bhattacharya A, Misra BN. Grafting: a versatile means to modify polymers: techniques, factors, and applications. Prog Polym Sci 2004;29:767-814.

103. Uyama Y, O.K.Kat, Ikada Y. Surface modification of polymers by grafting. Adv Polym Sci 1998;137:1.

104. Fukai R, Dakwa PHR, Chen W. Strategies toward biocompatible artificial implants: grafting of functionalized poly(ethylene glycol) to poly(ethylene terephthalate) surfaces. J PolySci Part A: Polym Chem 2004;42:5389-5400.

105. Abbasi F, Mirzadeh H, Katbab A-A. Modification of polysiloxanes for biomedical applications: a review. Polym Int 2001;50:1279-1287.

106. Papra A, Bernard A, Juncker D, Larsen NB, Michel B, Delamarche E. Microfluidic networks made of poly(dimethylsiloxane), Si, and Au coated with polyethylene glycol for patterning proteins onto surfaces. Langmuir 2001;17:4090-4095.

107. Ferguson GS, Chaudhury MK, Biebuyck HA, Whitesides GM. Monolayers in disordered substrates: self-assembly of alkyltrichlorosilanes on surface-modified polyethylene and poly(dimethyl siloxanes). Macromolecules 1993;26:5870-5875.

108. Unsworth LD, Tun Z, Sheardown H, Brash JL. Chemisorption of thiolated poly(ethylene oxide) to gold: surface chain densities measured by ellipsometry and neutron reflectometry. J Colloid Interface Sci 2005;281:112-121.

109. Zhu X-Y, Jun Y, Staarup DR, Major RC, Danielson S, Boiadjiev V. Grafting Of high-density poly(ethylene glycol) monolayers on Si(111). Langmuir 2001;17:7798-7803.

110. Vezenov DV, Mayers BT, Wolfe DB, Whitesides GM. Integrated fluorescent light source for optofluidic applications. Appl Phys Lett 2005;86:411041-411043.

111. Branch DW, Wheeler BC, Brewer GJ, Leckband DE. Long-term stability of grafted polyethylene glycol surfaces for use with microstamped substrates in neuronal cell culture. Biomaterials 2001;22:1035-1047.

112. Grange JDL, Markham SL, Kurkjian CR. Effect of surface hydration on the deposition of silane monolayers on silica. Langmuir 1993;9:1749-1753.

113. Kohli P, Blanchard GJ. Applying polymer chemistry to interfaces: layer-by-layer and spontaneous growth of covalently bound multilayers. Langmuir 2000;16:4655-4661.

114. Sharma S, Johnson RW, Desai TA. Ultrathin poly(ethylene glycol) films for silicon-based microdevices. Applied Surface Science 2003;206:218-229.

115. Zdyrko B, Klep V, Luzinov I. Synthesis and surface morphology of high-density poly(ethylene glycol) grafted layers. Langmuir 2003;2003(19):10179-10187.

116. Feng W, Brash JL, Zhu S. Non-biofouling materials prepared by atom transfer radical polymerization grafting of 2-methacryloloxyethyl phosphorylcholine: separate effects of graft density and chain length on protein repulsion. Biomaterials 2006;27:847-855.

117. Allen C, Santos ND, Gallagher R, Chiu GNC, Shu Y, Li WM. Controlling the physical behavior and biological performance of liposome formulations through use of surface grafted poly(ethylene glycol). Bioscience Reports 2002;22:225-250.

118. Soong R, Macdonald PM. PEG molecular weight and lateral diffusion of PEG-ylated lipids in magnetically aligned bicelles. Biochim Biophys Acta 2007;1768:1805-1814.

119. Hristova K, Needham D. Phase behavior of lipid/polymer mixture in aqueous medium. Macromolecules 1995;28:991-1002.

120. Harder P, Grunze M, Dahint R, Whitesides GM, Laibinis PE. Molecular conformation in oligo(ethylene glycol)-terminated self-assembled monolayers on

gold and silver surfaces determines their ability to resist protein adhesion. J Phys Chem B 1998;102:426-436.

121. Groll J, Ademovic Z, Ameringer T, Klee D, Moeller M. Comparison of coatings from reactive star shaped PEG-s*tat*-PPG prepolymers and grafted linear polymers PEG for biological and medical applications. Biomacromolecules 2005;6:956-962.

122. Wei J, Ravn DB, Gram L, Kingshott P. Stainless steel modified with poly(ethylene glycol) can prevent protein adsorption but not bacterial adhesion. Colloids and Surf B: Biointerfaces 2003;32:275-291.

123. Seah MP, Qiu JH, Cumpson PJ, Castle JE. Simple method of depth profiling (stratifying) contamination layers, illustrated by studies on stainless steel. Surface and Interface Analysis 1994;21:336-341.

124. Roach P, Farrar D, Perry CC. Interpretation of protein adsorption: surface-induced conformational changes. J Amer Chem Soc 2005;127:8168-8173.

125. Absolom DR, Zingg W, Neumann AW. Protein adsorption to polymer particles: Role of surface properties. J Biomed Mater Res 1987;21:161-171.

126. Lin FYH, Policova Z, Yueh HK, Moy E, Neumann AW. Application of freezing front technique and axissymmetric drop shape analysis-profile for the determination of surface tension of adsorbed proteins. Coll Surf B: Biointerfaces 1993;1:23-32.

127. Horbett TA. Principles underlying the role of adsorbed plasma proteins in blood interactions with foreign materials. Cardiovasc Pathol 1993;2:137S-148S.

128. Anderson JM, Ziats NP, Azeez A, Brunstedt MR, Stack S, Bonfield TL. Protein adsorption and macrophage activation on poly(dimethyl siloxane) and silicone rubber. J Biomater Sci Polym Ed 1995;7:159-169.

129. Bodas D, Khan-Malek C. Formation of more stable hydrophilic surfaces of PDMS by plasma and chemical treatments. Microelectronic Eng 2006;83:1277-1279.

130. Irvine DJ, Mapes AM, Stija SK, Barker JG, Sofia-Allgor SJ, Griffith LG. Comparison of tethered start and linear poly(ethylene oxide) for control of biomaterials and surface properties. J Biomed Mater Res 1997;40:498-509.

131. Irvine DJ, Mayes AM, Griffith-Cima L. Self-consistent field analysis of grafted star polymers. Macromolecules 1996;29:6037-6043.

132. Hooper R, Lyons LJ, Moline DA, West R. Novel siloxane polymers as polymer electrolytes for high energy density lithium batteries. Silicone Chem 2002;1:121-128.

133. Allcock HR, O'Connor SJM, Omeijer DL, Napierala ME, Cameron CG, Kuharcik SE, et al. Effect of oligo(ethyleneoxy)cyclotriphosphazenes, tetraglyme, and other small molecules on the ionic conductivity of the poly[bis(methoxyethyoxyethyoxy)phosphazene] (MEEP)/lithium triflate system. Electrochim Acta 1998;43:1143.

134. Dvornic PR. Thermal properties of polysiloxanes. Dordrecht: Kluwer Academic Publishers,2000.

135. Menard KP. Dynamic mechanical analysis. A practical introduction. Boca Raton, FL: Kluwer Academic Publishers,1999.

APPENDIX A

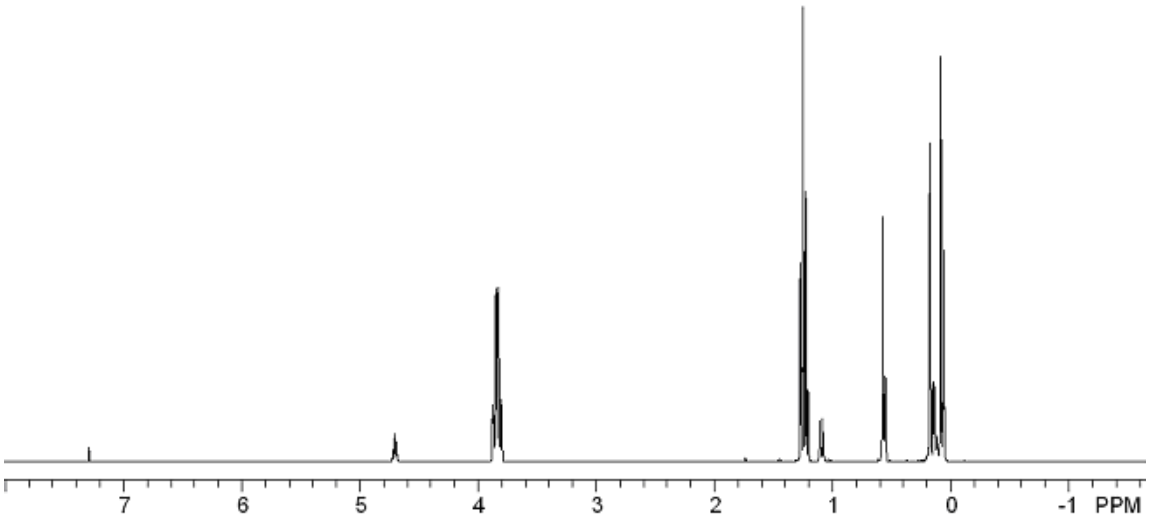

^{1}H NMR of α-triethoxysilylethyl-ω-silane-ODMS$_0$ (**1**)

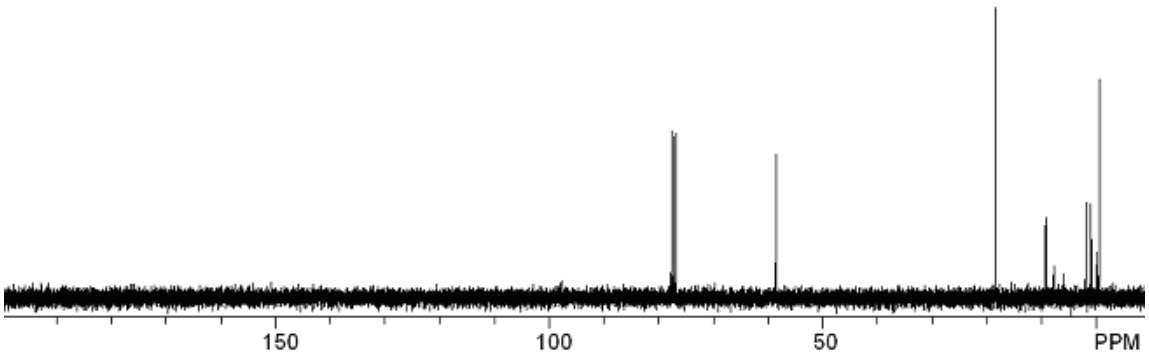

^{13}C NMR of α-triethoxysilylethyl-ω-silane-ODMS$_0$ (**1**)

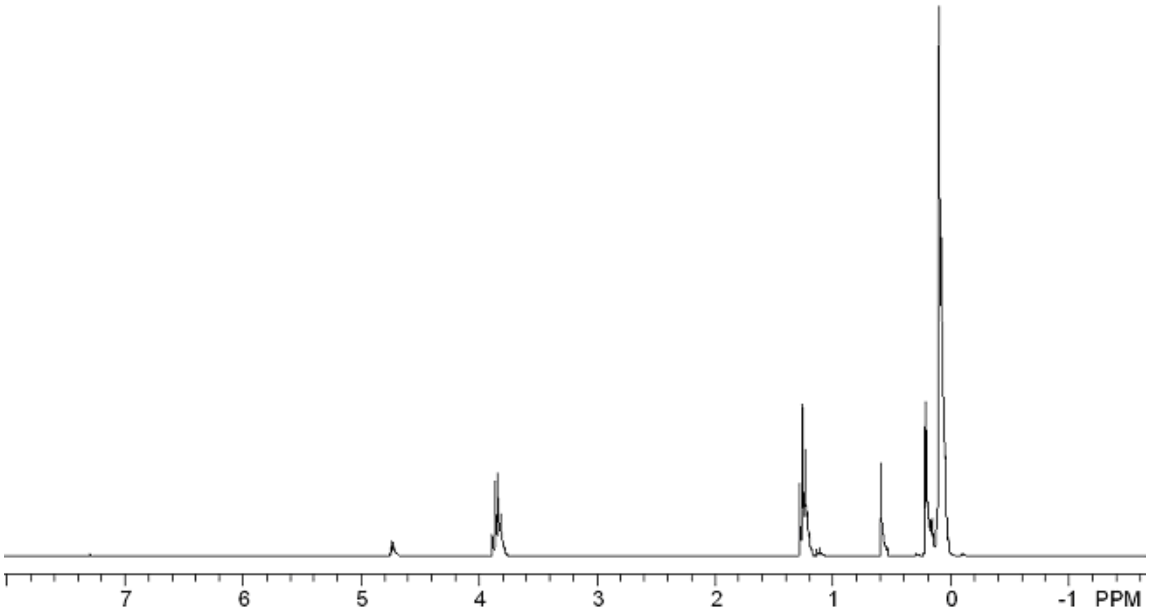

^{1}H NMR of α-triethoxysilylethyl-ω-silane-ODMS$_4$ (**2**)

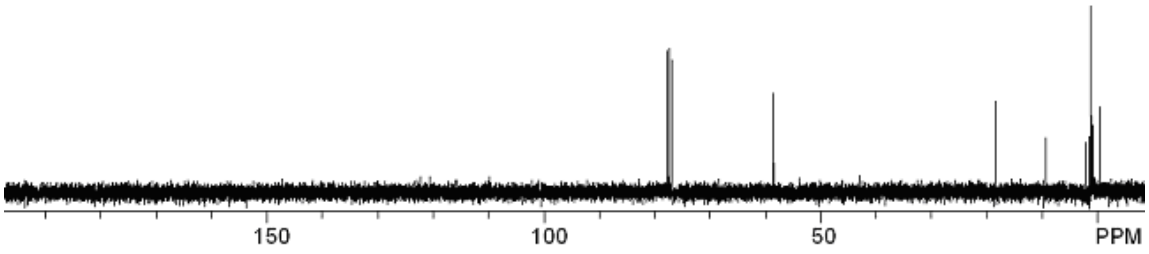

^{13}C NMR of α-triethoxysilylethyl-ω-silane-ODMS$_4$ (**2**)

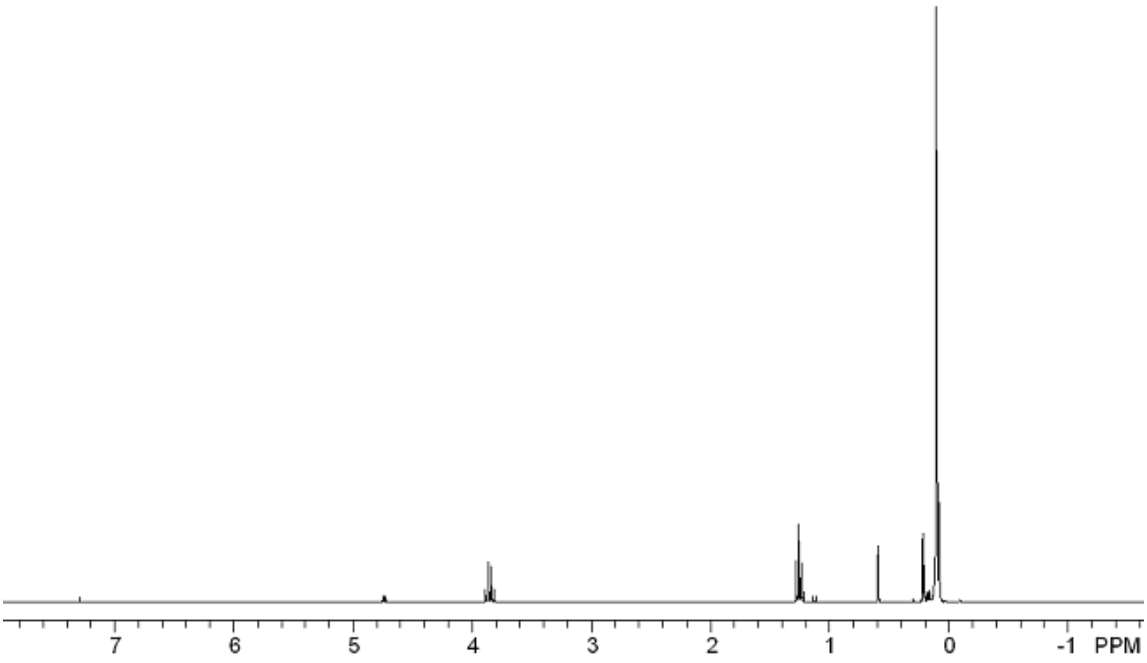

^{1}H NMR of α-triethoxysilylethyl-ω-silane-ODMS$_{13}$ (**3**)

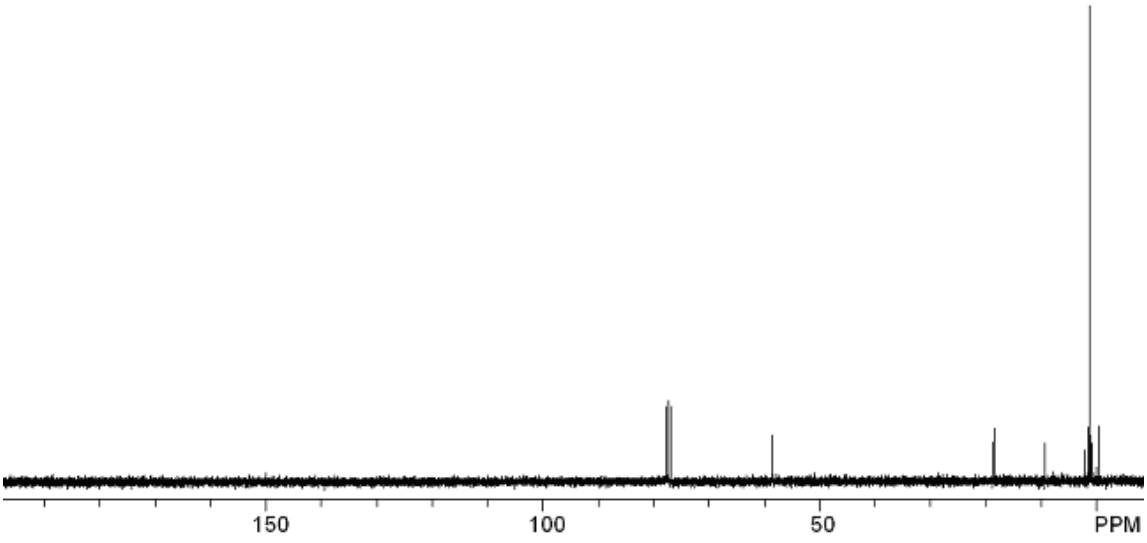

^{13}C NMR of α-triethoxysilylethyl-ω-silane-ODMS$_{13}$ (**3**)

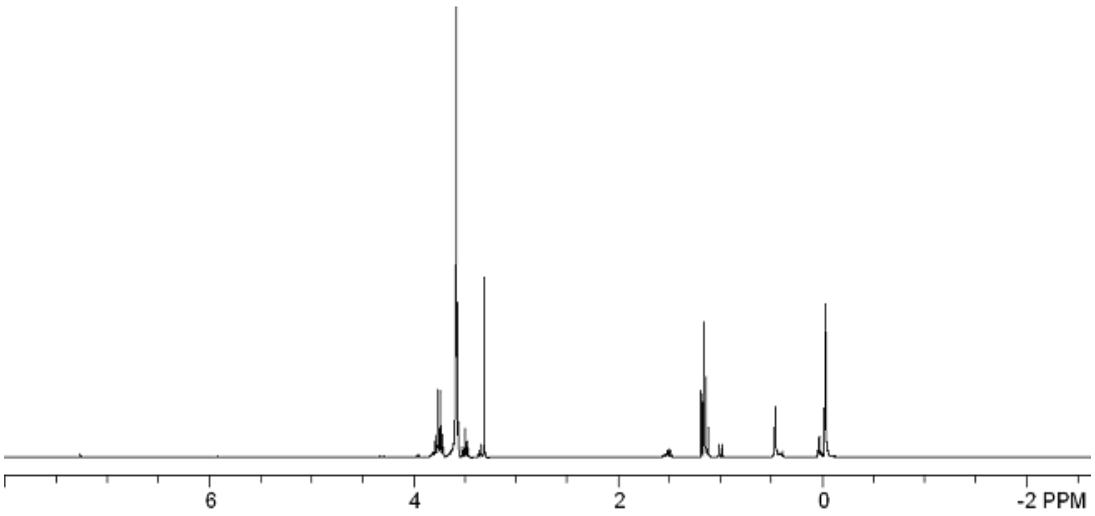

^{1}H NMR of triethoxysilylethyl-ODMS$_{0}$-*block*-poly(ethylene oxide)$_{8}$ (**a**)

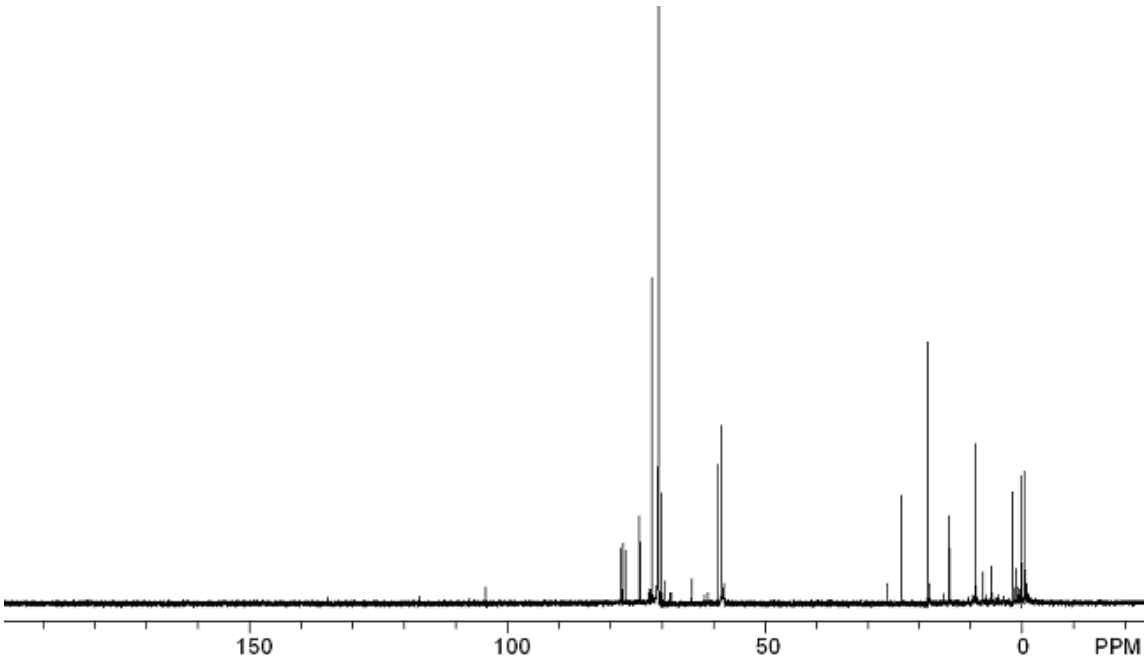

^{13}C NMR of triethoxysilylethyl-ODMS$_{0}$-*block*-poly(ethylene oxide)$_{8}$ (**a**)

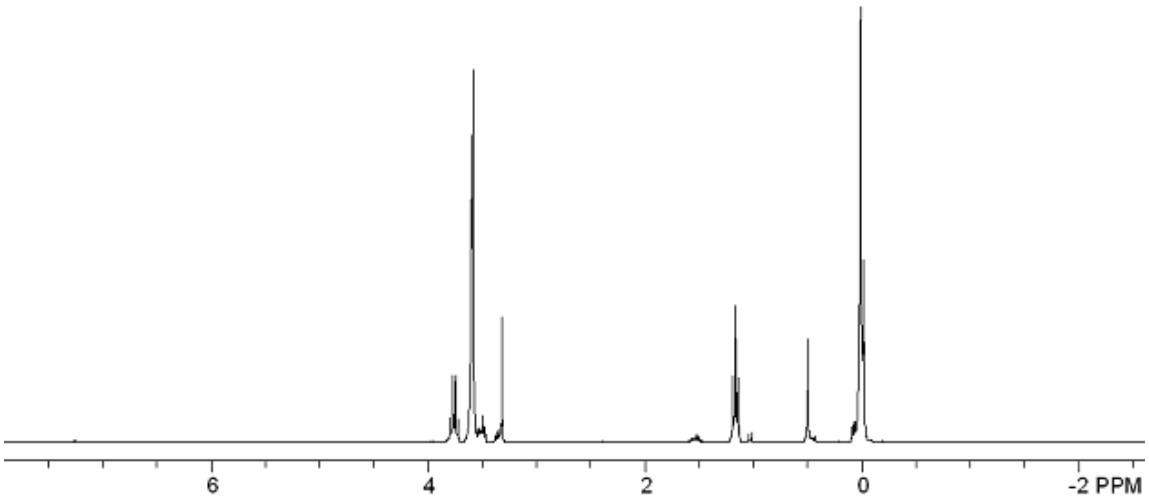

^{1}H NMR of triethoxysilylethyl-ODMS$_4$-*block*-poly(ethylene oxide)$_8$ (**b**)

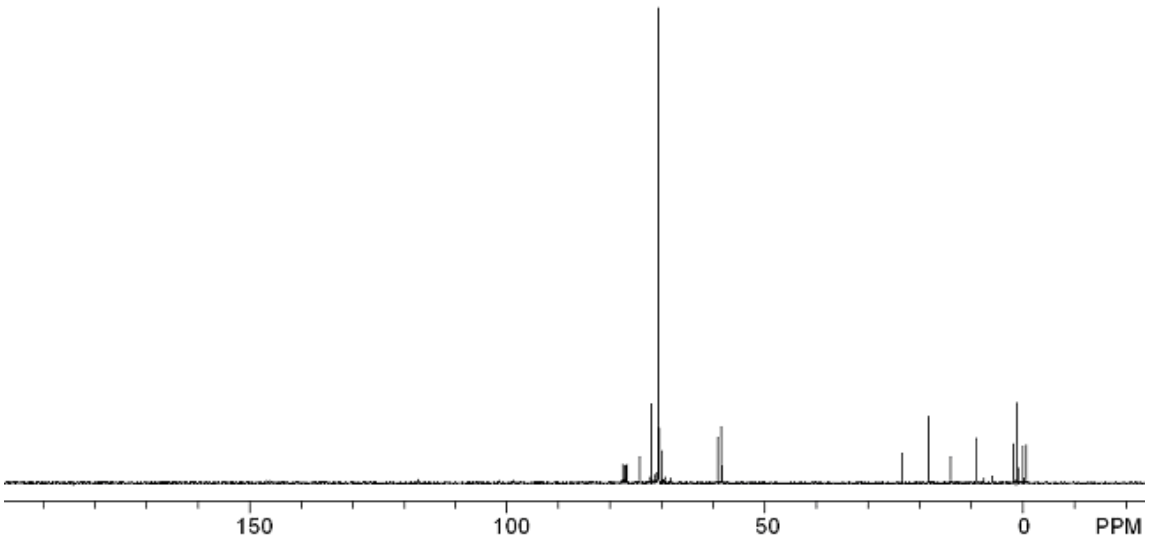

^{13}C NMR of triethoxysilylethyl-ODMS$_4$-*block*-poly(ethylene oxide)$_8$ (**b**)

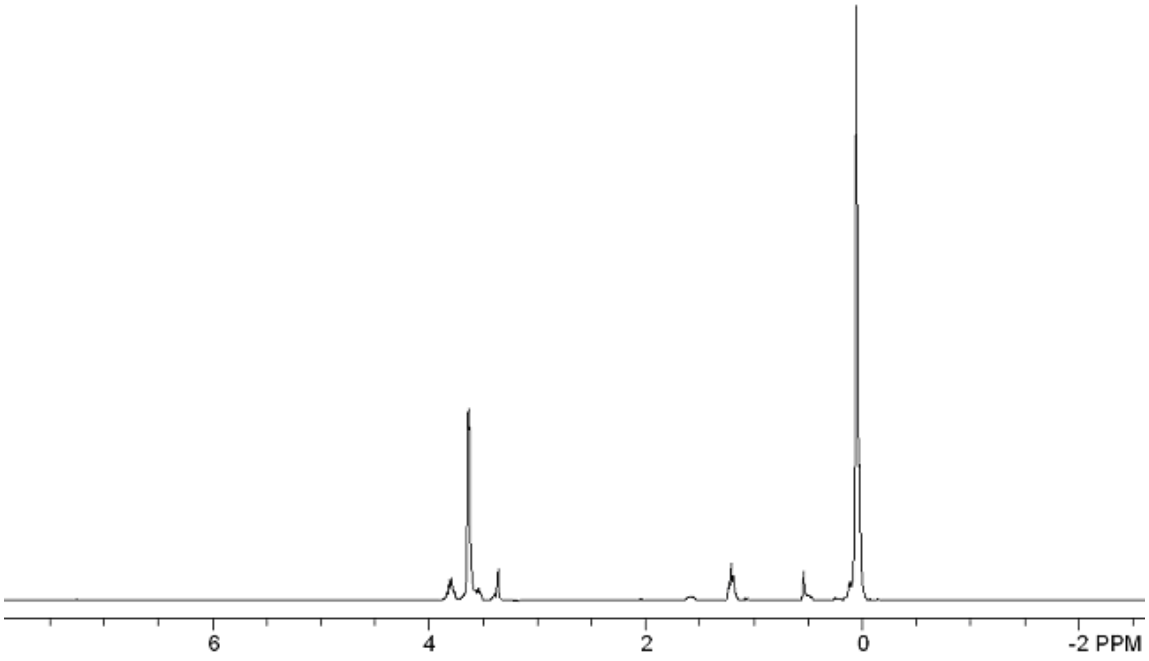

^{1}H NMR of triethoxysilylethyl-ODMS$_{13}$-*block*-poly(ethylene oxide)$_{8}$ (**c**)

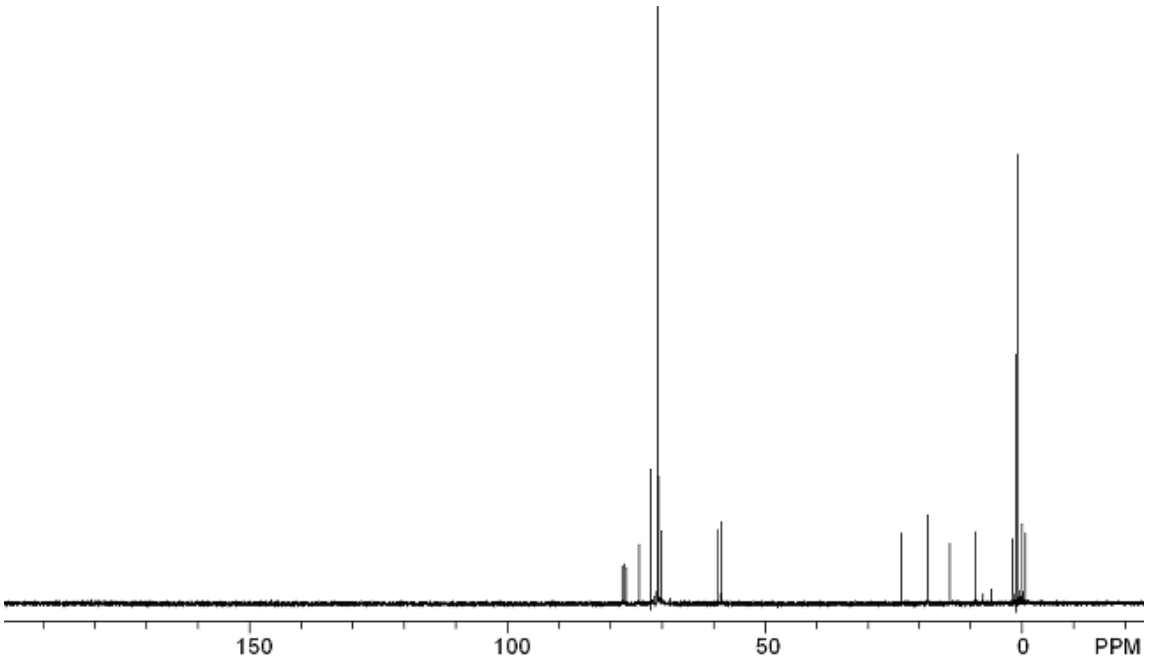

^{13}C NMR of triethoxysilylethyl-ODMS$_{13}$-*block*-poly(ethylene oxide)$_{8}$ (**c**)

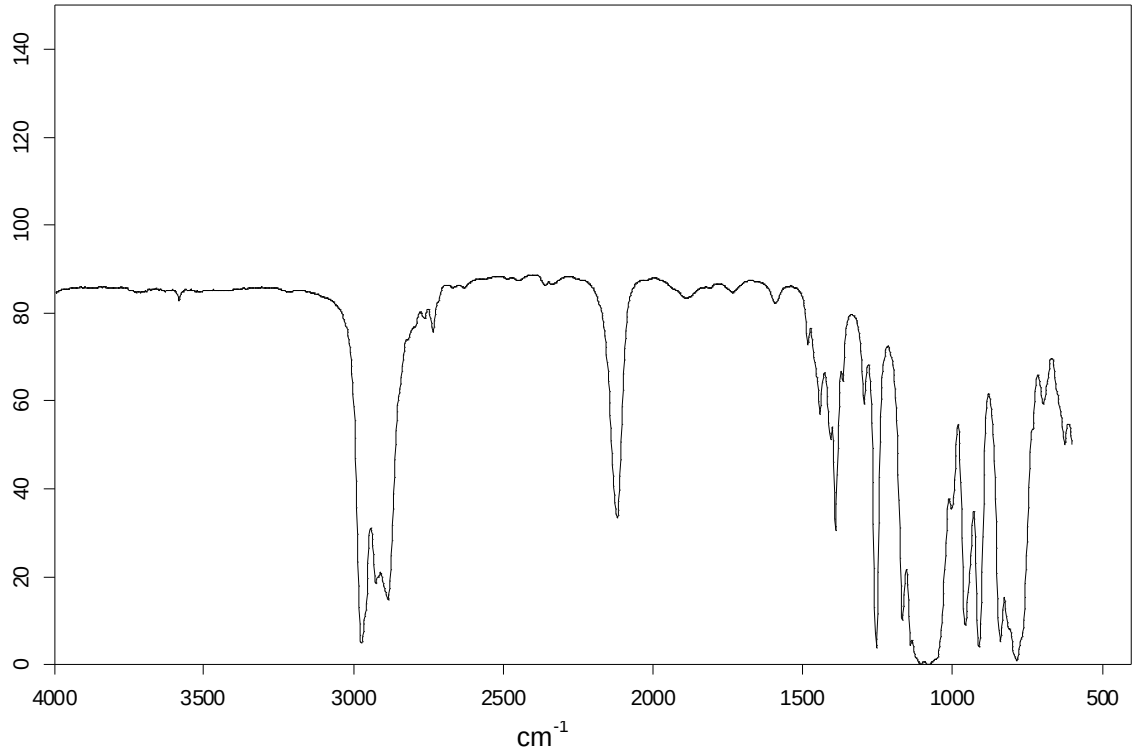

IR of α-triethoxysilylethyl-ω-silane-ODMS$_0$ (**1**)

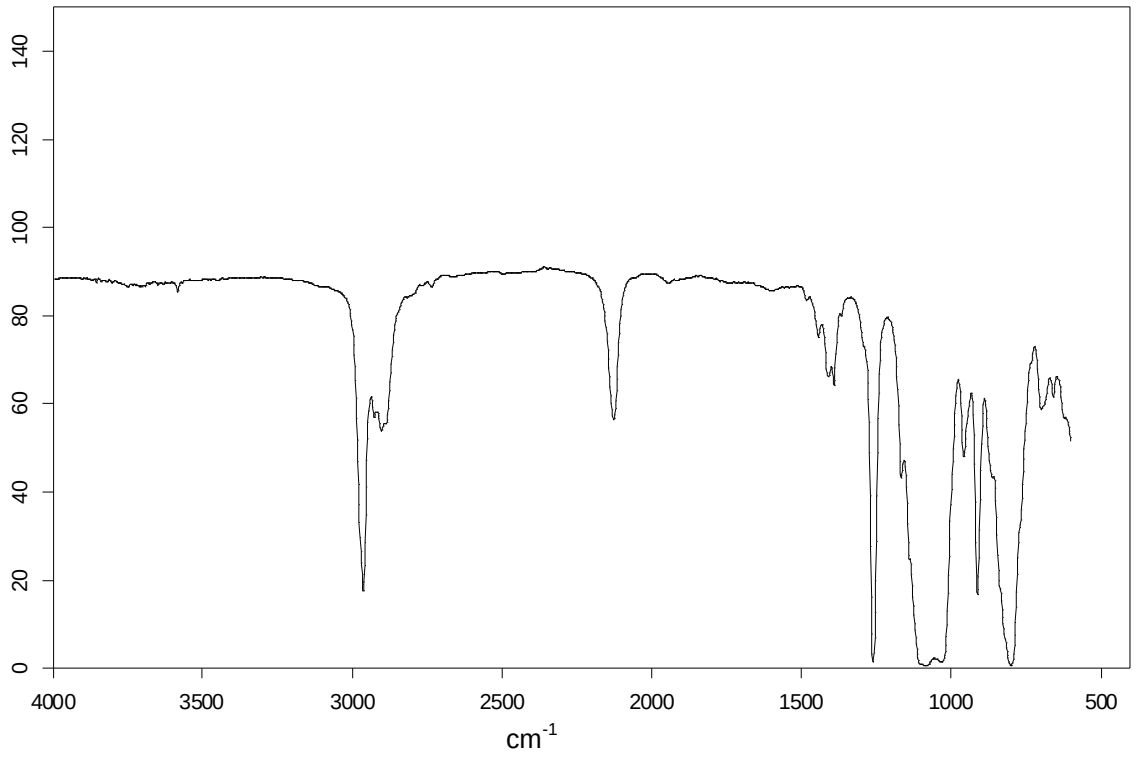

IR of α-triethoxysilylethyl-ω-silane-ODMS$_4$ (**2**)

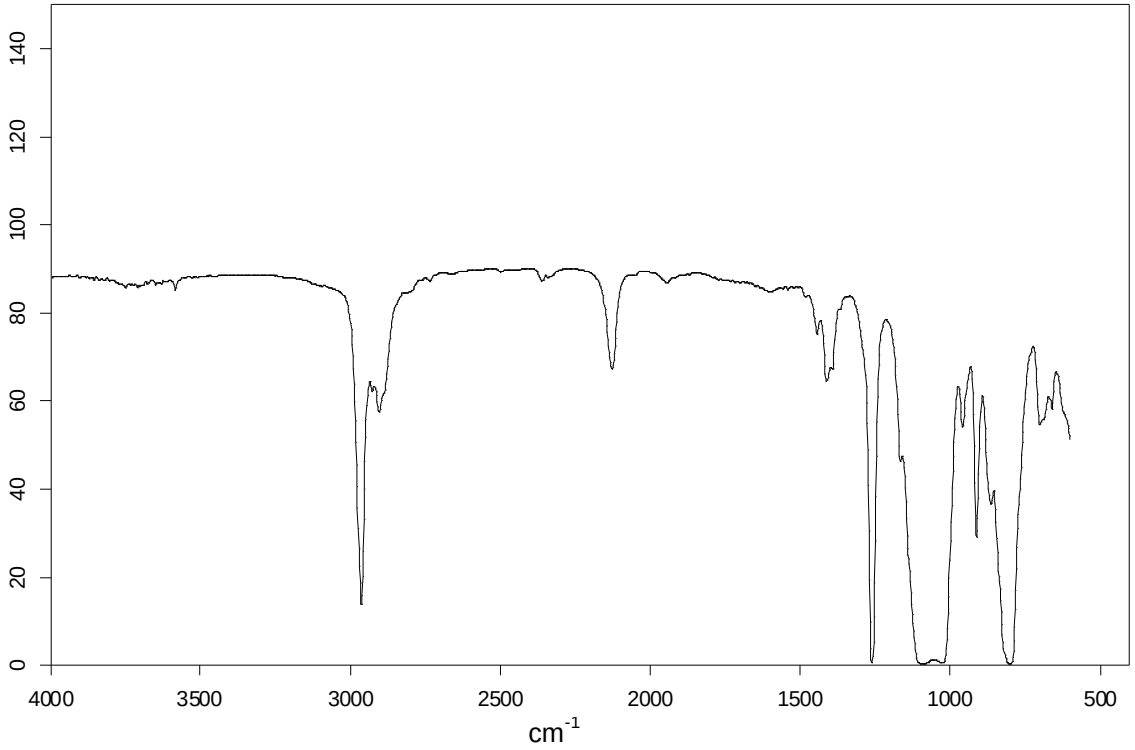

IR of α-triethoxysilylethyl-ω-silane-ODMS$_{13}$ (**3**)

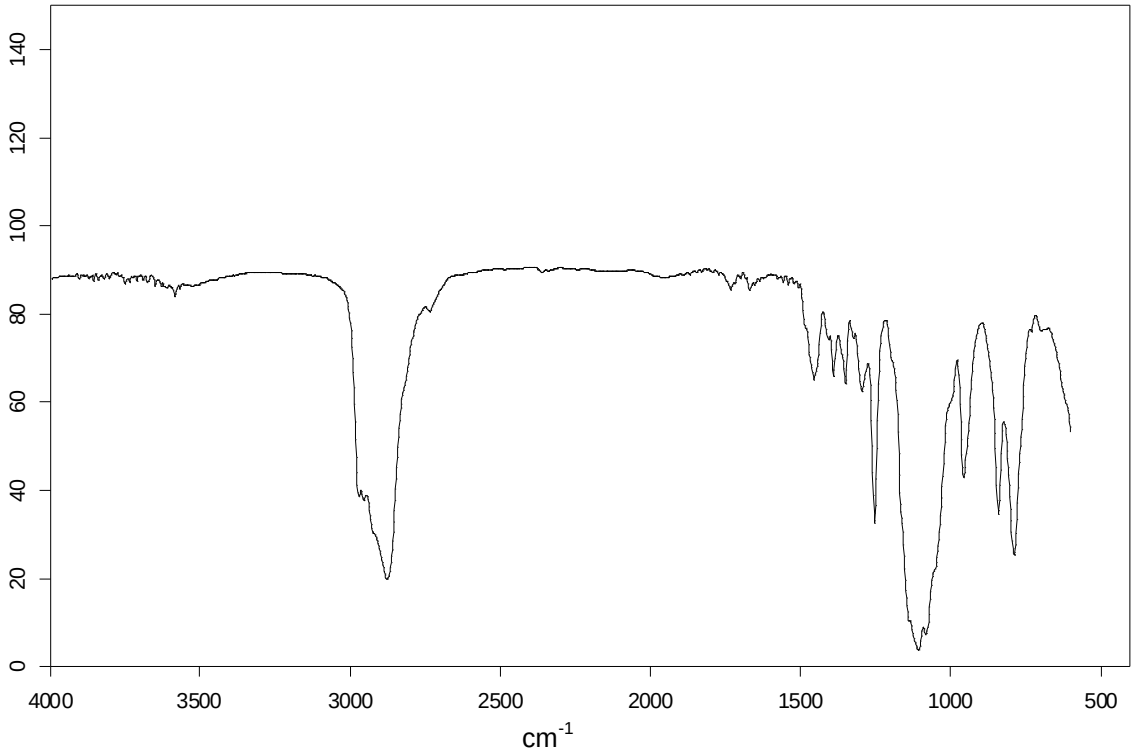

IR of triethoxysilylethyl-ODMS$_0$-*block*-poly(ethylene oxide)$_8$ (**a**)

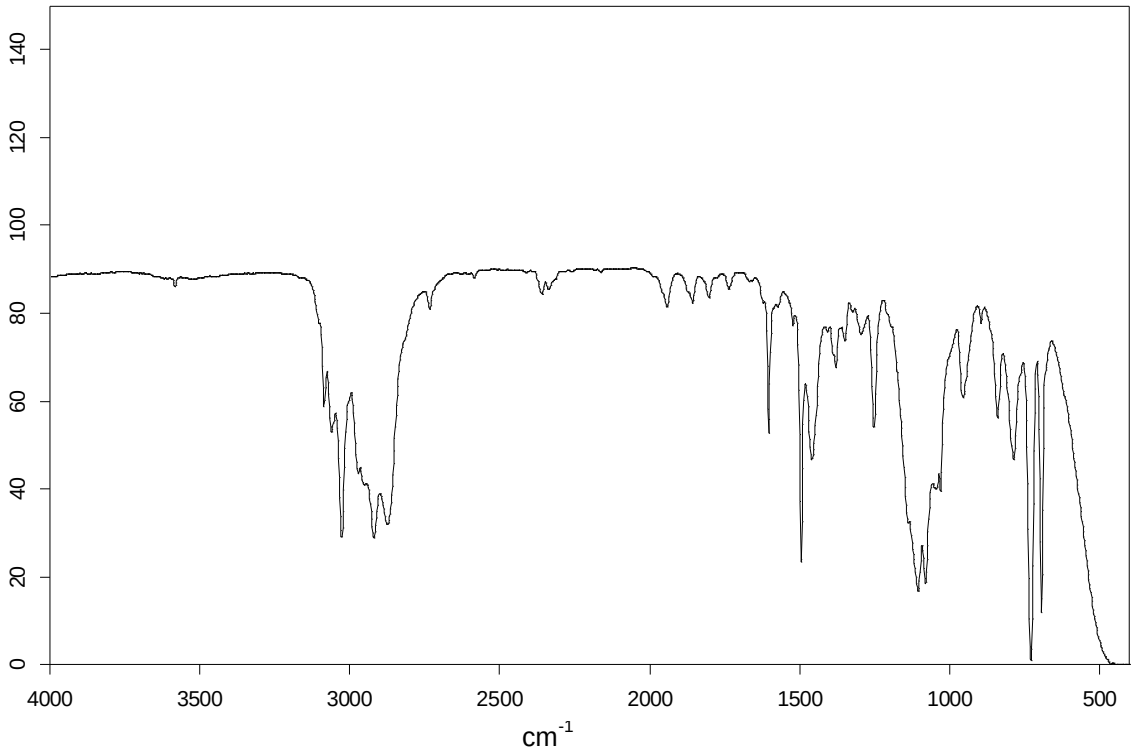

IR of triethoxysilylethyl-ODMS$_4$-*block*-poly(ethylene oxide)$_8$ (**b**)

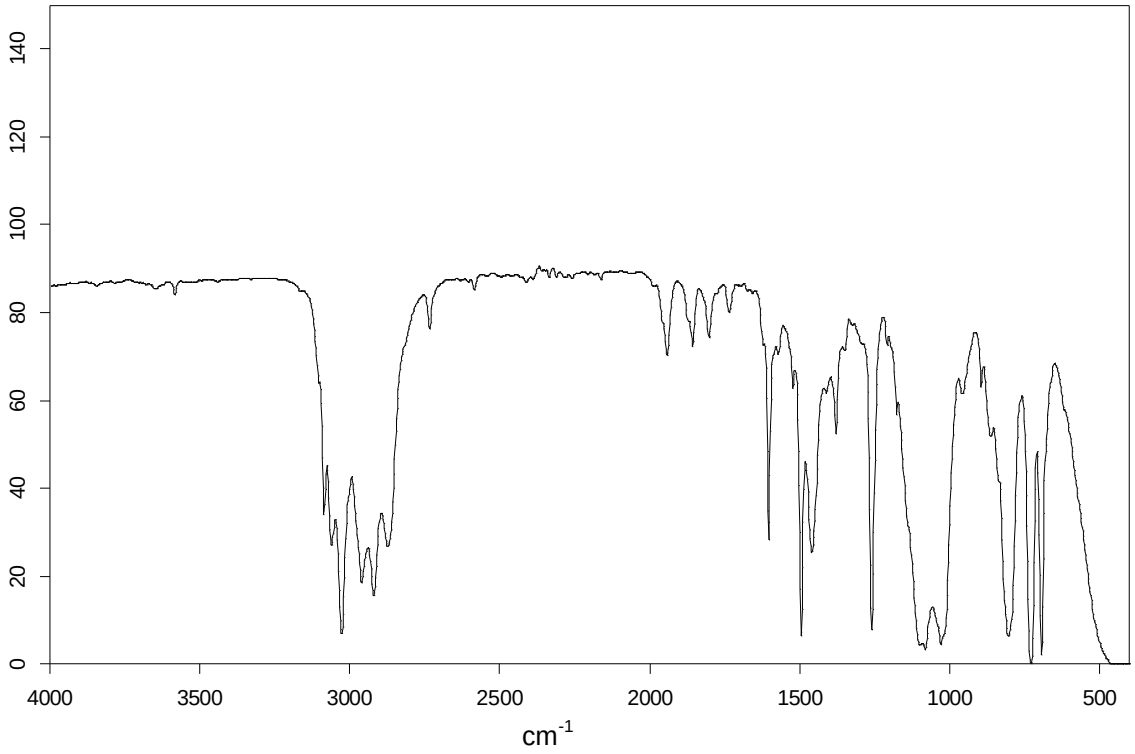

IR of triethoxysilylethyl-ODMS$_{13}$-*block*-poly(ethylene oxide)$_8$ (**c**)

APPENDIX B

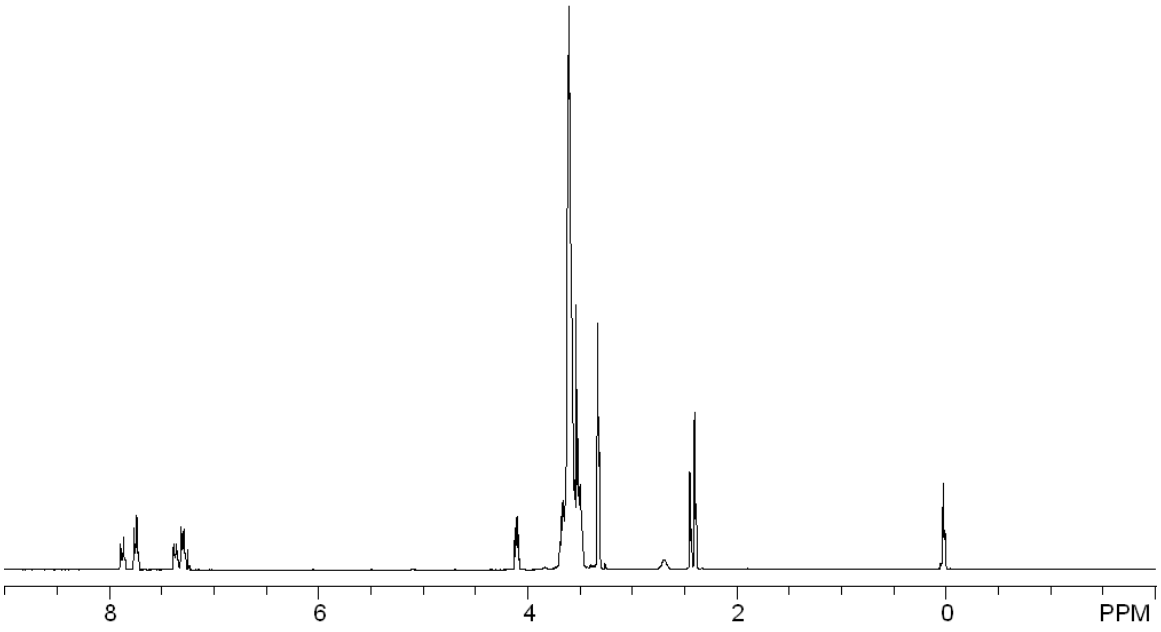

^{1}H NMR of TsO-poly(ethylene oxide)$_{6}$-M (**A**)

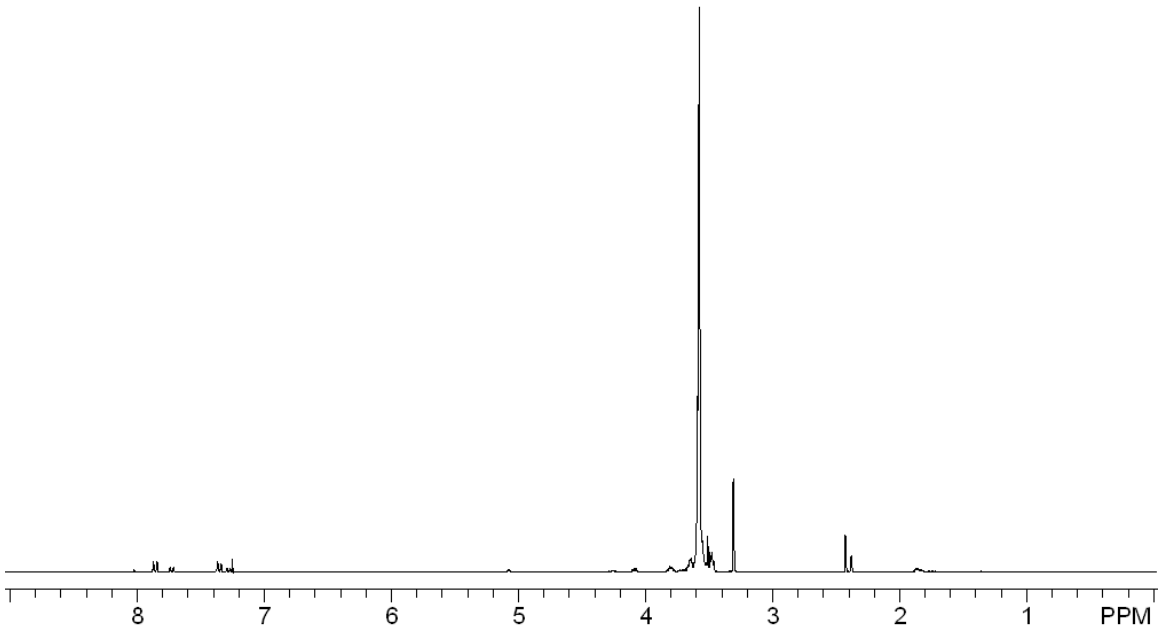

^{1}H NMR of TsO-poly(ethylene oxide)$_{12}$-M (**B**)

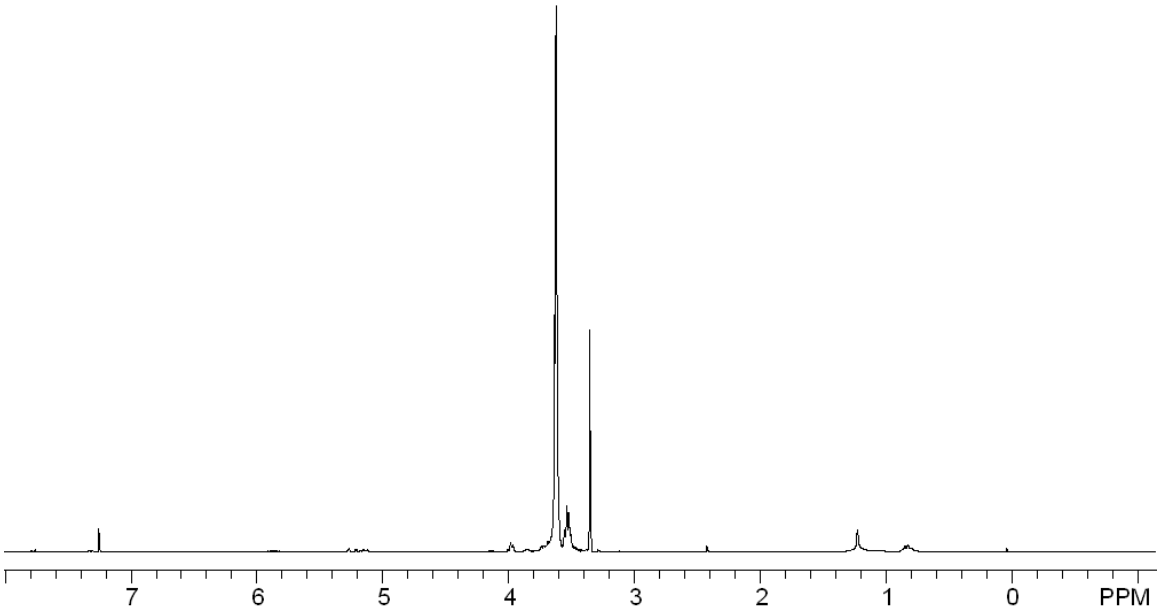

^{1}H NMR of Allyl-poly(ethylene oxide)$_{6}$-M (**a**)

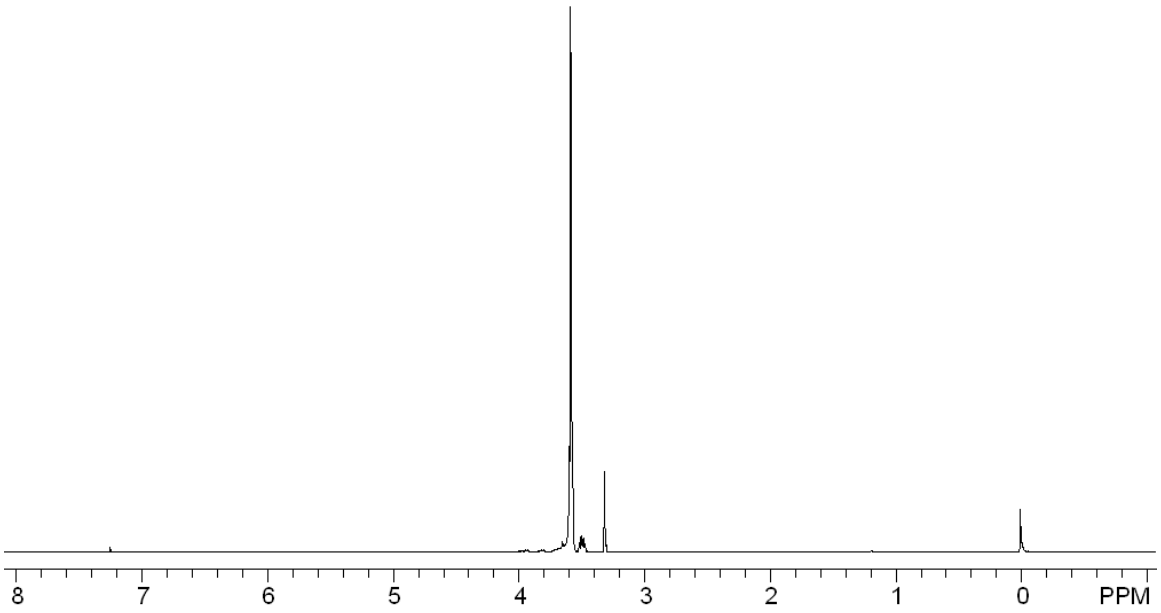

^{1}H NMR of Allyl-poly(ethylene oxide)$_{6}$-M (**b**)

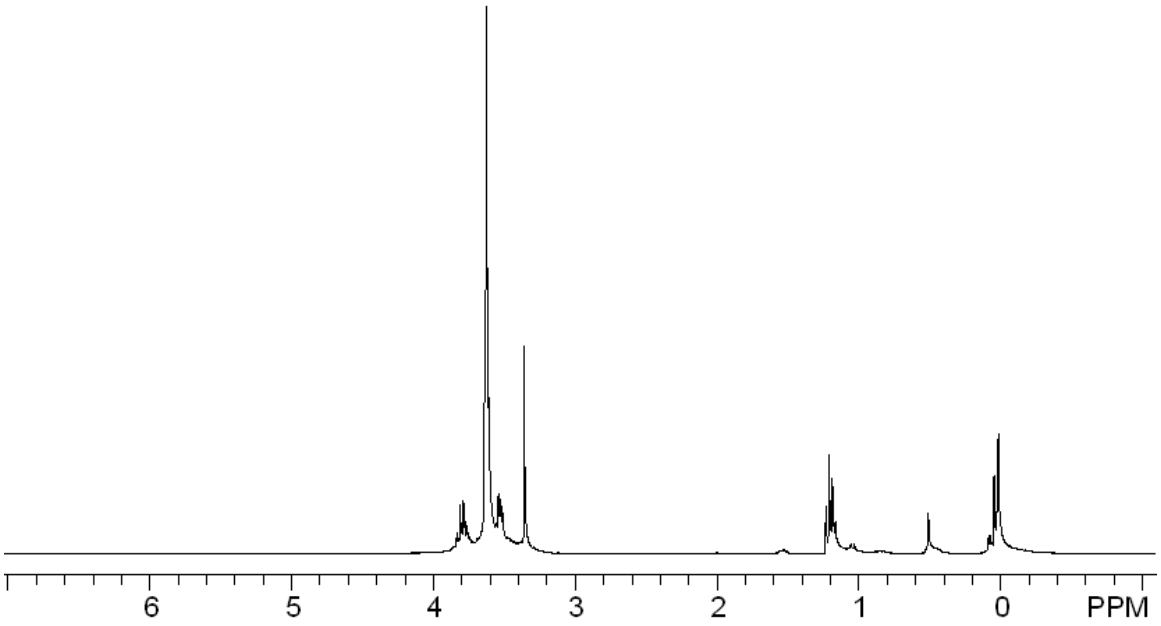

^{1}H NMR of triethoxysilylethyl-ODMS$_{0}$-*block*-[poly(ethylene oxide)$_{2}$]$_{6}$ (**1a**)

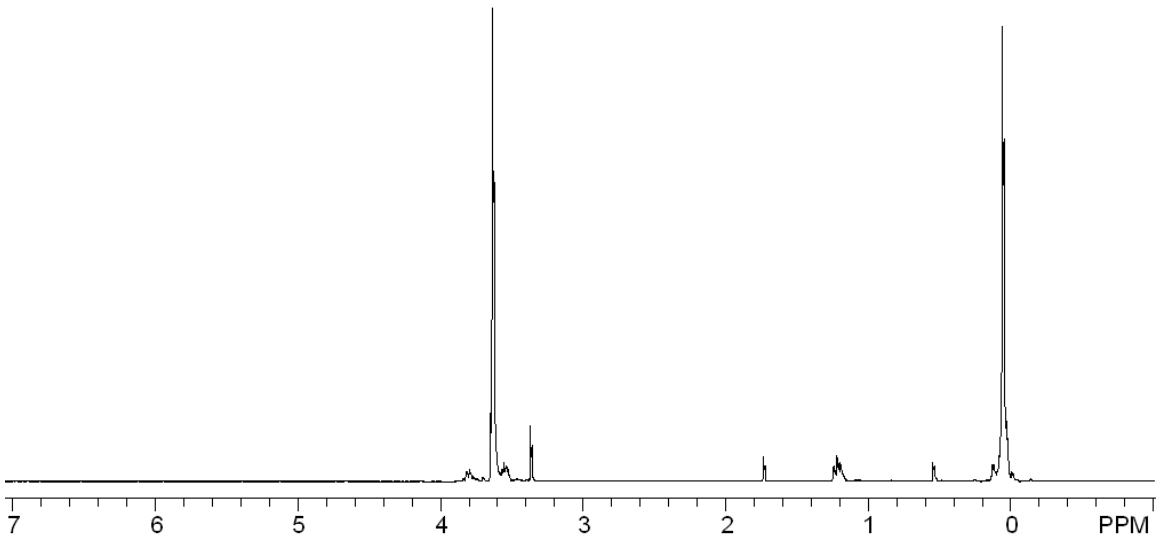

^{1}H NMR of triethoxysilylethyl-ODMS$_{0}$-*block*-[poly(ethylene oxide)$_{2}$]$_{12}$ (**1b**)

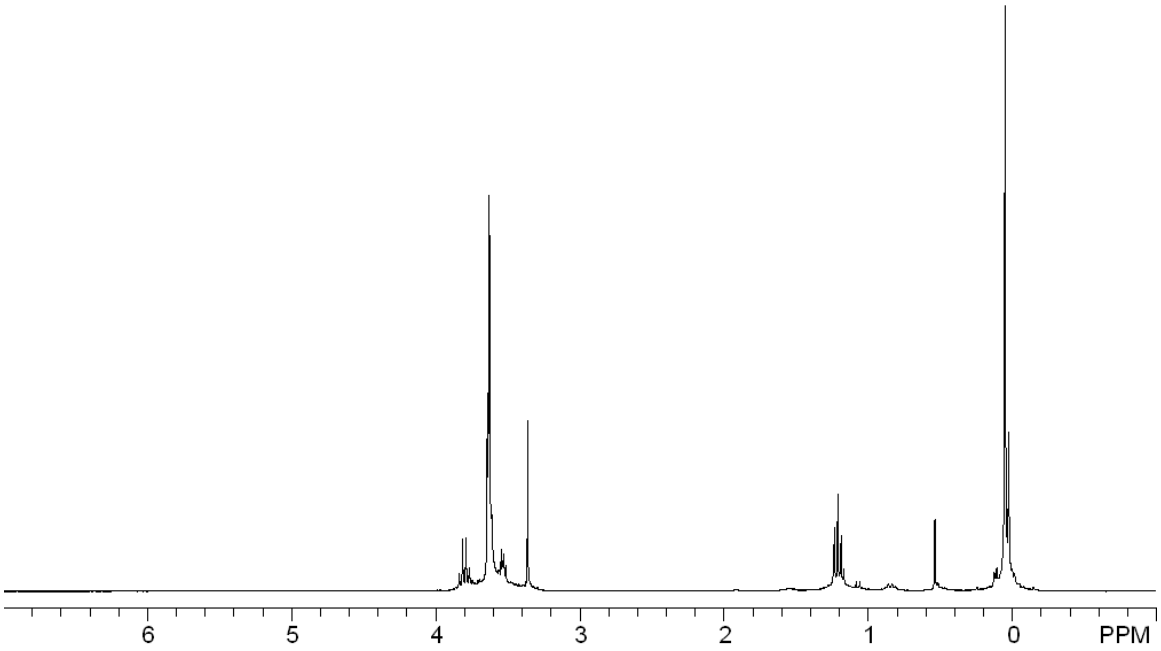

^{1}H NMR of triethoxysilylethyl-ODMS$_4$-*block*-[poly(ethylene oxide)$_2$]$_6$ (**2a**)

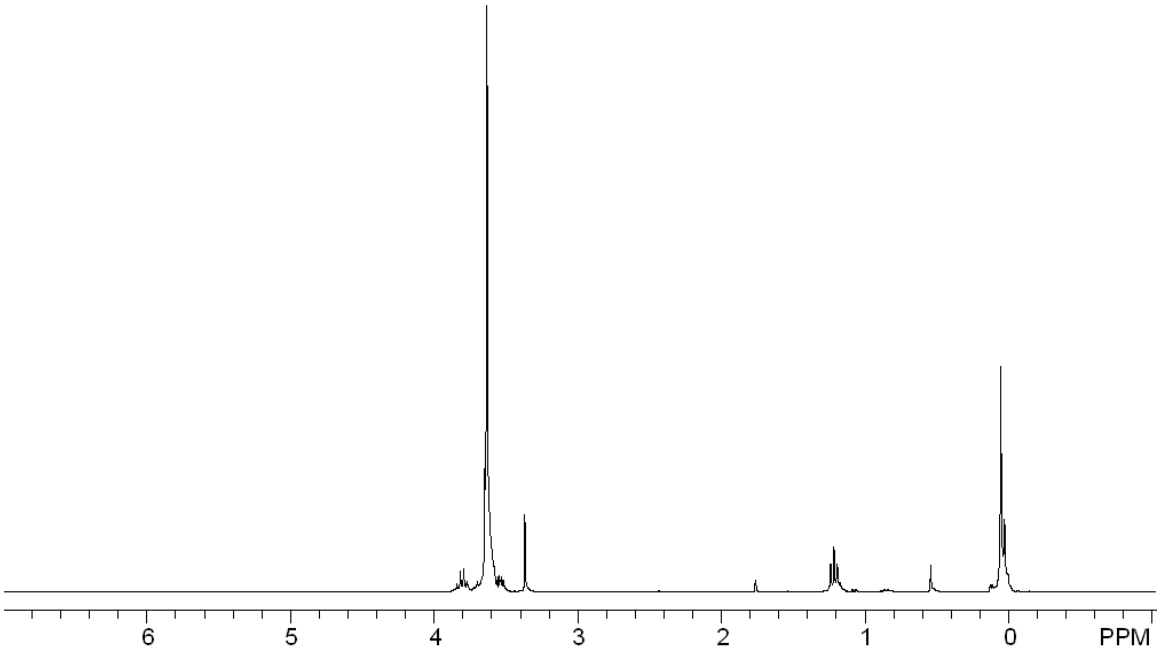

^{1}H NMR of triethoxysilylethyl-ODMS$_4$-*block*-[poly(ethylene oxide)$_2$]$_{12}$ (**2b**)

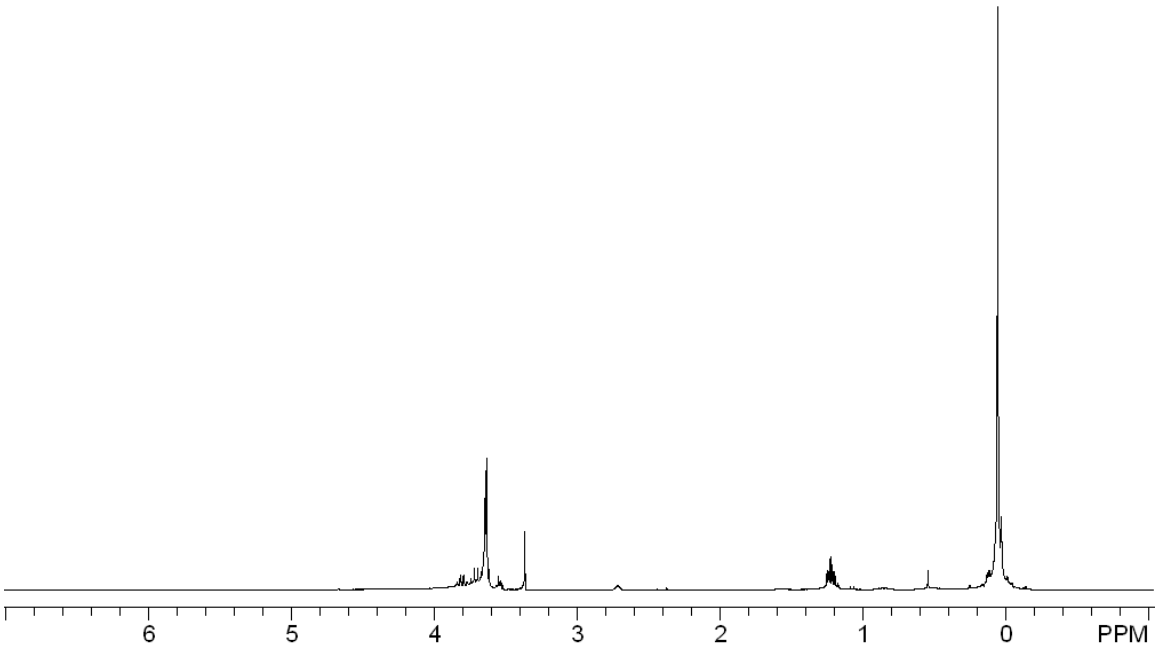

^{1}H NMR of triethoxysilylethyl-ODMS$_{13}$-*block*-[poly(ethylene oxide)$_{2}$]$_{6}$ (**3a**)

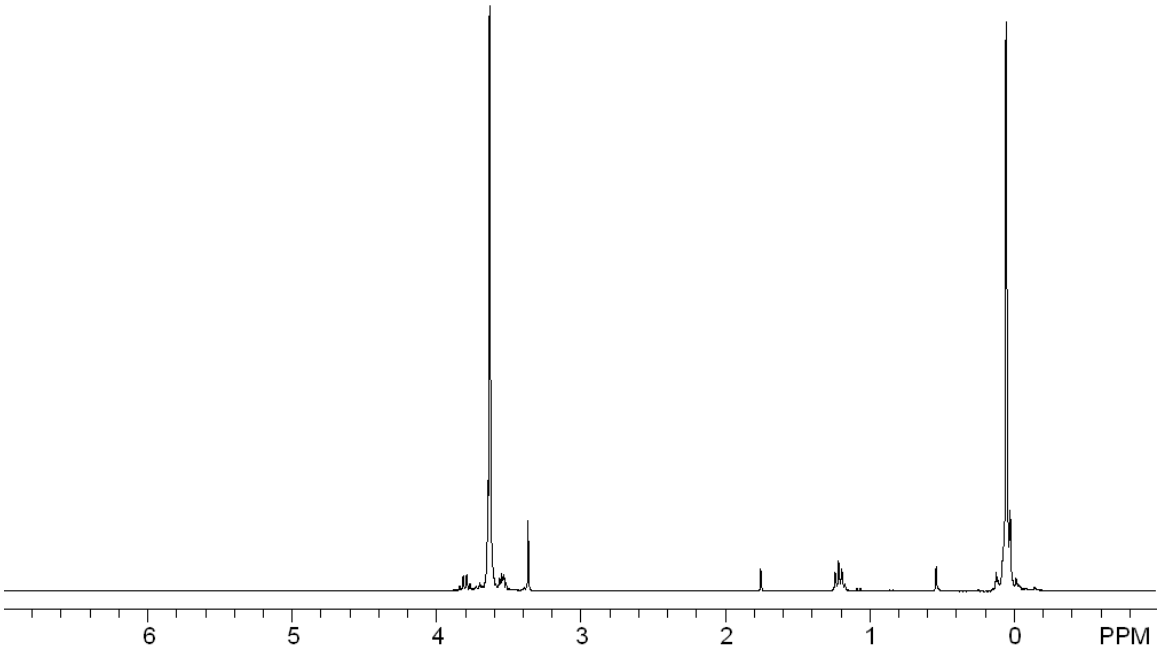

^{1}H NMR of triethoxysilylethyl-ODMS$_{13}$-*block*-[poly(ethylene oxide)$_{2}$]$_{12}$ (**3b**)

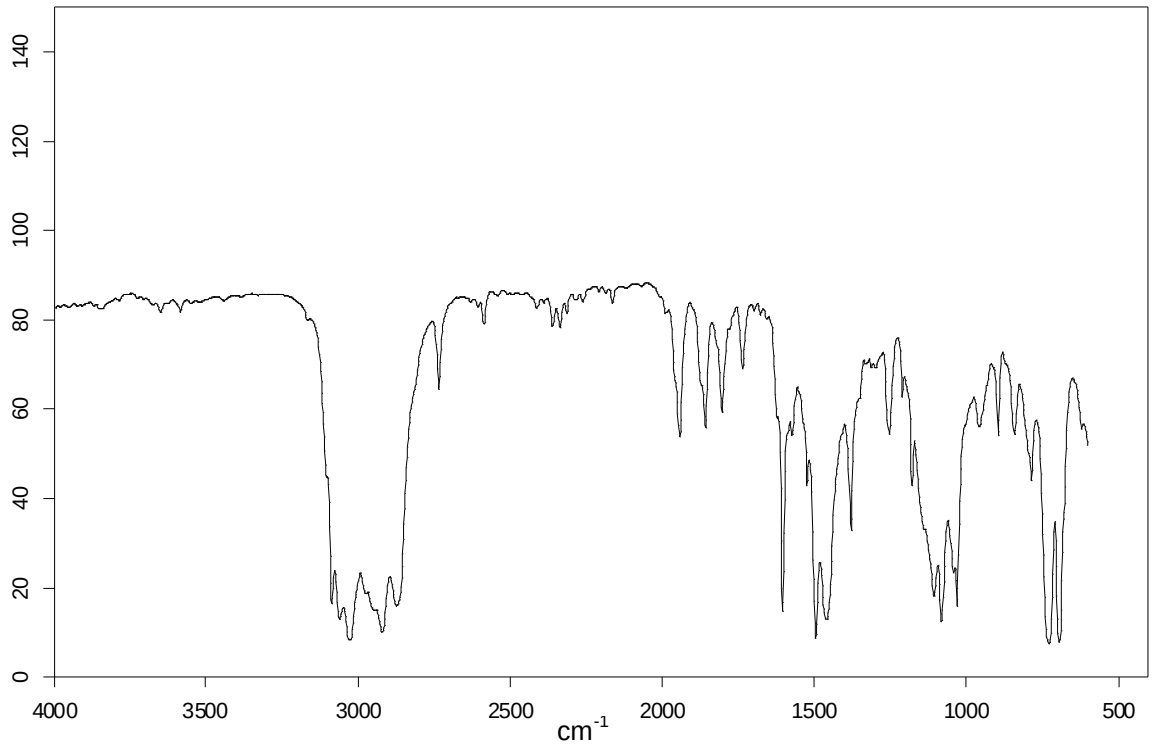

IR of triethoxysilylethyl-ODMS$_0$-*block*-[poly(ethylene oxide)$_2$]$_6$ (**1a**)

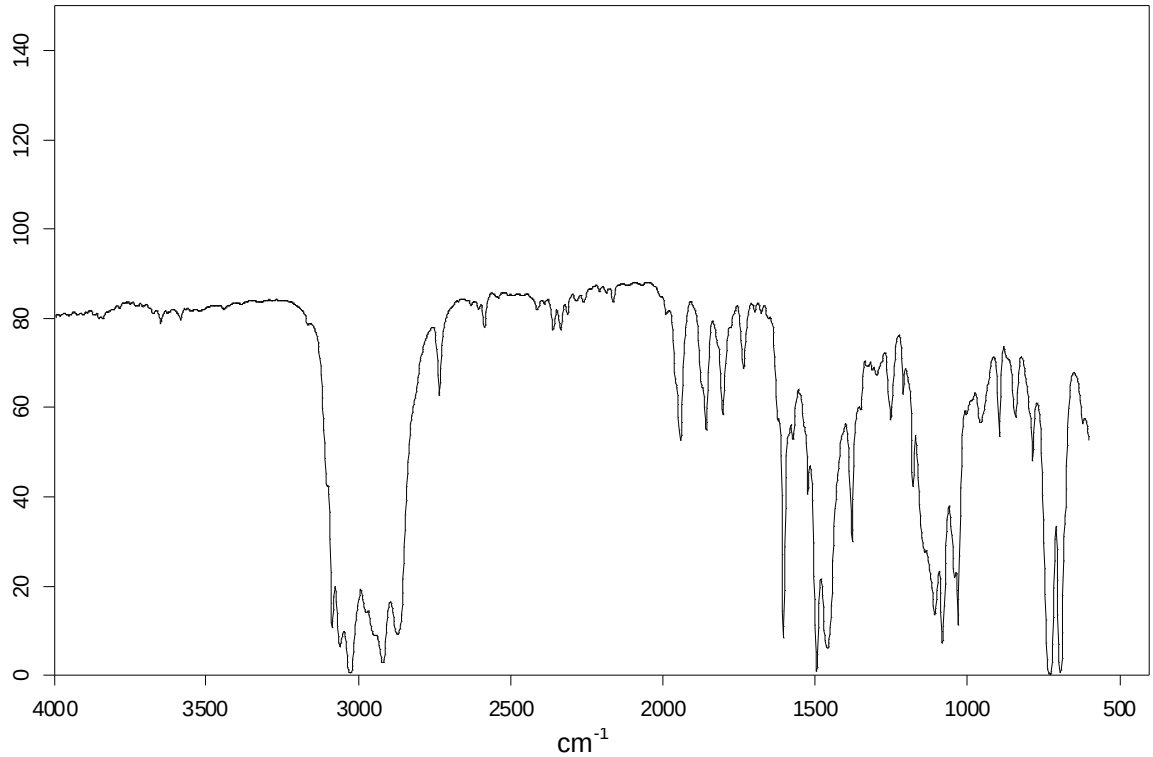

IR of triethoxysilylethyl-ODMS$_0$-*block*-[poly(ethylene oxide)$_2$]$_{12}$ (**1b**)

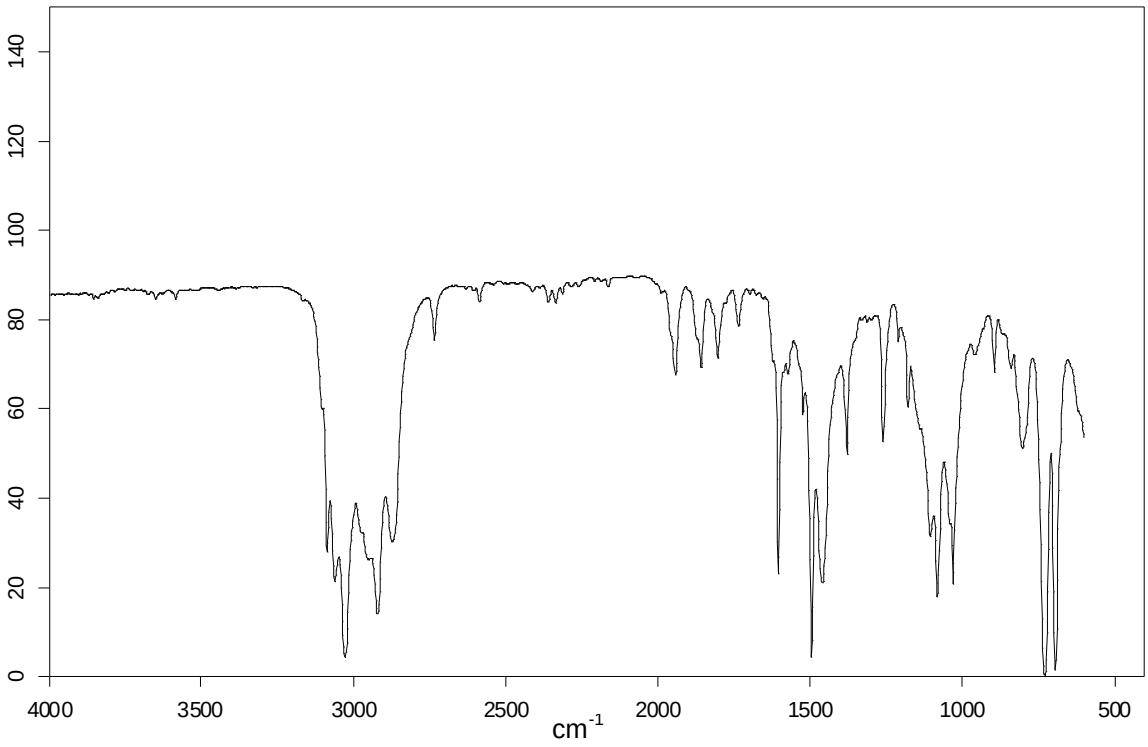

IR of triethoxysilylethyl-ODMS$_4$-*block*-[poly(ethylene oxide)$_2$]$_6$ (**2a**)

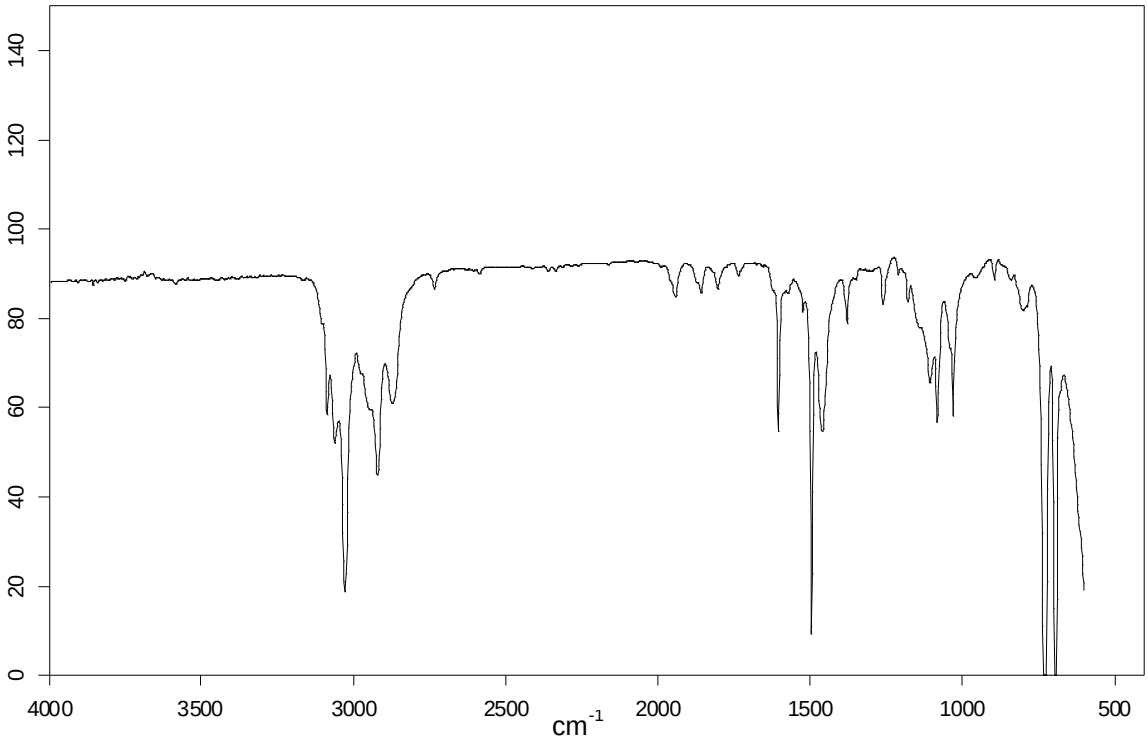

IR of triethoxysilylethyl-ODMS$_4$-*block*-[poly(ethylene oxide)$_2$]$_{12}$ (**2b**)

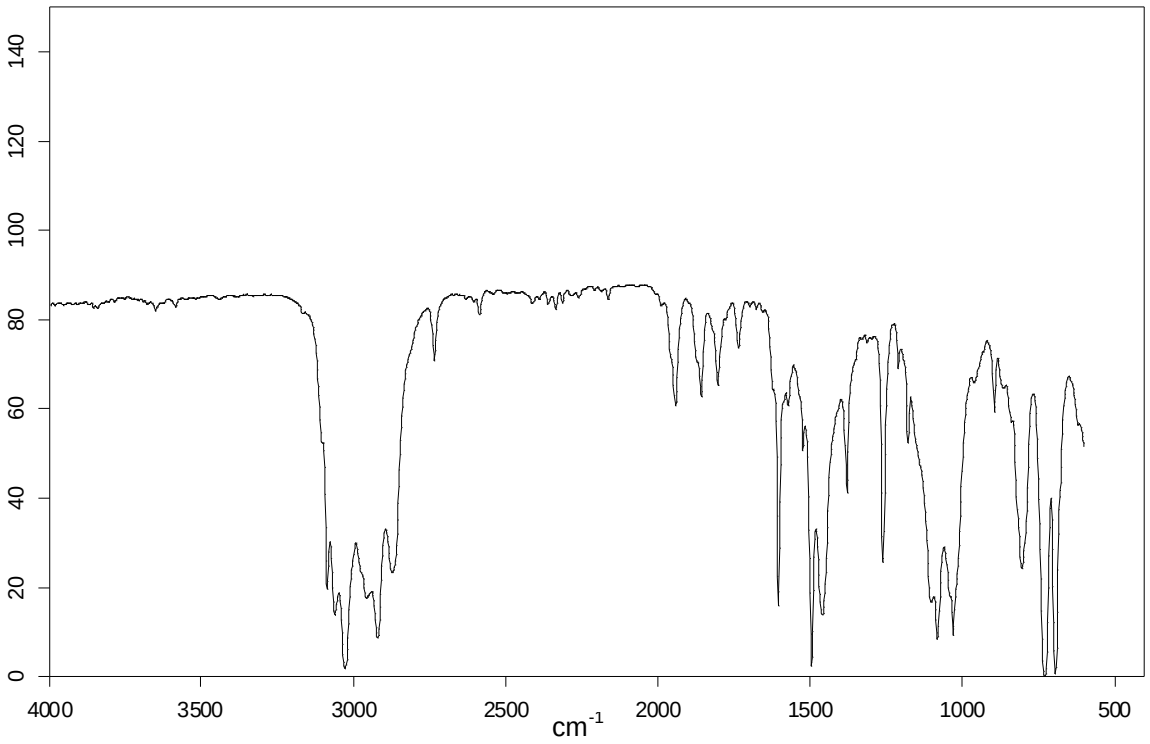

IR of triethoxysilylethyl-ODMS$_{13}$-*block*-[poly(ethylene oxide)$_2$]$_6$ (**3a**)

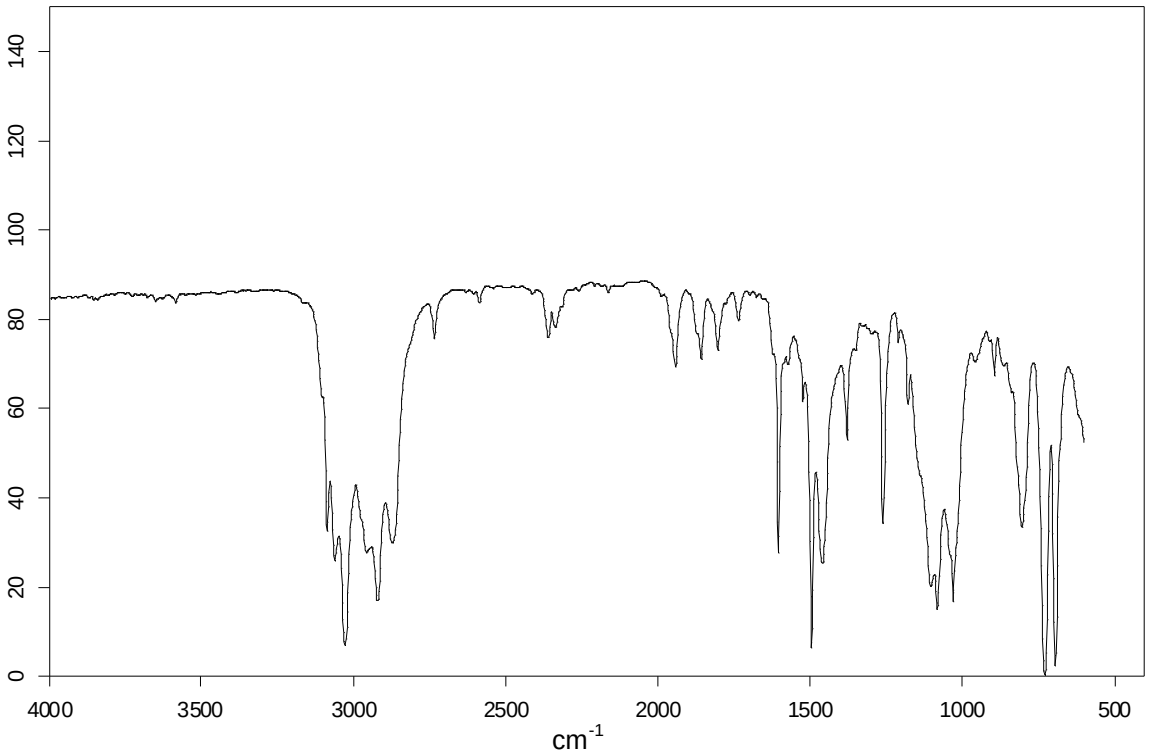

IR of triethoxysilylethyl-ODMS$_{13}$-*block*-[poly(ethylene oxide)$_2$]$_{12}$ (**3b**)

VITA

Ranjini Murthy received her Bachelor of Science degree in Journalism and a minor in English from Arkansas State University, Jonesboro, AR in 2000. She entered into the Chemistry program at Arkansas State University, Jonesboro, AR in August 2001 and received her Master of Science in August 2003. She later joined the Materials Science and Engineering program at Texas A&M University, College Station, TX in January 2005 and received her Doctor of Philosophy degree in May 2009. Her research interests include enhancing the antifouling properties of siloxane polymers, organic synthesis & characterization of novel (polyethylene oxide)-silanes, preparation and characterization of crosslinked silicone coatings and surface grafted films from PEO-silanes and organic synthesis of biodegradable polymers for use in tissue-engineering scaffolds. Expertise in spectroscopic, thermal, mechanical, surface, and microscopy techniques, including: (1) Nuclear Magnetic Resonance (NMR), (2) Fourier-Transform Infrared Spectroscopy (FTIR), (3) Gel Permeation Chromatography (GPC), (4) Thermal Gravimetric Analysis (TGA), (5) Dynamic Mechanical Analysis (DMA), (6) Differential Scanning Calorimetry (DSC), (7) Tensile Testing, (8) Goniometry/Contact Angle Analysis, (9) X-Ray Photoelectron Spectroscopy (XPS), (10) Fluorescence Microscopy, and (11) Ellipsometry.

Ranjini Murthy may be contacted through Prof. Melissa A. Grunlan at the Biomedical Engineering Department, Texas A&M University, College Station, TX 77843-3120.